PROFILING METHYLENETETRAHYDROFOLATE REDUCTASE THROUGHOUT MOUSE OOCYTE AND PREIMPLANTATION EMBRYO DEVELOPMENT

KYLA YOUNG

Thesis submitted to the University of Ottawa in partial fulfillment of the requirements for the Masters of Science in Cellular and Molecular Medicine

Department of Cellular and Molecular Medicine
Faculty of Medicine
University of Ottawa

Abstract

The global DNA methylation pattern is erased and re-established during oogenesis and again in preimplantation (PI) embryo development. Understanding where these methyl groups come from and how the process of methylation is regulated is important, as disruptions could result in detrimental effects. The methionine cycle that produces the cellular methyl pool is linked to the folate cycle. The key enzyme linking theses cycles is Methylenetetrahydrofolate Reductase (MTHFR) which converts 5,10-methylenetetrahydrofolate to 5-methyltetrahydrofolate. *Mthfr* RNA and protein are present throughout mouse oocyte and PI embryo development, including the germinal vesicle, MII egg, 1-cell embryo, 2-cell embryo, morula and blastocysts. In MII eggs the protein appears to be heavier than in any other stage. This was reversed by treatment with Lambda Protein Phosphatase (LPP), indicating that MTHFR is phosphorylated in MII eggs. MTHFR was progressively phosphorylated beginning shortly after initiation of meiotic maturation, reaching maximal levels in MII eggs before decreasing after egg activation using strontium chloride. Potential kinases responsible for the phosphorylation of MTHFR have been identified however not in oocytes or PI embryos. DYRK1A/1 and GSK3A/B have both been suggested to mediate the phosphorylation, however when inhibited showed no effect on the oocyte sample. An LC-MS/MS assay was attempted to measure the activity of MTHFR in wildtype and knockout mouse liver samples, however unsuccessful in the amounts needed to be used for comparison to oocytes. Overall, MTHFR is present in the developing stages of interest and is mediated in some capacity by phosphorylation modifications around the MII stage of development.

List of Tables

List of Figures

List of Abbreviations

ACVS: Animal Care and Veterinary Services

AHCY: Adenosylhomocysteinase

ANOVA: Analysis of variance

APC: Anaphase-promoting complex

BHMT: Betaine-homocysteine methyltransferase

bp: Base pair

cAMP: Cyclic Adenosine Monophosphate

CPM: Counts per million

CBS: Cystathionine beta synthase

cGMP: Cyclic Guanosine Monophosphate

CDKs: Cyclin Dependent Kinases

CDK1: Cyclin Dependent Kinase 1

CEEFs: Cumulus Expansion-Enabling Factor

CL: Corpus Luteum

COC: Cumulus oocyte complex

CSF: Cytostatic Factor

CTH: Cystathionine gamma-lyase

DMRs: differentially methylated regions

DNA: deoxyribonucleic acid

dpc: days post coitum

FSH: Follicle-stimulating hormone

GV: Germinal vesicle

GVBD: Germinal vesicle breakdown

hCG: human chorionic gonadotropin

ICM: Inner cell mass

ip: intraperitoneally

IP3: Inositol triphosphate

IU: international units

IVF: *in vitro* fertilization

IVM: *in vitro* maturation

KFHM: Potassium supplemented flushing-holding medium

KSOM: Potassium supplemented optimized medium

LH: Luteinizing hormone

LPP: Lambda Protein Phosphatase

MEM: Minimum Essential Medium

MI: Meiotic metaphase I

MII: Meiotic metaphase II

MAT: S-adenosylmethionine synthetase enzyme

MPF: Maturation Promoting Factor

MTHFR: Methylenetetrahydrofolate Reductase

MTR: Methionine synthase

MTX: methotrexate

NCBI: National Center for Biotechnology Information

NPPC: Natriuretic peptide type C

OCM: One Carbon Metabolism

PCR: Polymerase chain reaction

PI: Preimplantation embryo

PKA: Protein Kinase A

PLC: Phospholipase C

PLP: pyridoxal 5'-phosphate

PMSG: Pregnant Mare Serum Gonadotropin

PVA: Polyvinyl alcohol

RFC: reduced folate carrier

RNA: ribonucleic acid

SAH: S-adenosyl homocysteine

SAM: S-adenosyl methionine

SHMT: Serine hydroxymethyltransferase

TBST: Tris Buffered Saline + Tween

THF: Tetrahydrofolate

ZP: Zona Pellucida

Acknowledgements

The work compiled in this thesis was performed under the supervision of Dr. Jay Baltz (Department of Obstetrics and Gynecology and Cellular and Molecular Medicine, University of Ottawa Faculty of Medicine; Ottawa Hospital Research Institute, Chronic Disease Program). I would like to thank Dr. Baltz for not only supporting me academically but also for the assistance in finding a career path that aligns with what I am truly passionate about. I feel very fortunate to have studied under Dr. Baltz for his academic excellence, endless patience and witty personality.

Additionally I would like to thank the members of my Thesis Advisory Committee: Dr. Johné Liu (Department of Biochemistry, Microbiology and Immunology, University of Ottawa; Ottawa Hospital Research Institute, Chronic Disease Program), Dr. Shannon Bainbridge (Department of Cellular and Molecular Medicine and Interdisciplinary School of Health Sciences, University of Ottawa; Ottawa Hospital Research Institute, Chronic Disease Program) and Dr. Amanda MacFarlane (Department of Biology, Carleton University; Nutrition Research Division, Health Canada). The expertise and feedback given by these scientists was crucial in the ultimate success of this project and I am grateful for the meetings we had together.

As well, I would like to thank the members of the Baltz Lab who contributed to this work. This includes Megan Meredith for teaching me the basics of mouse work, training me to do all the necessary techniques and for always being available to help me whether she was in the lab or not. Dr. Allison Tscherner, who helped me immensely with the impossible task of trouble-shooting western blots into the wee hours of the morning, thoroughly teaching me PCR (and everything that comes with it), performing the qPCR experiments when I was unable to be trained and for her friendship that continues to guide and support me through all of my endeavours. Taylor McClatchie, who took on any extra work to assist with the enormous sample

collections that were needed for this project (mostly at 7am), the maintenance of all the mice I could ever need, performing the final activity assay when I was unable to do so and also for her friendship that continues to support me outside of the lab. Dr. Baohua Zhang, who did the preliminary work on this project and whose results helped me kickstart my Master's degree. Dr. Angus Macaulay, for all his assistance on wrapping my brain around bioinformatics.

Others who contributed to this work and deserve a thank you include Jeremy Zhang from the Ottawa Hospital Clinical Investigation Unit Pharmacokinetics Laboratory who performed the LC-MS/MS assays. The StemCore unit in the Ottawa Hospital Research Institute. Gareth Palidwor of the Bioinformatics Core Facility. Hannah Gillis and Scott Gunn, who also assisted in the western blot trouble-shooting process.

Finally, I would like to thank my mom and dad, Nicole and Dave, for making sure I finished this degree and supporting me in any way they could to ensure that happened.

This graduate work was supported by the Canadian Institute of Health Research (CIHR) (MOP 97972) obtained by Dr. Baltz. I would also like to thank the University of Ottawa Faculty of Graduate and Postdoctoral Studies Admission Scholarship for the contribution to my studies.

1. Introduction

1.1 Folliculogenesis and Oogenesis

The developing ovary supplies the female with primordial germ cells, which will eventually become oocytes and contribute to reproduction. The primordial germ cells are first found in the developing fetus in the extraembryonic mesoderm and will migrate to the posterior portion of the primitive streak (Ginsburg et al. 1990) and then to the endoderm of the developing hindgut (Anderson et al. 2000). At approximately 9 days post coitum (dpc) in the mouse, the primordial germ cells will migrate to the genital ridge (Molyneaux et al. 2001) and proliferate rapidly until 13.5 dpc (Ginsburg et al. 1990). The primordial germ cells will form germ cell clusters, called cysts or nests, until they begin meiosis and their transformation into oocytes (Jagarlamundi and Rajkovic 2012). When the germ cells cysts begin to break down, they will form primordial follicles while also losing a significant amount of germ cells so that the final products are primordial follicles each containing a single oocyte (Pepling and Spradling 2001).

Each primordial follicle contains a prophase-arrested oocyte surrounded by pre-granulosa cells that will differentiate to form granulosa cells. Primordial follicles will either remain quiescent, die, or be activated to finish development until ovulation (Zheng et al. 2012). The primordial follicles will become primary follicles after the granulosa cells change from flattened to cuboidal (Pedersen and Peters 1968). The oocyte will continue to grow and the granulosa cells will proliferate with an additional layer of theca cells surrounding the follicle to make a secondary follicle (Eppig 2001).

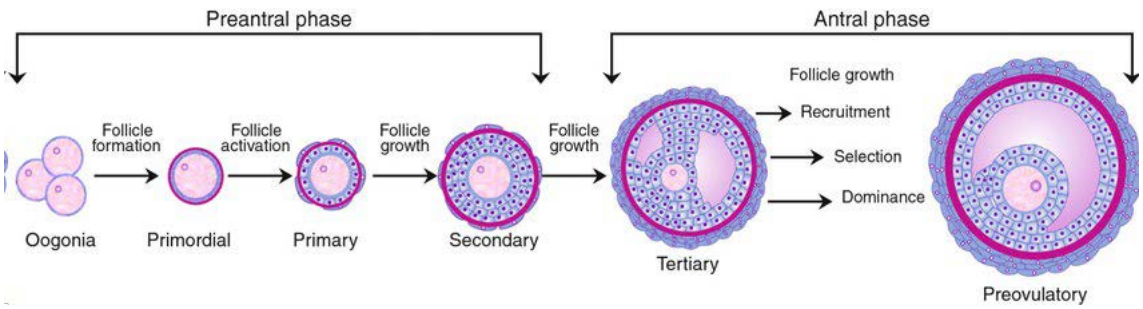

Figure 1. Schematic sequence of Folliculogenesis.

Preantral phase: Formation, growth and activation of primordial follicles and growth of primary and secondary follicles. Antral phase: Formation of tertiary follicles, growth continues through recruitment, selection, dominance and preovulatory stage of follicular waves. Oogonia develop from a primordial germ cell and differentiate into an oocyte in the ovary. Primordial follicles have one layer of granulosa cells. Primary follicles have one layer of cuboidal granulosa cells. Secondary follicles have two or more layers of cuboidal granulosa cells and some theca cells. Tertiary follicles have several granulosa cell layers, theca cells, and primary oocyte and is characterized by an antral cavity which contains follicular fluid. Preovulatory or Graafian follicles are larger, have more antral fluid and contain a secondary oocyte; this is the last stage of follicle development. Light Pink: Oocyte; Dark Pink: Zona Pellucida; Light Purple: Granulosa Cells; Dark Purple: Theca Cells. This image was obtained with permission from Araújo et al (2014).

Small fluid-filled cavities form within the secondary follicle, eventually coalescing into the antrum. The follicle at this stage is therefore an antral follicle. The granulosa cells are separated into cumulus cells around the oocyte and mural granulosa cells in multiple layers lying inside the follicle wall. Follicle-stimulating hormone (FSH) is what induces antral follicle growth. Fully grown antral follicles, called Graafian follicles, will survive and develop to the preovulatory stage. These have outcompeted the other follicles that were recruited to grow in the same cycle by producing more estrogen, having greater granulosa cell proliferation, and producing more FSH receptors, thus allowing them to survive the decrease in FSH that occurs as ovulation approaches. These form the preovulatory follicles (several in mice and one in humans) and are deemed dominant follicles (Figure 1). During most of their growth, oocytes are not capable of resuming meiosis. However, when the oocyte reaches approximately three-quarters of its final size, it develops meiotic competence, which allows the oocyte to resume meiosis (Wassarman et al, 1979). Resumption of meiosis will normally occur *in vivo* in response to luteinizing hormone (LH) stimulation and the oocyte will be ovulated in response to the LH surge. After ovulation into the oviduct, they await fertilization.

1.2 Prophase I arrest

Growing oocytes are arrested at the diplotene stage of prophase I of meiosis. Several pathways allow for this arrest to be maintained, with several overlapping to ensure meiotic resumption does not occur. During growth, oocytes are not meiotically competent because they lack the molecular machinery to exit prophase and complete meiotic maturation. However, they accumulate the molecular components of cell cycle control during growth and become meiotically competent as they approach full size (Harrouk & Clarke, 1995). Once this occurs,

oocytes require active inhibition of meiotic progression to remain arrested in prophase I. Oocytes arrested at prophase I can be distinguished by their large nucleus, called a GV.

High activity of protein kinase A (PKA) is necessary to maintain meiotic arrest and cyclic adenosine monophosphate (cAMP) is required to activate PKA (Jaffe & Egbert, 2017). The downstream effect of high PKA activity in the GV oocyte is to maintain M-phase Promoting Factor (MPF) in an inactive state. MPF is a heterodimer made up of cyclin-dependent kinase 1 (CDK1) and cyclin B and PKA maintains CDK1 in an inactive from (Jaffe & Egbert, 2017). MPF must be activated for the oocytes to be released from GV arrest and re-enter meiotic progression. Fully-grown GV oocytes already contain cyclin B and CDK1 but they do not form the active MPF complex. The high levels of cAMP activate PKA which in turn phosphorylates and activates WEE1 kinase which phosphorylates and inactivates CDK1 (Jaffe & Egbert, 2017). PKA also phosphorylates and inhibits CDC25B phosphatase that dephosphorylates CDK1 to prevent removal of the inhibitory phosphate groups from CDK1 (Jaffe & Egbert, 2017). The inactivation of CDK1 allows for MPF to stay inactive and the oocytes to remain arrested in prophase I as a GV oocyte. The cAMP in arrested GV oocytes is produced by the oocytes themselves via adenylyl cyclase. This cyclase is activated by the G-protein coupled receptor GPR3, which is constitutively active in the oocyte and continually stimulates adenylyl cyclase activity.

The cAMP in the oocyte is maintained at a high level because it is produced continually through adenylyl cyclase and also because it is not degraded. In the oocyte, the mechanism of cAMP degradation is via the cAMP-specific phosphodiesterase PDE3A (Mehlmann, 2005). PDE3A is inactive in the arrested oocyte. It is maintained in an inactive state by its inhibition by cyclic guanosine monophosphate (cGMP) which acts directly on PDE3A. The cGMP in the

oocyte is synthesized in the cumulus granulosa cells that surround it and are coupled to it via gap junctions. In the cumulus cells, cGMP is synthesized by the receptor guanylyl cyclase NPR2 (Zhang et al, 2010). The ligand that activates NPR2 is natriuretic peptide precursor C (NPPC). NPPC is continually synthesized by mural granulosa cells and secreted into the antrum of the follicle to bind to NPR2 on the cumulus cells and thus maintain meiotic arrest.

1.3 Resumption of Meiosis and rearrest as an MII egg

During a reproductive cycle, fully-grown GV oocytes will re-enter meiosis by activating MPF which causes the oocyte's nuclear envelope to break down, termed germinal vesicle breakdown (GVBD). Following GVBD, the homologous chromosomes align on the first meiotic metaphase (MI) spindle and the oocyte completes the first round of meiosis by extrusion of the first polar body in which it discards half the chromosomes to reduce to the haploid state. It then progresses into the second meiotic metaphase (MII) where the remaining chromosomes align on the MII spindle.

The onset of GVBD involves several molecular cascades, beginning with LH produced by the pituitary gland. LH binds to its receptors on the mural granulosa cells, where it induces dephosphorylation of NPR2 which inactivates it and leads to a rapid block of cGMP production and to the cGMP in the oocyte diffusing back out into the cumulus cells (Jaffe & Egbert 2017). The decrease of cGMP in the oocyte leads to release of its inhibition of PDE3A and PDE3A activation. This acts to decrease cAMP levels, inactivating PKA, activating CDC25B, dephosphorylating CDK1 and thus activating MPF. These oocytes with activated MPF and metaphase I spindles are known as metaphase I (MI) oocytes.

The oocyte completes MI and then immediately transitions to MII. This involves separation of the homologous chromosomes through anaphase of the MI spindle and cytokinesis to extrude the first polar body. The oocyte then forms the MII spindle and arrests as a mature MII egg.

The mechanism of MII arrest is different from that of GV arrest. Second meiotic arrest is maintained by cytostatic factor (CSF) to prevent parthenogenesis. CSF activity via the MOS-MEK-MAPK pathway maintains MII arrest (Phillips et al, 2002). High levels of MPF trigger the translation of *Mos* mRNA and the expression of MOS, a MEK kinase found in germ cells. MOS protein synthesis triggers MEK activation and MAPK activation. MAPK induces MII arrest by ultimately inhibiting anaphase promoting complex (APC). APC targets cyclin B for degradation at the transition from metaphase to anaphase and allows progression (Maller et al, 2002). This arrest ends upon fertilization or parthenogenetic activation.

1.4 Ovulation

Ovulation follows the LH surge. In addition to inducing the resumption of meiosis in the oocyte, LH also causes the expansion of cumulus cells, rupturing of the follicle, and release of the cumulus-oocyte complex (COC) as a fertilizable oocyte into the oviduct. LH binds to its G-protein coupled receptor on mural GCs to induce an ovulatory response (Park et al, 2004). The oocyte excretes cumulus expansion enabling factors (CEEFs), which activate the cumulus cell dependent pathways leading to cumulus expansion (Vanderhyden et al, 1990). The cumulus expands by secretion of a hyaluronic acid extracellular matrix by the cumulus cells, which release their cell-cell contacts and move away from the oocyte surface to form a large mucinous mass. This coincides with the closure and then physical disruption of the gap junctions between the cumulus and oocyte and those between cumulus cells (Gilula et al, 1978).

The expanded COC is released from the follicle into the oviduct. This involves expression of enzymes that degrade the follicle wall and allow its rupture to release the COCs. The COCs are then captured by the fimbria of the proximal end of the oviduct and taken up into the ampulla of the oviduct where fertilization will take place.

When the oocyte is released, the remaining cells will be reprogrammed to form the corpus luteum (CL). The CL assists in establishing and maintaining pregnancy, mainly by secreting progesterone until the placenta takes over this function later in pregnancy (Kidder and Vanderhyden, 2010). The CL is maintained by chorionic gonadotropin that is secreted by the implanting embryo. If pregnancy does not occur, the CL quickly breaks down.

1.5 Fertilization and Preimplantation embryo development

When an ovulated haploid MII egg is met by a species-specific ejaculated haploid sperm in the oviduct, fertilization can occur to form a diploid zygote (Yanigamachi, R. 1994). The first step to achieving fertilization is the binding of the sperm's acrosome, the anterior part of the sperm able to release egg-penetrating enzymes, to the egg's zona pellucida (ZP). When binding occurs, the acrosomal reaction (exocytosis of the acrosomal vesicle) will take place, which will allow for penetration of the ZP. Next, the sperm will penetrate the ZP, reach the perivitelline space, and bind to the oocyte's plasma membrane, eventually fusing with it and releasing its nucleus into the egg cytoplasm. This is the point of fertilization where the egg is now deemed a zygote or 1-cell embryo.

When the sperm fuses with the egg membrane it activates the egg. This involves the release of the sperm-specific phospholipase, phospholipase C zeta (PLCζ), into the oocyte. PLCζ acts on inositol phospholipids in the oocyte membrane to release inositol triphosphate (IP3) in

the egg. IP3 in turn binds to its receptors on the egg endoplasmic reticulum to release Ca^{2+}. It is the increased intracellular Ca^{2+} concentration that activates the egg.

The increase in Ca^{2+} has two main actions. First, it activates the anaphase promoting complex which degrades cyclin B and inactivates MPF, releasing the egg from MII arrest. Second, it causes the exocytosis of the egg's cortical granules, which is the main block to polyspermy. The cortical granules contain the protease ovastacin. Ovastacin will activate to cleave a ZP glycoprotein, ZP2, and this will stop other sperm from being able to bind the plasma membrane, avoiding polyspermy (Burkart et al. 2012).

Egg activation and inactivation of MPF results in the completion of meiosis. Fertilization releases the oocyte from MII arrest and allows for discarding of the second polar body, while the remaining chromatids form the female pronucleus within the egg. 1-cell embryos contain two pronuclei, each one containing the maternal or paternal genome. The pronuclei remain separate until their nuclear envelopes break down just before the 1-cell embryo cleaves into a 2-cell embryo and the maternal and paternal genomes combine. After the first cleavage event, each cell will contain the new embryonic genome, and this will now be a 2-cell embryo (Cooper & Hausman, 2000).

Up until now, the embryo has relied on maternal genes for formation of structures and maintenance of development. Zygote genome activation occurs at the 2-cell stage in mice (Ram and Schultz, 1993). The zygote now undergoes several rounds of mitosis without an increase in total volume to form a 4-cell embryo and then an 8-cell embryo. At this stage, the embryo will undergo a process called compaction where the cells form tight junctions and there is an increase in intercellular adhesion, completed by the 16-cell stage in mice. Once compaction is complete, the embryo is called a morula.

The next process to occur is cavitation, where a fluid-filled cavity known as a blastocoel forms and the cells begin to differentiate into two distinct lineages: trophectoderm and inner cell mass (ICM) and the embryo is termed a blastocyst. The cells of the trophectoderm will form the extraembryonic tissues including the placenta, while the cells of the ICM will form its own two lineages: the epiblast which will form the fetus, umbilicus and innermost fetal membranes and the primitive endoderm which will form the intermediate layers of the extraembryonic membranes (Biggers et al, 1988; Rossant & Tam, 2009; Hudson et al, 2010). The embryo will then implant in the uterine wall on approximately day 5 following fertilization in mice (day 7 in humans) for the remainder of prenatal development as an embryo and fetus (Cockburn and Rossant, 2010).

1.6 In vitro maturation and embryo culture

The first successful *in vitro* maturation (IVM) technique in humans occurred in 1991 by Cha et al, proving that immature oocytes collected from unstimulated ovaries could be incubated outside the follicle using mature follicular fluid and result in successful *in vitro* fertilization (IVF) (Cha et al. 1991). The process of IVM begins with the oocyte in a COC as it is still surrounded by the follicle which contains all of the components the oocyte requires in the follicular fluid. The main benefit of IVM in humans is to reduce the gonadotropin stimulation in a patient which will remove the risk of ovarian hyperstimulation syndrome (Walls and Hart, 2018).

Media used for IVM have become standard to include necessary substrates and ions to produce a healthy, mature egg. Culture times for maturation vary from 24-40 hours with a high success rate. These media will include hormones, sources of protein, growth factors and amino acids all at optimal concentrations. In 1992, seven commercial media were compared for IVM

and it was concluded that IVM for bovine oocytes in either Eagle's Minimal Essential Medium alpha (MEMα) or SFRE 199-2 medium resulted in the highest development to blastocyst after fertilization *in vitro* and embryo culture (Rose and Bavister, 1992). For mice, MEMα has become the standard for IVM (Figure 2).

The first successful embryo transfer was of rabbit embryos in 1891, resulting in live offspring after transfer (Heape, 1891). Following this, the first successful culture of rabbit embryos occurred in 1912 (Brachet, 1912). The first successful human embryo IVF resulting in a live birth occurred in 1978 (Steptoe and Edwards, 1978). Different media has been deemed necessary for optimal embryo growth, compared to the immature oocyte. The first embryo culture media designed contained salt solutions, pyruvate, lactate and glucose but lacked amino acids. Presently, amino acids are added to the embryo culture media and while the solution is more complex, it is still relatively simple and cost effective to produce. The most widely-used embryo culture media for mouse embryos is KSOM (Lawitts and Biggers, 1993), which supports development from fertilized eggs through blastocysts.

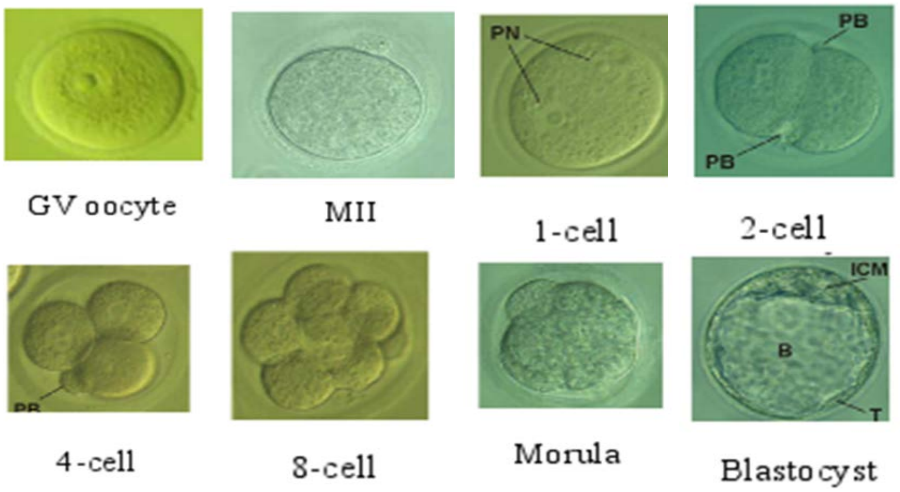

Figure 2. In vitro maturation and embryo culture.

Images of mouse oocyte and preimplantation embryos at various stages of development. The GV oocyte can be identified by its prominent nucleus at its center. MII eggs are recognizable by the first polar body extrusion. 1-cell embryos are flushed from mouse oviducts and cultured for up to 4 days. 2-cell, 4-cell and 8-cell embryos are identified by their cleavage. Morulas have a distinctly compact appearance. Blastocysts have two compartments: the inner cell mass and the blastocoel. PN: pronuclei, PB: polar body, ICM: inner cell mass, T: trophectoderm, B: blastocoele. Image obtained from the Baltz Lab.

1.7 Folate-mediated one carbon metabolism and the methionine cycle

Folate refers to a group of compounds including folic acid and its derivatives. One carbon metabolism (OCM) refers to the physiological pathways producing and utilizing one-carbon groups such as methyl (-CH3), methylene (-CH2-), methenyl (-CH=) and formyl (-CHO). OCM is the integration of folate and methionine metabolism, as well as the transsulfuration pathway, an alternative for homocysteine metabolism (Ikeda et al, 2012) (Figure 3).

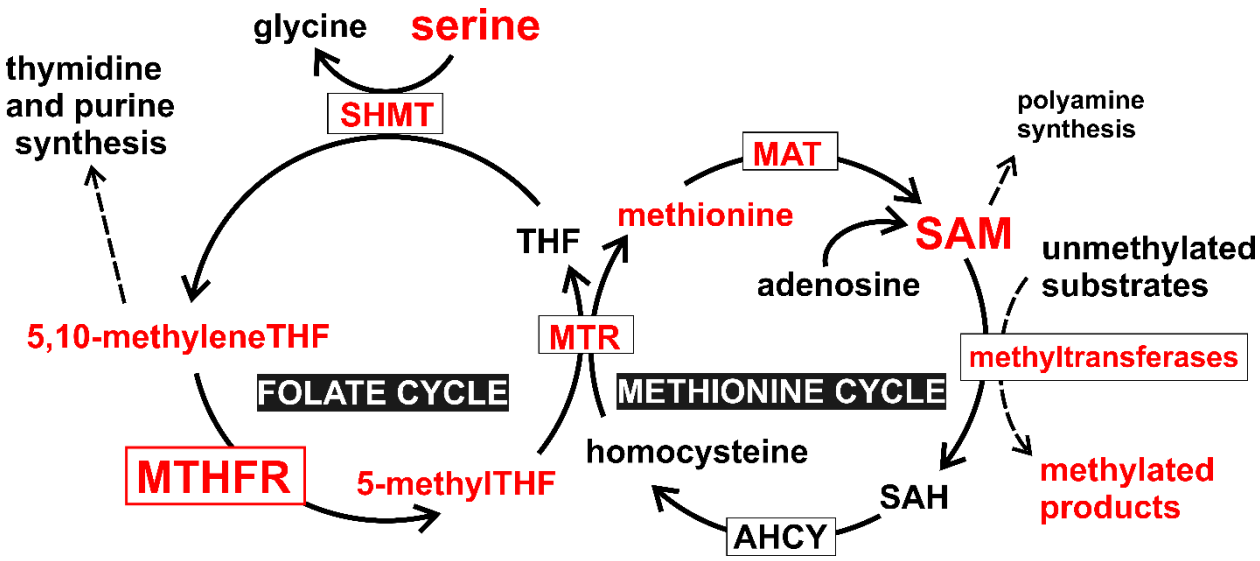

Figure 3. Folate and Methionine Cycles.

OCM depicted showing the connection between the folate and methionine cycles. The pathway of one carbon groups entering the folate cycle begins with serine, as shown in red. MTHFR shown in the red square is used to make 5-methylTHF from 5,10-methyleneTHF. This is the last reaction before methionine synthase (MTR in the diagram) which allows methyl groups to enter the methionine cycle and contribute to the production of SAM and the cellular methyl pool.

OCM occurs in three specific cellular compartments: the cytoplasm, the mitochondria and the nucelus. OCM in the cytoplasm is necessary to synthesize purines, thymidylate and to remethylate homocysteine to methionine. In the mitochondria, OCM is required for synthesis of formylated methionyl-tRNA, catabolism of choline, purines and histidine and interconversion of serine and glycine (Fox and Stover, 2008).

Pteroylmonoglutamic acid (folic acid) is the synthetic form of folate used in nutrional supplements. The natural form of folate is the 5-methyltetrahydrofolate (THF) form with a chain of polyglutamates, therefore animals will usually ingest folate as polyglutamates (Iyer and Tomar, 2009). Polyglutamates are hydrolyzed to monoglutamates and then absorbed into mucosal cells to be converted to 5-methylTHF (Ikeda et al, 2012). The process for folic acid is similar, however it is first reduced to dihydrofolate and then tetrahydrofolate. Demethylation of 5-methylTHF to THF is catalyzed by 5-methyltetrahydrofolate-homocysteine methyltransferase (MTR) with B12-derived methylcobalamin as a cofactor (Ikeda et al, 2012). The methyl group is used to methylate homocysteine which is the link to the methionine cycle. MTR is the rate limiting enzyme in which methyl groups reach their fate of entering the methionine cycle to contribute to the cellular methyl pool or staying within the folate cycle to be recycled.

Serine hydroxymethyl transferase (SHMT) catalyzes the transfer of the one-carbon group from serine to THF in order to produce 5,10-methyleneTHF and glycine while using pyridoxal 5'-phosphate (PLP) as a cofactor (Ikeda et al, 2012). 5,10-methyleneTHF is reduced to 5-methylTHF by MTFHR. As well, 5,10-methyleneTHF is the methyl donor in the reaction producing deoxythymidine monophosphate from deoxyuridine monophosphate for DNA synthesis. 5,10-methyleneTHF is also converted to 10-formyltetrahydrofolate by methylenetetrahydrofolate dehydrogenase for purine synthesis (Ikeda et al, 2012).

Methionine, produced from the transfer of the one-carbon methyl group from 5-methylTHF to homocysteine via MTR, can be adenosylated by methionine adenosyltransferase (MAT) to form SAM (Ikeda et al, 2012). SAM is the universal methyl donor for most methyltransferase enzymes and is responsible for methylating neurotransmitters, phospholipids, histones, RNA and CpG islands in DNA (Ikeda et al, 2012). When this methyl group is donated, SAM becomes S-adenosylhomocysteine (SAH). SAH can be hydrolyzed to homocysteine by the enzyme S-adenosylhomocysteine hydrolase (AHCY). Homocysteine can then be remethylated to methionine by the MTR enzyme or by betaine-homocysteine methyltransferase (BHMT) which uses betaine as the methyl donor (Ikeda et al, 2012).

In the transsulfuration pathway, homcysteine is instead condensed with serine using the enzyme cystathionine B-synthase and PLP as a cofactor to form cystathionine (Ikeda et al, 2012). This can then be converted to cysteine using cystathionase and PLP.

1.8 DNA methylation

DNA methylation is the addition of methyl groups from the universal methyl donor, SAM, to the DNA strand using DNA methyltransferases. This can affect the activation or repression of the gene being methylated. Methylation is important for normal development and contributes to processes like genomic imprinting, X-chromosome inactivation and repression of transposable elements.

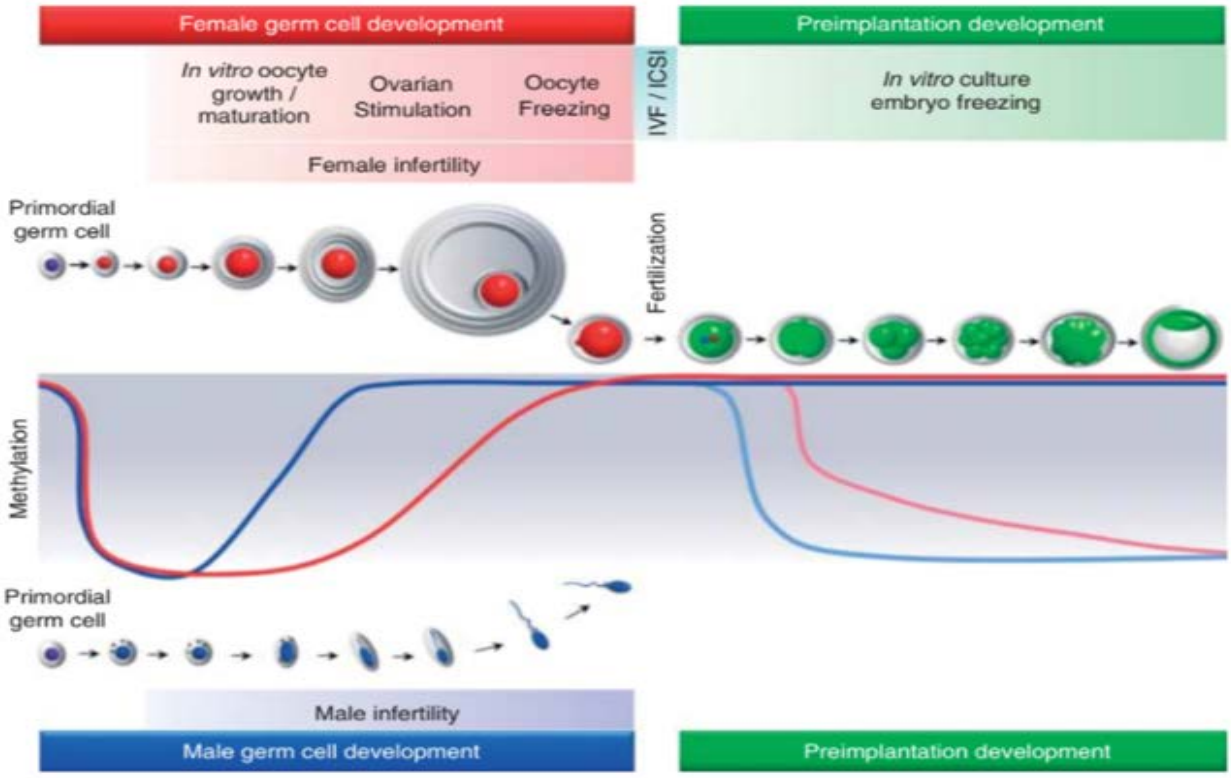

Figure 4. Methylation over the course of development.

The maternal line is seen in red displaying that DNA methylation is erased in primordial germ cells. The paternal line is seen in blue and is re-methylated faster than the female germ cells. After fertilization, the paternal genome is rapidly demethylated while the maternal genome is passively demethylated. This image was obtained with permission from Denomme & Mann 2012.

1.9 Epigenetic reprogramming

The pattern of DNA methylation in the developing embryo is erased and reprogrammed twice in the lifetime. The first erasure occurs in the primordial germ cells, allowing for genome-wide reprogramming and removal of the tissue-specific patterns from the DNA (Denomme & Mann, 2012). This erasure restores the cells to a totipotent state, allowing for cell differentiation (Reik and Walter, 2001). This allows for the gametes to gain their own sex-specific DNA methylation patterns during development (Denomme et al, 2012). After fertilization, the maternal genes are passively demethylated while the paternal genes are actively demethylated (Monk et al, 1987). Re-methylation takes place by the time the epiblast is formed in the ICM (Figure 4). During the second erasure, differentially methylated regions (DMRs) will remain untouched and these are called imprinted genes which will be discussed in the next section (Smallwood et al, 2011).

1.10 Imprinted genes

Genomic imprinting leads to sex-specific monoallelic expression of genes. The allele from only one parent will be normally expressed, and the other will be silenced by methylation-mediated imprinting, making them functionally non-equivalent. This imprinting occurs during gametogenesis, so the zygote will have gamete-specific imprinted genes inherited from each parent. Each are responsible for different features of development and will be highly expressed at prenatal stages. Approximately 150 imprinted genes have been identified in mice and 100 in humans (SanMiguel and Bartolomei, 2018). The maternal and paternal imprinted genes work together to allow for balanced fetal growth and placental development.

Imprinting errors can be catastrophic when it comes to the developing fetus. An example of an imprinting error disorder is Silver-Russel syndrome, caused by hypomethylation (Bartolomei and Ferguson-Smith, 2011). This syndrome is characterized by intrauterine growth restriction, poor growth after birth, body asymmetry and feeding difficulties. Other imprinting disorders include Angelman syndrome, a neurological disorder, and Beckwith-Wiedemann syndrome, an overgrowth disorder.

1.11 One-carbon metabolites in oocytes and preimplantation embryos

As OCM is a tightly regulated process with several pathways involved, any perturbations to the enzymes or substrates during oocyte and preimplantation embryo development can result in detrimental effects on viability. Mammalian oocytes and preimplantation embryos express almost all of the OCM enzymes needed to metabolize OCM nutrients as previously shown at either the transcript or protein level (An et al, 2020; Clare et al, 2021; Ikeda et al, 2012; Ikeda et al. 2010; Kwong et al, 2010).

An example of the effects manipulation can have was provided by Menezo et al 1989, who inhibited methionine metabolism with ethionine and found suppression of blastocyst development, but when reproduced by another lab, saw no effect on morula compaction (Ikeda et al. 2012). Partial restoration of blastocyst development was found with supplementation of SAM in the ethionine-culture (Ikeda et al, 2012). On the other hand, when methionine is added to the media of IVF bovine zygotes, the yield of blastocysts will increase in a dose dependent manner between 7-21 μM (Bonilla et al, 2010).

Another example is the addition of methotrexate (MTX), an antimetabolite of folate, to the culture media at the 1-cell, 2-cell and 8-cell stages significantly inhibited cell division

(O'Neill, 1998). For 1-cells, the progression to 2-cells was reduced to 17%, while the rate to blastocyst formation was 0%. This inhibition could also be reversed with the addition of thymidine, proving the reduction was due to the lack of DNA synthesis.

Folates are transported into the preimplantation embryo using the folate receptor FOLR1 and into the COC through the Reduced Folate Carrier-1 (RFC1) (Kooistra et al, 2013). During murine oocyte growth, there is a distinct peak of folate transport when the oocytes are almost fully grown (Meredith et al, 2016). This is important as early preimplantation embryos could support their own development without supplemental folate if the oocyte accumulates enough folate during growth.

Hyperhomocysteinemia, a condition caused by elevated levels of homocysteine, can occur from folate deficiencies or a common genetic mutation of MTHFR (C677T) that reduces its enzyme activity. Addition of homocysteine to culture media will also suppress blastocyst development in the case of murine and bovine preimplantation embryos (Menezo et al, 1989, Ikeda et al, 2010). Homocysteine produces reactive oxygen species which can exert cytotoxic effects that could be contributing to the developmental suppression, as oxidative stress is known to be detrimental to embryos (Welch and Loscalzo, 2010, Guerin et al, 2001).

BHMT is another enzyme that has been manipulated and shown to affect blastocyst development. Betaine (N, N, N-trimethylglycine) is an organic osmolyte that has osmoprotective properties in the mouse embryo (Biggers et al, 1993). As mentioned previously, in OCM, betaine is catabolized to dimethylglycine and donates a methyl group to homocysteine by the enzyme BHMT. Lee et al proved that betaine is retained in the embryo and metabolized by BHMT to contribute to the cellular methyl pool of SAM in the blastocyst (Lee et al, 2012). Zhang et al targeted BHMT knockdown with antisense morpholinos and inhibited the folate cycle with

MTX, with purine and thymidylate added to rescue DNA and purine synthesis. Both of these treatments had affected blastocyst development individually, however when used simultaneously, blastocyst development was significantly decreased, SAM levels were significantly lower and 5-meC staining showed significantly lower levels as well (Zhang et al, 2015). These results suggest that neither BHMT nor the folate cycle (SAM) are absolutely necessary for blastocyst development. Instead, they are working with a compensatory mechanism to ensure development will occur as often as possible.

In bovine embryos, the knockdown of MTHFR expression by siRNA-mediated interference from the 8-16 cell stage resulted in decreased development to the blastocyst stage and decreased cell numbers in both trophectoderm and inner cell mass (Ishitani et al, 2020).

Restriction of vitamin B12, folate and methionine from the diet of female sheep from 8 weeks before conception to 6 days after conception showed elevated homocysteine levels in plasma, ovarian follicular fluid, and granulosa cell lysates (Sinclair et al, 2007). The ratio of SAM to SAH was significantly reduced in granulosa cells. The same study shows that male sheep at 22 months of age in the treatment group were proportionately fatter compared to control males and exhibited signs of insulin resistance. Blood pressure was also increased in males whose mothers were exposed before their conception and during periconception, but not in females. Immune function was also altered. The status of CpG islands were also investigated and the methylation status of treated animals varied greatly from that of untreated animals. These results are important in drawing attention to the timeline at which these effects occur. Folate supplementation is suggested to expecting mothers around the time of conception, whereas it should be supplemented during the periconceptional period to ensure high enough folate levels for the sought-after beneficial effects.

Experiments investigating the lack of methyl donors in oocyte culture show similar effects in that the results show decreased antral follicle development, a decrease in polar body extrusion rate and morphologically abnormal GVBD-arrested oocytes (Anckaert et al, 2010). However, DNA methylation of regulatory sequences of several imprinted genes were minimally affected by the lack of methyl donors in the culture media. Of the four genes investigated, *Mest*, was the only one to show a significant reduction in DNA methylation (Anckaert, 2010). This is thought to be due to the fact that *Mest* acquires methylation later than most imprinted genes, at late-stage oocyte growth. In culture, the methyl groups could be consumed by the increasing follicular growth resulting in low methionine levels by the time *Mest* requires methylation.

1.12 Methylenetetrahydrofolate reductase (MTHFR)

MTHFR catalyzes the reaction of 5,10-methylenetetrahydrofolate to 5-methyltetrahydrofolate in the folate cycle (Fox and Stover, 2008). This reaction is important as it is nearly irreversible *in vivo* and ensures that one-carbon units enter the methionine cycle via the methionine synthase reaction to ultimately contribute to the cellular methyl pool (Appling, 1991). The methionine produced is used mainly to form SAM, which is the universal methyl donor in cells (Ikeda et al, 2012).

The sole function of 5-methylTHF in mammals is to remethylate homocysteine and thus produce methionine (Yamada et al, 2005). Methionine is then complexed with adenosine to produce SAM. Therefore, MTHFR is the enzyme that controls the transfer of one carbon units from the folate cycle into the methionine cycle.

1.12.1 Isoforms

MTHFR has been shown to have two major isoforms that are derived from alternative splicing of exon 1, MTHFR A and MTHFR B (Tran et al, 2002). These encode for proteins which have predicted molecular weights of 77 kDa and 70 kDa, respectively (Tran et al, 2002). Two major promoters in the *Mthfr* gene have been identified, an upstream and downstream promoter (Pickell et al, 2005). When transcription begins at the upstream promoter and translation begins at the downstream AUG, the 77 kDa isoform A protein is made. Alternately, transcription from the downstream promoter and translation from the upstream AUG produces the 70 kDa isoform B protein (Tran et al, 2002). *Mthfr* has shown temporal- and tissue-specific regulation (Pickell et al, 2011). For example, when 10.5-dpc embryo and placenta tissues were examined for promoter activity compared to neonates and adults, activity was found in the 10.5-dpc embryo and placenta and in the brain and epididymis of neonates while in the adults, there was more expression in the brain and testis while it was no longer present in the epididymis (Pickell et al, 2011). MTHFR A showed more expression in the brain, germ cells and Sertoli cells while MTHFR B showed more expression in endothelial cells lining the aorta and other embryonic blood vessels (Pickell et al, 2011).

1.12.2 Phosphorylation

MTHFR activity has been shown to be mediated by phosphorylation and allosteric inhibition (Yamada et al, 2005). Thr34 has been identified as the priming site for phosphorylation, which leads to subsequent phosphorylation of a series of serines in the N-terminal catalytic domain (Yamada et al, 2005). The phosphorylated protein is less active than the unphosphorylated one (Yamada et al, 2005). When the SAM/SAH ratio is low, MTHFR phosphorylation modification is decreased so the enzyme becomes more active and less susceptible to inhibition by SAM (Yamada et al, 2005).

1.12.3 Potential Kinases for Phosphorylation of MTHFR

As mentioned previously, MTHFR has been known to be regulated by multisite phosphorylation (Yamada et al, 2005). The kinases responsible for this phosphorylation have been investigated recently and some potential candidates in MDA-MB-468 cells have been identified. DYRK1A/2 and GSK3A/B have been proven to be able to contribute to the phosphorylation of MTHFR (Zheng et al, 2019). The proposed scheme of phosphorylation begins with the priming site, T34, phosphorylated by DYRKs, which leads to the phosphorylation of S30 and S26 by GSK3. Next, S33 is phosphorylated by CK1, triggering the phosphorylation of S29, S25 and S21 by GSK3. Lastly, S23, S20 and S18 are phosphorylated by CK2.

The study above used the DYRK specific inhibitor, harmine, on wild-type and S30A-MTHFR overexpressing cells to confirm the role of DYRK in the phosphorylation of MTHFR. The results show that the mutated cells were rapidly dephosphorylated, suggesting DYRK involvement. As well, they used the GSK3 inhibitor, CHIR99021, on MTHFR-overexpressing cells which gave similar results (Zheng et al, 2019). These results were obtained with exogenous MTHFR expressed in cell lines, and whether these kinases operate for physiological regulation of MTHFR phosphorylation in most cells is not known.

1.12.4 Polymorphisms and Human Relevance

MTHFR polymorphisms are a potential risk factor for hyperhomocysteinemia which can lead to several comorbidities. Two common polymorphisms of human MTHFR have been identified, 677C>T and 1298A>C. The 677C>T mutation leads to the substitution of Ala-222 by valine and the 1298A>C mutation leads to the replacement of Glu-429 by alanine.

The first identification of reduced MTHFR activity due to a thermolabile enzyme was associated with coronary artery disease (Kang et al, 1993). The C677T mutation moderately decreases activity of the enzyme by making it less thermostable (Yamada et al, 2001). It is also associated with decreased preimplantation embryo quality and increased aneuploidy (Enciso et al, 2016). It is the most common genetic cause of mild elevation of homocysteine in plasma (Schwahn and Rozen, 2001) and also leads to reduced folate concentrations in the plasma (Jacques et al, 1996). Similarly, the A1298C mutation leads to a reduction in MTHFR activity and has been associated with an increased risk of neural tube defects (van der Put et al, 1998; Weisberg et al, 1998).

Mild elevation of blood homocysteine is an established risk factor for cardiovascular disease (Boushey et al, 1995). Forty percent of patients with coronary artery disease were found to have high plasma homocysteine compared to only 15% of healthy individuals (Welch et al, 1997). The mechanism by which the elevated levels of homocysteine effect the risk of cardiovascular disease is still unknown. Treatment to lower homocysteine levels did not reduce the risk of cardiovascular associated complications (Bonaa et al, 2006).

The C677T mutation has been associated with several other diseases but most have only been identified in specific subpopulations. Baiqiu et al identified a relationship between the mutation and psoriasis in the Chinese population, while Vasku et al saw the same pattern in the Caucasian population (Baiqiu et al, 2000; Vasku et al, 2009). Other studies report neurological and psychiatric diseases stemming from hyperhomocysteinemia (Bottiglieri, 1996). The destabilization of the DNA could lead to potentially malignant transformations, with increasing depletion of thymidine and misincorporation of uracil (McKinnon and Caldecott, 2007; Choi and Mason, 2002).

Importantly, for this research, the polymorphism has been associated with infertility and recurrent pregnancy loss (Wei et al, 2012; Wu et al, 2012; Cao et al, 2013). If a polymorphism is associated with the loss of the phosphorylation priming site, this could have downstream effects on the activity of MTHFR and the ability for the cellular methyl pool to have adequate methyl supplies. Rima Rozen's group was able to rescue the lack of methylation in mice with dietary supplementation of methionine. This further emphasizes the importance of folate supplementation before and during pregnancy, along with pre-screening of potential risk factors.

1.13 Summary

Despite the important role MTHFR plays between the folate and methionine cycles, much is unknown about its expression and regulation in oocytes and preimplantation embryos. MTHFR expression has not been investigated in mouse oocytes or embryos and its regulation has not been identified in any species. A study of the metabolome of maturing mouse oocytes has been reported and SAM increased approximately 2.5-fold within hours of the GV oocyte's release from meiotic arrest and then decreased to baseline again in mature MII eggs (Li et al, 2020). Such a decrease in SAM should allosterically activate MTHFR to maintain SAM levels (Yamada et al, 2005) which apparently does not occur as SAM levels remain low in MII eggs. A possibility of this could be that MTHFR activity is downregulated as oocytes mature and this could be due to the phosphorylation of the enzyme.

I used my project to elucidate the mRNA and protein patterns of MTHFR in mice. I also investigated the phosphorylation pattern of MTHFR over the course of development, how this phosphorylation was being regulated and if it affected the activity of the enzyme.

2. Objectives and Specific Aims

Objective

The objective of this project was to elucidate when MTHFR is present throughout the course of oocyte and preimplantation embryo development and in what forms, phosphorylated (less active) or dephosphorylated (more active). As MTHFR is a key enzyme in the folate cycle, it contributes to the accumulation of the universal methyl donor SAM and therefore the cellular methyl pool. Knowing when this enzyme is present, in what form and how active it is will assist in the growing understanding of the tightly regulated process of DNA methylation and what implications this could have on a growing oocyte or embryo.

2.1 Specific Aims and Hypotheses

Specific Aim 1: To characterize the pattern of MTHFR protein expression and the presence of *Mthfr* mRNA during oocyte maturation and preimplantation embryo development.

It is known that *Mthfr* mRNA, along with other enzymes in the one-carbon metabolic pathway, are present in bovine embryos (Ikeda et al. 2010). The pattern of MTHFR protein in oocytes and preimplantation embryos of any species has yet to be reported.

I hypothesized that both Mthfr RNA and MTHFR *protein would be found at all stages of development from the GV oocyte to the blastocyst.*

2.2 Specific Aim 2: To determine the pattern of phosphorylation of MTHFR protein during oocyte maturation and preimplantation embryo development and identify the potential kinases responsible for this phosphorylation.

Previous studies have reported that MTHFR can be phosphorylated and that the phosphorylated protein is less active than the unphosphorylated version (Yamada et al, 2005). Two kinases could be responsible for the phosphorylation of MTHFR, which are DYRKs and GSK3A/B (Zheng et al, 2019). Inhibitors for these kinases, harmine and CHIR99021 respectively, were used on various cell lines and produced data which suggest that DYRKs are responsible for the phosphorylation of the priming site T34, while GSK3 is responsible for the subsequent phosphorylations (Zheng et al, 2019).

Therefore, I hypothesized that some, but not all stages of development would have phosphate modifications on the MTHFR *protein and that harmine and CHIR99021 will inhibit the kinase activity of DYRKs and GSK3 in GV oocytes and not allow for oocyte MTHFR to be phosphorylated during overnight culture to MII eggs.*

2.3 Specific Aim 3: Develop an assay based on LC-MS/MS to measure MTHFR activity within oocytes.

Phosphorylated MTHFR has been shown to be less active than the unphosphorylated form and more readily allosterically inhibited by SAM (Yamada et al, 2005). MII eggs should show less activity than GV oocytes because MTHFR in MII eggs is more phosphorylated than in GV oocytes. To address this aim, I was intending to measure MTHFR activity using a published assay which would run the MTHFR reaction of 5,10-methylenetetrahydrofolate to 5-methyltetrahydrofolate in reverse removing the 5-methyl group and producing a radiolabelled product that can be isolated and detected by scintillation counting (Christensen et al, 1997). This was dependent on obtaining radioactively-labelled 5-methyltetrahydrofolate and the ability to miniaturize the assay to be effective on oocyte samples. Unfortunately, the radioactively-labelled product has been discontinued and is no longer commercially available from any source so we

attempted to develop a different activity assay. To pursue this assay, the product has to be synthesized, and then assessed using LC-MS/MS to determine the limit of detection of the product of interest. Next, if the limit of detection is sufficiently low, we would use liver samples to validate the MTHFR activity assay and its specificity using *Mthfr* wildtype and knockout samples. Lastly, we would use the optimized assay to determine whether there was a difference in activity between GV oocytes and MII eggs.

Therefore, I hypothesize that this LC-MS/MS assay can be developed and that MII eggs will have a lower activity of MTHFR than GV oocytes.

3. Materials and Methods

3.1 Chemicals and Pharmacological Agents

All chemicals and compounds used are listed in Table 1 with their sources. All pharmacological agents and their sources are listed in Table 2. All antibodies are listed in Table 3.

Table 1. Summary of chemicals and compounds used.

Name of Chemical or Compound	Source	Catalogue Number
2-mercaptoethanol	Sigma (St. Louis, MO, USA)	M-3148
2-Propanol	Sigma (St. Louis, MO, USA)	I9516
2X Laemmli Sample Buffer	Bio-Rad Laboratories (Mississauga, ON, Canada)	1610737
30% Acrylamide/Bis Solution 37.5:1	Bio-Rad Laboratories (Mississauga, ON, Canada)	1610158
4X Laemmli Sample Buffer	Bio-Rad Laboratories (Mississauga, ON, Canada)	161-0747
5,5-Dimethyl-1,3-cyclohexanedione	Sigma (St. Louis, MO, USA)	38490
Acetic acid	Sigma (St. Louis, MO, USA)	A6283
Agarose	Sigma (St. Louis, MO, USA)	A9539
Amersham ECL Prime Western Blotting Detection Reagent	GE Healthcare (Chicago, IL, USA)	RPN2236
Ammonium persulfate	Sigma (St. Louis, MO, USA)	A3678
Aprotinin	Roche Diagnostics (Mannheim, Germany)	10236624001
BSA Standard (1.38mg/mL)	Bio-Rad Laboratories (Mississauga, ON, Canada)	500-0007
Calcium chloride dihydrate	Sigma (St. Louis, MO, USA)	C7902

Clarity Western ECL Substrate	Bio-Rad Laboratories (Mississauga, ON, Canada)	170-5060
D-(+)-Glucose	Sigma (St. Louis, MO, USA)	G6152
DC Protein Assay Reagent A	Bio-Rad Laboratories (Mississauga, ON, Canada)	500-0113
DC Protein Assay Reagent B	Bio-Rad Laboratories (Mississauga, ON, Canada)	500-0114
DC Protein Assay Reagent S	Bio-Rad Laboratories (Mississauga, ON, Canada)	500-0115
Dimethyl Sulfoxide	EMD Millipore (Burlington, MA, USA)	317275
Ethidium bromide	Sigma (St. Louis, MO, USA)	E8751
Ethylenediaminetetraacetic acid disodium salt dihydrate	Sigma (St. Louis, MO, USA)	E5134
Formaldehyde Solution	Sigma (St. Louis, MO, USA)	15512
Glycine	Sigma (St. Louis, MO, USA)	G8898
HEPES	Sigma (St. Louis, MO, USA)	H6147
Hyaluronidase	VWR International (Radnor, PA, USA)	37326-33-3
Hydrochloric Acid, 0.120 Normal	Ricca Chemical Company (Arlington, TX, USA)	3611-16
Instant Skim Milk Powder	Compliments (Canada)	
Lambda Protein Phosphatase	New England BioLabs (Ipswich, MA, USA)	PO7535
Leupeptin hemisulfate salt	Sigma (St. Louis, MO, USA)	L2884
Magnesium sulfate heptahydrate	Sigma (St. Louis, MO, USA)	M2773
MassRuler DNA Ladder Mix	ThermoFisher scientific (Rockford, IL, USA)	SM0403
MassRuler DNA Loading Dye (6X)	ThermoFisher scientific (Rockford, IL, USA)	R0621

MEM Alpha (1X)	Life Technologies/Gibco (Burlington, ON, Canada)	12561-056
Methanol	ThermoFisher scientific (Rockford, IL, USA)	A412P-4
Methanol for HPLC >99.9%	Sigma (St. Louis, MO, USA)	34860
Mineral Oil	Sigma (St. Louis, MO, USA)	M8410-1
Penicillin G potassium salt	Sigma (St. Louis, MO, USA)	P7794
Phenylmethylsulfonyl fluoride	Roche Diagnostics (Mannheim, Germany)	10837091001
Pierce RIPA Buffer	ThermoFisher scientific (Rockford, IL, USA)	89900
Poly(vinyl alcohol)	Sigma (St. Louis, MO, USA)	P8136
Potassium chloride	Sigma (St. Louis, MO, USA)	P5405
Potassium buffered saline (10X)	Life Technologies/Gibco (Burlington, ON, Canada)	70011-044
Potassium phosphate monobasic	Sigma (St. Louis, MO, USA)	P5655
Precision Plus Protein Kaleidoscope	Bio-Rad Laboratories (Mississauga, ON, Canada)	161-0375
RNeasy Micro Kit	Qiagen (Hilden, Germany)	74004
Sodium bicarbonate	Sigma (St. Louis, MO, USA)	S5761
Sodium chloride	Sigma (St. Louis, MO, USA)	S9888
Sodium DL-lactate solution	Sigma (St. Louis, MO, USA)	L7900
Sodium dodecyl sulfate	Sigma (St. Louis, MO, USA)	L3771
Sodium hydroxide	Sigma (St. Louis, MO, USA)	S8045
Sodium pyruvate	Sigma (St. Louis, MO, USA)	P4562
Streptomycin sulfate salt	Sigma (St. Louis, MO, USA)	S1277
Strontium chloride	Sigma (St. Louis, MO, USA)	439665
Superscript IV	invitrogen (Carlsbad, CA, USA)	18091050

Supersep Phos-tag gels	FUJIFILM Wako Pure Chemical Corporation (Osaka, Japan)	195-16391
Taq DNA Polymerase	invitrogen (Carlsbad, CA, USA)	10342-053
TEMED	Bio-Rad Laboratories (Mississauga, ON, Canada)	161-0800
Tris(hydroxymethyl)aminomethane	Sigma (St. Louis, MO, USA)	252859
Tween 20	Sigma (St. Louis, MO, USA)	P9416

Table 2. Summary of pharmacological agents used.

Pharmacological agent	**Source**	**Catalogue Number**	**Action**
CHIR99021	Sigma (St. Louis, MO, USA)	SML1046	GSK3A/B inhibitor.
Harmine	Sigma (St. Louis, MO, USA)	286044	DYRK inhibitor.
Human Chorionic Gonadotropin	Prospec (Sturgeon County, AB, Canada)	HOR-250	Stimulation of ovulation in mice (hormone).
Pregnant Mare Serum Gonadotropin	Prospec (Sturgeon County, AB, Canada)	HOR-272	Stimulation of ovarian follicle growth in mice (hormone).

Table 3. Summary of all antibodies used.

Antibody	**Source**	**Catalogue Number**
Anti-GADPH primary antibody	Santa Cruz (Dallas, TX, USA	sc-25778
Anti-MTHFR primary antibody	Abcam (Cambridge, MA, USA)	ab203786

Anti-rabbit IgG, HRP-linked antibody	Cell Signaling Technology (Danvers, MA, USA)	7074S
Anti-vinculin primary antibody	Abcam (Cambridge, MA, USA)	ab129002

3.2 Animals

All animal protocols for handling and manipulating mice were approved by the Animal Care Committee at the University of Ottawa Faculty of Medicine. Animals were kept in the Animal Care and Veterinary Services (ACVS) Facility and wellness-checked by veterinary technicians. The mice were kept on a 12 hour light-dark cycle and all handling and manipulation were done during their light cycle. All animals had unlimited access to Teklad Global 18% protein rodent diet (Envigo, Indianapolis, IN) and water.

3.2.1 Experimental Mice

Female CD1 mice were purchased from Charles River Canada, QC and used at the ages of 5-8 weeks old for experimentation. Oocytes were collected from the adult females upon euthanization. Preimplantation embryos were produced by mating the adult CD1 females to BDF1 males overnight and separating them in the morning. Mice were sacrificed using cervical dislocation.

3.2.2 Mthfr Knockout Mouse Line

Mthfr knockout mice were originally produced from Rima Rozen's Lab at McGill University. A neogene was transfected to interrupt exon 3 of the *Mthfr* gene in embryonic stem cells. The positive clones were injected into blastocysts from BALB/c female mice and transferred into BDF1 pseudopregnant mice to produce chimeric offspring. Breeding of the

chimeric mice with BALB/cAnNCrBr mice (Charles River Canada, QC) generated heterozygotes which were bred to each other to produce homozygous *Mthfr* knockout mice (Chen et al., 2001).

Further manipulation of the mutant mouse line led to the null allele being backcrossed to a C57/Bl6 strain of mice for more than 13 generations by Jacquetta Trasler's lab at McGill University (Lawrence et al, 2010). Heterozygous matings allowed for production of wildtype, heterozygous and knockout offspring. Our lab obtained the *Mthfr* mutant mice on the C57/Bl6 background from Trasler's group and these were used for validating the MTHFR antibody. The mutant mice were maintained under the same conditions as the CD1 mice.

3.2.3 Superovulation

A superovulation protocol was used to maximize the number of oocytes or preimplantation embryos produced by each mouse (Dawson and Baltz, 1997). 5-8 week old, female CD1 mice (Charles River, QC) were injected intraperitoneally (ip) with 5IU pregnant mare serum gonadotropin (PMSG; Prospec). Approximately 44 hours post-PMSG injection, female mice were euthanized for GV oocyte collection.

For the collection of MII eggs, mice that had been injected with PMSG received a second ip injection 48 hours later with 5IU human chorionic gonadotropin (hCG; Prospec), to mimic the effect of LH and the induction of ovulation. MII eggs were ready for collection approximately 15 hours post-hCG injection.

For preimplantation embryos, mice that had been injected with both PMSG and hCG were caged overnight with a BDF1 male mouse (Charles River, QC) to mate. Times for collection of each stage of embryo can be found in Table 4.

Table 4. Collection times for each stage of development.

Day	**-2**	**-1**	**0**	**1**	**2**	**3**	**4**
AM			GV oocytes 11am-1pm (44-46 hr post-PMSG)	MII eggs 6-8am (14-16 hr post-hCG)	2 cell 9-11am (42-44 hr post-hCG)		Blastocyst early 10-11am (91-92 hr post-hCG)
PM	PMSG Injection 4pm		hCG Injection 3pm	1 cell 12-3pm (21-24 hr post-hCG)		Morula 7pm (76 hr post-hCG)	Blastocyst fully expanded 12-1pm (93-94 hr post-hCG)

3.3 Media

Four different media were used depending on what stage of oocyte or embryo was being collected or cultured and what experiment was being performed.

3.3.1 Collection Media

Potassium-supplemented flushing-holding medium (KFHM) was used for the handling and collection of oocytes and preimplantation embryos. This medium is made up of NaCl (95 mM),

KCl (2.5 mM), KH_2PO_4 (0.35 mM), $MgSO_4 \cdot 7H_2O$ (0.2 mM), Na lactate (10 mM), Glucose (0.2 mM), Na pyruvate (0.2 mM), $NaHCO_3$ (4 mM), Hepes (21 mM), $CaCl_2 \cdot 2H_2O$ (1.7 mM), EDTA (tetra Na) (0.01 mM), K penicillin G (0.16 mM), Streptomycin SO_4 (0.03 mM). 1 mg/mL of polyvinyl alcohol (PVA) was added. The medium was used at an osmolarity of 240 mOsM and was adjusted to a pH of 7.4 using sodium hydroxide (Lawitts and Biggers, 1993). All components came from Sigma and were cell culture grade or embryo tested (St. Louis, MO, USA).

This medium was modified slightly for the collection of any samples prepared to run in a Phos-tag gel. The KH_2PO_4 was removed to eliminate any interference with the phosphate groups being detected.

3.3.2 GV Oocyte Culture Medium

GV oocytes were cultured in MEMα (Life Technologies) with the addition of 1 mg/mL PVA.

3.3.3 Embryo Culture Medium

Preimplantation embryos were cultured in potassium-supplemented simplex optimized medium (KSOM) without glutamine and 1 mg/mL PVA was used in place of bovine serum albumin (Lawitts and Biggers, 1993). This medium contains NaCl (95 mM), KCl (2.5 mM), KH_2PO_4 (0.35 mM), $MgSO_4 \cdot 7H_2O$ (0.2 mM), Na lactate (10 mM), Glucose (0.2 mM), Na pyruvate (0.2 mM), $NaHCO_3$ (25 mM), $CaCl_2 \cdot 2H_2O$ (1.7 mM), EDTA (tetra Na) (0.01 mM), K penicillin G (0.16 mM), Streptomycin SO_4 (0.03 mM). KSOM was used at an osmolarity of 250 mOsM and all components came from Sigma and were cell culture grade or embryo tested (St. Louis, MO, USA).

3.3.4 Egg activation Medium

Calcium-free KSOM was used for the activation medium. This was the standard embryo culture KSOM, but omitting $CaCl \cdot 2H_2O$. 10 mM strontium chloride (Sigma) was added to the calcium-free KSOM to make Sr-KSOM for MII egg activation.

3.4 Collection

3.4.1 GV Collection

The ovaries from superovulated mice were dissected and placed in a drop of KFHM approximately 44 hours post-PMSG injection. Ovaries were mechanically minced with a razor blade in their drop and then submerged in a dish of KFHM where COCs were retrieved and isolated into a separate KFHM drop. GV oocytes were denuded of their cumulus cells by repeated pipetting using a mouth-operated narrow flame-pulled Pasteur pipette and washed through 3 drops of KFHM to remove any debris.

3.4.2 MII Egg Collection

The oviducts from superovulated mice were dissected and placed in a drop of KFHM. Each oviduct was then separated into its own drop of KFHM containing 300 μg/mL of hyaluronidase (VWR). Oviducts were flushed using a blunt-tipped syringe of KFHM+hyaluronidase in the infundibulum, forcing any MII eggs into the drop to have the hyaluronic acid digested. The eggs were in the enzyme for 1-2 minutes and then washed through 3 drops of KFHM to remove any debris or residual hyaluronidase using a mouth operated flame-pulled Pasteur pipette.

3.4.3 Preimplantation Embryo Collection

Embryos at the 1-cell stage were collected from superovulated and mated mice the same way as MII eggs. Fertilization was confirmed by the observation of two pronuclei.

Embryos at the 2-cell stage were collected from superovulated and mated mice by flushing KFHM using a blunt-tipped syringe inserted into the infundibulum of dissected oviducts. These embryos were washed through 3 drops of KFHM using a mouth operated flame-pulled Pasteur pipette.

Morulas and blastocysts were collected using the same protocol as 2 cell embryos, however a small piece of the uterus was included in the dissection to collect morulas and the entire uterus was dissected to collect blastocysts.

3.5 Culture

3.5.1 Oocyte Culture

Fully grown GV oocytes were cultured in 50 µL drops of MEMα (Life Technologies) under oil in pools of approximately 15. Three 50 µL drops were pipetted into a 35 mm dish and covered in KSOM-washed mineral oil. These dishes were placed in the incubator for approximately two hours with 5% CO_2 in air at 37°C and 100% humidity to equilibrate. GV oocytes were washed through the first two drops and left in the third and final drop for culture. Culture duration was dependent on each experiment.

3.5.2 Preimplantation Embryo Culture

Preimplantation embryo culture was performed using the same protocol as oocyte culture, with the use of KSOM instead of MEMα for the culture media.

3.5.3 MII Egg Activation

MII eggs were collected as per the regular protocol. After washing through KFHM, the eggs were transferred into pre-equilibrated dishes of Sr-KSOM and cultured for 2 hours in 5% CO_2 at 37°C in 100% humidity. After 2 hours, the eggs were transferred into pre-equilibrated KSOM dishes and left to culture for as long as experimentally necessary. Activation was confirmed by the presence of 2 pronuclei, 2 polar bodies and a slightly granular, darker cytoplasm.

3.6 Inhibition of Kinase Activity

GV oocytes were collected as per the regular protocol. MEMα (Life Technologies) was used as the culture media with 1 μM or 10 μM of either DMSO (Millipore) as a vehicle control, 1 μM or 10 μM of the DYRK inhibitor harmine (Sigma) or 1 μM or 10 μM of the GSK3A/B inhibitor CHIR99021 (Sigma) added. Oocytes were washed through 3 drops of MEMα plus inhibitor or DMSO before being placed in their final drop. 4-well plates were used for a 24 hour culture in 5% CO_2 at 37°C in 100% humidity.

3.7 Molecular Biology Techniques

3.7.1 Polymerase Chain Reaction

3.7.1.1 DNA extraction and Genotyping PCR

All genotyping was performed by the lab technician, Taylor McClatchie. Ear-notch samples were collected from mice at weaning and used for genomic DNA. 200 µL of 50 mM NaOH was added to the sample before incubation in a thermocycler at 95°C for 30 minutes. 17 µL of 1 mM Tris was added to the samples which were then vortexed. 1.5 µL of total DNA from the ear-notch was used per PCR reaction. Primers to detect a wildtype MTHFR or knockout band used were: 5'-GACTAGCTGGCTATCCTCTCATCC-3', 5'-GAAGCAGAGGGAAGGAGGCTTCAG-3' and 5'-AGCCTGAAGAACGAGATCAGCAGC-3'.

3.7.1.2 RNA extraction

RNA extraction was completed using the RNeasy Micro Kit (Qiagen Cat. No. 74004). Liver or testis were used as the control tissue. Fresh samples were dissected from C57/Bl6 mice and prepared using the instructions provided in the kit.

For oocyte samples, the same protocol was followed, however, 20 ng of carrier t-RNA was added to the sample of 50 oocytes before extraction. This eluted RNA was then used for the reverse transcription reaction.

3.7.1.3 Reverse Transcription

Reverse transcription was performed using the Superscript IV Kit (Invitrogen Cat. No.: 18091050). Eluted RNA was prepared using the instructions provided in the kit.

3.7.1.4 Primer Design

Primers were designed for the common region of MTHFR and for regions specific to isoform A and isoform B. The primer sequences for the common region were 5'-TGGCTACAGAGTAACCTGCC-3' for the forward primer and 5'-GATGTGGTAGTTGACCCGCA-3' for the reverse primer. The melting temperatures were 58°C and 62°C, respectively. These primers had 55% GC content and produced a 283 bp amplicon.

The primers made for the isoform A specific region were 5'-TGGGCACTGTTATCCATCCC-3' for the forward primer and 5'-AGTCCATTCTGCGCCTCATC-3' for the reverse primer. The melting temperatures were 63°C for both primers. These primers had 55% GC content and produced an amplicon of 251 bp.

The primers for the isoform B specific region were 5'-GCCACCGATCTGACGCAA-3' for the forward primer and 5'-AACAGCTCCCTCAGCAGTTC-3' for the reverse primer. The melting temperatures were 64°C and 60°C, respectively. These primers had 61% and 55% GC content, respectively and produced an amplicon of 253 bp (Figure 5).

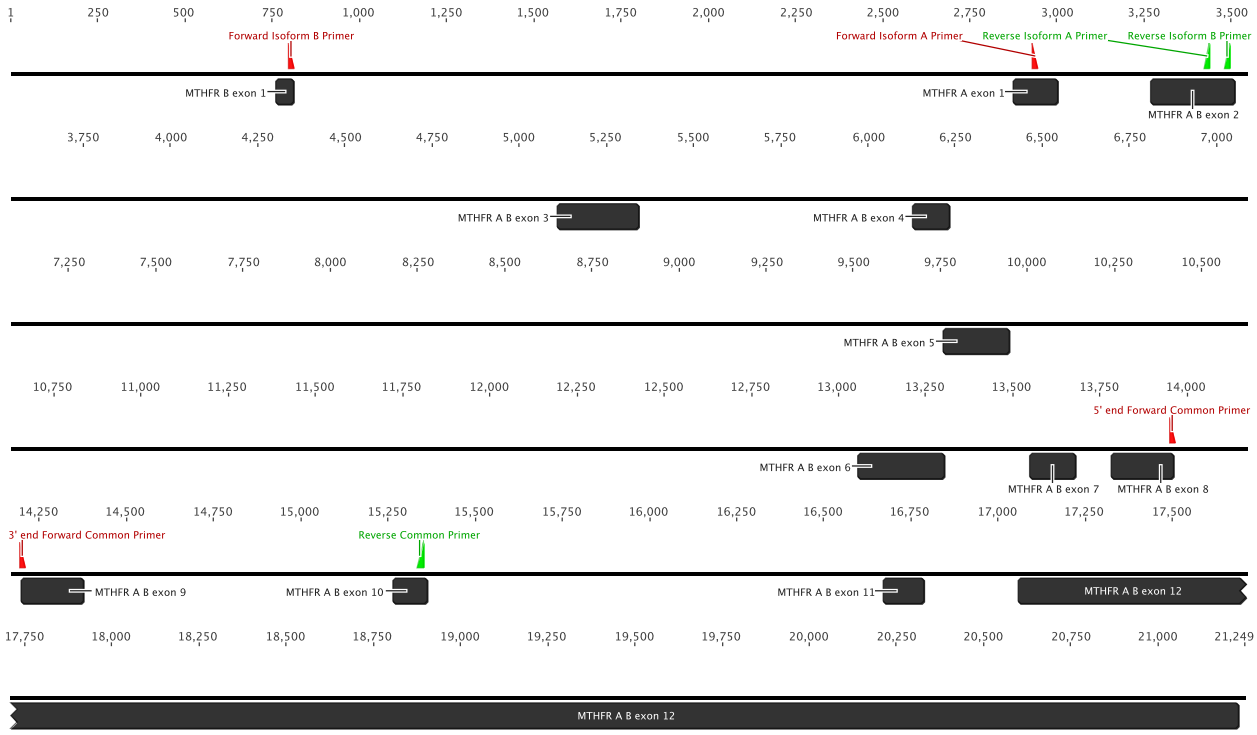

Figure 5. MTHFR DNA annotated with primer pairs for each region.

Primers for the common region of *Mthfr* were placed between exon 8 and exon 10. Isoform specific primers for *Mthfr* A were placed between exon 1 and 2, along with isoform specific primers for *Mthfr* B as this is the only unique region to both isoforms.

3.7.1.5 PCR

cDNA synthesized from the RT reaction was mixed with 10 mM dNTP mix, which was made up of equal parts dCTP, dATP, dTTP and dGTP in water, 10 µM primer solutions, 10X $MgCl_2$ buffer, 50 mM $MgCl_2$ and Taq polymerase (Invitrogen). These reactions were run at various temperatures for a different number of cycles depending on the primer pair as specified, in a Bio-Rad T100 Thermocycler.

3.7.1.6 qRT-PCR

All qRT-PCR experiments were performed by Allison Tscherner, a postdoctoral fellow in the Baltz Lab, as I was not permitted to be trained on the qPCR instrumentation due to Covid-19 restrictions that were in place. She provided this description of the methods used:

"Total cellular RNA was isolated using the Arcturus PicoPure RNA isolation system (Applied Biosystems, Foster City, CA catalog #KIT0204) with on-column DNase digestion using RNase-Free DNase Set (Qiagen, Toronto, Ontario, Canada, catalog #79254), as reproducible detection of infrequent MTHFR variant transcripts could not be achieved when RNA was isolated using the previously mentioned system. RNA was isolated from pools of 34 oocytes. Total RNA was reverse transcribed with Superscript IV Kit (Invitrogen, Carlsbad, CA, catalog #18091050). CDNA was diluted so that an equivalent of 3 oocytes per QPCR reaction were used as a template.

Quantitative reverse-transcription PCR was carried out on a 7500 FAST Real-Time system (Applied Biosystems, Foster City, CA) Reactions were carried out using PowerUp SYBRGreen Master Mix (Applied Biosystems, Foster City, CA catalog #A25742) with MicroAmp Fast optical 96-well reaction plates and Adhesive Film (Applied Biosystems, Foster City, CA catalog #4346907 and #4311971). Identical primer sets as those described for conventional RT-PCR were used for MTHFR variant A, variant B and MTHFR common region.

In addition, the following primers were designed to amplify a 150bp segment of the transcript for the gene *RNMT*, which was used as a reference gene:

Forward: 5'- TGCTCTTAAAACGAATGCAGGC-'3,

Reverse: 5'- CTGACTTACTTAAGGTTCCCAGAG-'3.

Samples were loaded in duplicate wells, which were averaged for one independent repeat. The qPCR program of 50°C (2 min), followed by 95°C (10 min), followed by 35 cycles of 95°C (15sec), 60°C(15sec), 72°C (1min). Following amplification, a melt curve from 60-95°C was performed to confirm the presence of a single PCR product.

RNA abundance in oocytes was calculated by absolute quantification using a standard curve of known cDNA concentration (1:10 serial dilution from 1000 femtograms to 0.01 femtograms) obtained from mouse liver for each primer set. The standard curve was run adjacent to oocyte samples on each independent replicate, and was also used to calculate the amplification efficiency of each primer set (acceptable range within 90-110%). A total of N=3 independent replicates were performed."

3.7.1.7 Gel Electrophoresis

A 1.5% agarose gel was made using 1.5 g agarose, 100 mL of 1X TAE, and 6 µL ethidium bromide. PCR samples were mixed with 4 µL 6X MassRuler Loading Dye and 20 µL of this sample was loaded in each lane. MassRuler DNA Ladder Mix was loaded in each gel to confirm band sizes. The gel was run for 1 hour at 110V in the Thermo Scientific Owl EasyCast B2 mini gel electrophoresis system. Visualization was done on the ChemiDoc-It^{TS2} 810 Imager.

3.7.1.8 Sequencing

Amplicons were extracted from agarose gels and prepared using the QIAquick Gel Extraction Kit (Qiagen Cat. No.: 28704) and sent for sequencing to the Ottawa Hospital Research Institute StemCore facilities. Sequences were matched to the predicted region using BLAST by the National Centre for Biotechnology Information (NCBI).

3.7.2 Western Blot

3.7.2.1 Protein Extraction

Liver lysates were used as a control on most western blots. They were prepared by dissecting a piece of fresh mouse liver and washing it in 1X PBS (Life Technologies) to remove any excess blood. The liver was then placed in 1 mL of RIPA lysis buffer (Thermofisher) with the addition of 5 µg/mL aprotinin (Roche), 5 µg/mL leupeptin (Sigma) and 1 mM PMSF (Roche) and incubated on ice for 15 minutes. Samples were then moved between liquid nitrogen and warm water 3-4 times and then homogenized. The homogenates were centrifuged at 11000 rpm for 10 minutes at 4°C in the Eppendorf Centrifuge 5810 R and the supernatant was collected. Supernatants were analyzed using the Biorad Microplate Assay Protocol and read by a spectrophotometer at 650 nm. A standard curve was made using a bovine serum albumin commercial standard of 1.38 mg/mL (Bio-Rad) for comparison.

3.7.2.2 Western Blot Optimization

Our lab originally acquired an anti-MTHFR primary antibody from Rima Rozen's lab at McGill University and previous members of the lab did preliminary work using and validating it. This antibody was specific for MTHFR protein however could not produce a clean background when using this antibody for the weak signals associated with oocyte and preimplantation

embryos, although following the original protocol, the protein bands were dark enough that the films were able to be used. However, Rozen's group eventually transferred the antibody to Sigma and their own laboratory stocks were depleted, so our lab purchased this product once our aliquots of the original antibody ran out. The Sigma antibody was unable to be optimized despite attempts at optimizing every aspect of the western blot protocol. Each attempt made and the modification that was tried is outlined in Table 7 beginning with the original Rozen antibody that worked. Several new commercial antibodies were then purchased and tested for MTHFR specificity. Abcam anti-MTHFR was the antibody that gave the best results and the one we chose to move forward with for all experiments. The Western blot optimization is described in detail in Results.

Other antibodies tested at the same time as the Abcam anti-MTHFR monoclonal antibody and found not to work (see Results) are listed in Table 6. Once the Abcam antibody showed specificity, I optimized the western blot conditions for this antibody as described in Results. Conditions tested included: 2X and 4X loading dye with various amount of liver protein, 10% precast gels were compared to various percentages of poured gels and number of oocytes required for detection between 10-100 GV oocytes. The conditions settled on were 10% poured gels, with 1-5 μg of liver protein as a control or 75 oocyte/embryos, using 2X or 4X loading dye, run for 6 hours at 70V, transferred overnight at 4°C at 15V to a PVDF membrane, blocked in 5% milk for 1 hour at room temperature, incubated in 1:2000 Abcam anti-MTHFR in 5% milk overnight at 4°C, then 1:5000 Cell Signalling HRP Goat AntiRabbit secondary for 1 hour at room temperature, ECL Prime kit for visualization. More details can be found in the General Western Blot section.

Table 5. Anti-MTHFR antibodies tested and found to not work.

Antibody	Source	Catalogue Number
Anti-MTHFR rabbit polyclonal	Biorbyt	orb214275
Anti-MTHFR rabbit polyclonal	MyBioSource	MBS820888
Anti-MTHFR goat polyclonal	ProSci	42-899
Anti-MTHFR goat polyclonal	Novus	NBP2-27549
Anti-MTHFR goat polyclonal	Abnova	PAB24568
Anti-MTHFR rabbit polyclonal	Biorbyt	orb161862
Anti-MTHFR rabbit polyclonal	MyBioSource	MBS9209113
Anti-MTHFR rabbit polyclonal	Bioworld	BS2946

3.7.2.3 General MTHFR Western Blot

The volume of oocyte and embryo samples were measured and made uniform by the addition of RIPA lysis buffer (ThermoFisher). The samples were mixed with Laemmli buffer (2X or 4X, Bio-Rad) and 2-mercaptoethanol (Sigma) and boiled for 5 minutes at 100°C. These samples were loaded into a 10% acrylamide SDS-PAGE gel and run for 6 hours at 70V. The Precision Plus Protein Kaleidoscope molecular weight ladder was also loaded in each gel to confirm band sizes. The gel was transferred to a PVDF membrane (Millipore Cat. No.: IPVH00010, pore size 0.45 μm) overnight at 4°C at 15V. The membrane was blocked with 5%

milk for 1 hour at room temperature and incubated overnight at 4°C in 1:1000 anti-MTHFR (Abcam) in 5% milk. The next day, the membrane was washed with Tris-Buffered Saline + Tween 20 (TBST) for 10 minutes, 3 times then incubated in 1:5000 anti-rabbit IgG, HRP-linked secondary antibody in 5% milk for 1 hour at room temperature. After 3 10-minute washes in TBST, the membrane was visualized using the ECL Prime Detection kit (GE Healthcare) on autoradiography film (Denville Scientific Inc, Cat. No.: E3018). After visualization, the membrane was washed 3 times with TBST for 10 minutes each, and incubated overnight at 4°C in 1:1000 anti-vinculin (Abcam) in 5% milk as a loading control. The following day, the membrane was washed 3 times with TBST for 10 minutes each and incubated in 1:5000 anti-rabbit IgG, HRP-linked secondary antibody for 1 hour at room temperature and then washed 3 more times. Visualization was done with the ECL Prime Detection kit (GE Healthcare). Some earlier blots used 1:200 anti-GAPDH (Santa Cruz) as a loading control in 5% milk and used the Clarity Western ECL Substrate (Bio-Rad) for visualization.

3.7.2.4 Lambda Protein Phosphatase (LPP) Treatment

Oocytes and embryos were collected using the regular protocol and stored in 2 µL of RIPA buffer (ThermoFisher) until needed for an LPP (NEB) western blot experiment. Samples were thawed and the volumes were measured, RIPA buffer was added to ensure all samples were at the same volume. These samples were split in half to have uniform samples in the control and LPP treated groups. Each group was mixed with 10X $MnCl_2$ and 10X PMP Buffer (NEB). The treated group was mixed with 300 units of LPP and water, while the control group received the same volume of water. These mixtures were incubated in a water bath or thermocycler for 1 hour at 30°C. After incubation, the samples were prepared to run in an SDS PAGE gel as per the regular protocol.

3.7.2.5 Phos-tag Western Blot

The Phos-tag gels (Fujifilm Wako Pure Chemical Corporation) were obtained as precast gels and samples were loaded as per the standard western blot protocol. These gels were 12.5% acrylamide and contained 50 μmol/L Mn^{2+}-Phos-tag. The Phos-tag gels ran at 70V for 4 hours. After electrophoresis, the gel was soaked in a standard transfer buffer + 1mmol/L EDTA for 3 10-minute washes. This was to remove manganese ions from the gel to increase the efficiency of the transfer. Next, the gel was soaked in a standard transfer buffer for 3 10-minute washes and the regular western blot protocol was followed beyond that.

3.7.2.6 Western blot analysis: ImageJ

The blots from a given experiment were subjected to ImageJ analysis if, in the set of blots from that experiment, a clear shift was visible between any two lanes or if the intent was to prove a lack of shift on the blots. Each scanned image was opened in ImageJ and adjusted using the Rotate function to be horizontal. A rectangle was placed around the visible bands in the first lane and the data was collected using the Gels function as gray scale vs. distance in inches, showing a clear difference between where bands were present and where there was only background. This rectangle moved horizontally across the image collecting data from each lane. These data were plotted in Prism and the distance in inches was converted to molecular weight. Films of each blot were used to measure the molecular weight (MW) ladder which had visible bands from 250 kDa to 50 kDa, which were used to make a standard curve for each blot using Rf value vs logMW. Once the curve was made, a visible peak (the darkest band) was measured on the film and converted to MW using the standard curve. Using this conversion, all distances were able to be converted to MW.

3.8 Dimedone Formaldehyde Adduct (Formaldemethone) Synthesis

Formaldemethone crystals were produced in order to create a standard curve to report the linear range and the limit of detection in the LC-MS/MS system. 0.4% dimedone solution in water was mixed with a 3.4 nmole formaldehyde solution pH 4.5 overnight to produce a formaldemethone precipitate. This solution was filtered through a Buchner funnel attached to a vacuum filtration apparatus. The crystals collected from this were washed with distilled water and dried in a 37°C drying oven overnight. The adduct was then recrystallized twice by dissolving the product in 99.9% methanol and then adding an excess of distilled water to re-precipitate the crystals. This solution was filtered through a Buchner funnel attached to a vacuum filtration apparatus again, washed with distilled water and left in a 37°C drying oven overnight. The crystals (formaldemethone) were then weighed and the percent yield was calculated as 73%. The crystals were dissolved in toluene and allowed to evaporate overnight before being given to the Pharmacokinetics Laboratory of the Clinical Investigations Unit of the Ottawa Hospital, where Jeremy Zhang performed LC-MS/MS on the sample to create a standard of detectable formaldemethone in the system. This technique allows for separation using High Performance Liquid Chromatography and detection using mass spectrometry. The dimedone formaldehyde adduct was separated using liquid chromatography by resuspension in 100 µL or 200 µL 0.1% formic acid in 4:1 acetonitrile:water. Next, the samples were injected into a tandem mass spectrometer (MS/MS).

3.9 Bioinformatics

Datasets used were drawn from RNAseq studies including mouse, human and cow

samples at varying stages of development. Gareth Palidwor of the Bioinformatics Core Facility re-aligned these data to the newest versions of the mouse, human and cow genomes. The files were converted to either single or paired end reads as appropriate and FASTQ files were generated. The files were examined with FASTQC and the reads were processed in Salmon. These reads were assigned to transcripts in Salmon using recent GENCODE assemblies. The counts per million (CPM) values from Salmon are the number of counts for a transcript divided by the total number of mapped counts multiplied by 1 million. The exclusion criterion was reads mapped were less than 100,000. In addition to *Mthfr*, genes of interest were chosen that encoded enzymes from the folate and methionine cycles associated with MTHFR including *Bhmt*, *Mtr*, *Mat1a*, *Mat2a*, *Mat2b*, *Ahcy*, *Shmt1* and *Shmt2*. CPM was graphed from each study for each stage of development available from the datasets, showing the average and standard error.

Table 6. List of datasets used for Bioinformatics graphs listed with their respective GEO numbers.

Replicate	GEO Number
Mouse GV Rep 1	GSM1903780
Mouse GV Rep 2	GSM1903781
Mouse GV Rep 3	GSM1903782
Mouse GV Rep 4	GSM1664631
Mouse GV Rep 5	GSM1664632
Mouse GV Rep 6	GSM3333253
Mouse GV Rep 7	GSM3333254
Mouse GV Rep 8	GSM3611277
Mouse GV Rep 9	GSM3611279
Mouse MII Rep 1	GSM1080195
Mouse MII Rep 2	GSM1080196
Mouse MII Rep 6	GSM2588668
Mouse MII Rep 7	GSM1811753
Mouse MII Rep 8	GSM3333267

Mouse 1 Cell Rep 1	GSM1080197
Mouse 1 Cell Rep 2	GSM1080198
Mouse 1 Cell Rep 3	GSM1080199
Mouse 1 Cell Rep 4	GSM1811765
Mouse 1 Cell Rep 5	GSM3333259
Mouse 1 Cell Rep 6	GSM3333260
Mouse 1 Cell Rep 7	GSM3611291
Mouse 1 Cell Rep 8	GSM3611293
Mouse 2 Cell Rep 1	GSM1080200
Mouse 2 Cell Rep 2	GSM1080201
Mouse 2 Cell Rep 3	GSM1080202
Mouse 2 Cell Rep 4	GSM3611305
Mouse 2 Cell Rep 5	GSM3611306
Mouse 2 Cell Rep 6	GSM2588670
Mouse 2 Cell Rep 7	GSM2588671
Mouse 2 Cell Rep 8	GSM1811721
Mouse 2 Cell Rep 9	GSM3611307

Mouse 4 Cell Rep 1	GSM1080203
Mouse 4 Cell Rep 2	GSM1080204
Mouse 4 Cell Rep 3	GSM1080205
Mouse 4 Cell Rep 4	GSM4118739
Mouse 4 Cell Rep 5	GSM4118740
Mouse 4 Cell Rep 6	GSM2588674
Mouse 4 Cell Rep 7	GSM2588675
Mouse 4 Cell Rep 8	GSM1811726
Mouse 8 Cell Rep 1	GSM1080206
Mouse 8 Cell Rep 2	GSM1080207
Mouse 8 Cell Rep 3	GSM1080208
Mouse 8 Cell Rep 4	GSM4118741
Mouse 8 Cell Rep 6	GSM2588678
Mouse 8 Cell Rep 7	GSM2588679
Mouse 8 Cell Rep 8	GSM1811732
Mouse 16 Cell Rep 1	GSM2253495
Mouse 16 Cell Rep 2	GSM2253497

Mouse 16 Cell Rep 3	GSM2253499
Mouse 16 Cell Rep 4	GSM2253496
Mouse 16 Cell Rep 7	GSM2253500
Mouse 16 Cell Rep 8	GSM2253501
Mouse 16 Cell Rep 9	GSM2253502
Mouse 16 Cell Rep 10	GSM2253503
Mouse 16 Cell Rep 11	GSM2253504
Mouse Morula Rep 1	GSM1080209
Mouse Morula Rep 2	GSM1080210
Mouse Morula Rep 3	GSM1080211
Mouse Morula Rep 4	GSM2588681
Mouse Morula Rep 5	GSM2588682
Mouse Morula Rep 6	GSM1811747
Mouse Morula Rep 7	GSM1811748
Mouse Blastocyst Rep 1	GSM1502476
Mouse Blastocyst Rep 2	GSM1502477
Mouse Blastocyst Rep 3	GSM4118743

Mouse Blastocyst Rep 4	GSM4118744
Mouse Blastocyst Rep 6	GSM1811738
Mouse Blastocyst Rep 7	GSM1811739
Mouse Blastocyst Rep 8	GSM3611320
Mouse Blastocyst Rep 9	GSM3611321
Mouse Blastocyst Rep 10	GSM3611322
Human GV Rep 1	GSM1861606
Human GV Rep 2	GSM1861607
Human GV Rep 3	GSM2706233
Human GV Rep 4	GSM2706234
Human GV Rep 7	GSM2514771
Human GV Rep 8	GSM2514773
Human GV Rep 9	GSM2514775
Human MII Rep 1	GSM1160112
Human MII Rep 2	GSM1160113
Human MII Rep 3	GSM1160114
Human MII Rep 4	GSM1861610

Human MII Rep 5	GSM1861611
Human MII Rep 6	GSM2706235
Human MII Rep 7	GSM2706236
Human MII Rep 8	GSM2514772
Human MII Rep 9	GSM2514774
Human MII Rep 10	GSM2514776
Human 1 Cell Rep 2	GSM1160119
Human 1 Cell Rep 3	GSM1833283
Human 1 Cell Rep 4	GSM1833284
Human 1 Cell Rep 5	GSM1833285
Human 1 Cell Rep 6	GSM1833286
Human 1 Cell Rep 7	GSM1833287
Human 2 Cell Rep 8	GSM1160120
Human 2 Cell Rep 9	GSM1160121
Human 2 Cell Rep 10	GSM1160122
Human 2 Cell Rep 11	GSM1861614
Human 2 Cell Rep 12	GSM1861615

Human 2 Cell Rep 13	GSM1833288
Human 2 Cell Rep 14	GSM1833291
Human 2 Cell Rep 15	GSM2706237
Human 2 Cell Rep 16	GSM2706238
Human 2 Cell Rep 17	GSM2706239
Human 2 Cell Rep 18	GSM2706260
Human 2 Cell Rep 19	GSM2706261
Human 4 Cell Rep 1	GSM1160123
Human 4 Cell Rep 2	GSM1160124
Human 4 Cell Rep 3	GSM1160125
Human 4 Cell Rep 4	GSM1160126
Human 4 Cell Rep 5	GSM1833292
Human 4 Cell Rep 6	GSM1833296
Human 4 Cell Rep 7	GSM2706240
Human 4 Cell Rep 8	GSM2706241
Human 8 Cell Rep 1	GSM1160127
Human 8 Cell Rep 2	GSM1160128

Human 8 Cell Rep 3	GSM1160129
Human 8 Cell Rep 4	GSM1160130
Human 8 Cell Rep 5	GSM1160131
Human 8 Cell Rep 6	GSM1160132
Human 8 Cell Rep 7	GSM1160133
Human 8 Cell Rep 8	GSM1160134
Human 8 Cell Rep 9	SM1160135
Human 8 Cell Rep 10	GSM1160136
Human 8 Cell Rep 11	GSM1160137
Human 8 Cell Rep 12	GSM1833297
Human 8 Cell Rep 13	GSM1833302
Human 8 Cell Rep 14	GSM1833304
Human 8 Cell Rep 15	GSM2706242
Human 8 Cell Rep 16	GSM2706243
Human 8 Cell Rep 17	GSM2706264
Human 8 Cell Rep 18	GSM2706265
Human Morula Rep 1	GSM1160138

Human Morula Rep 2	GSM1160139
Human Morula Rep 3	GSM1160140
Human Morula Rep 4	GSM1861616
Human Morula Rep 5	GSM1861617
Human Morula Rep 6	GSM1833307
Human Morula Rep 7	GSM1833314
Human Blastocyst Rep 1	GSM1833316
Human Blastocyst Rep 2	GSM1833324
Human Blastocyst Rep 3	GSM1833326
Human Blastocyst Rep 5	GSM3144752
Human Blastocyst Rep 6	GSM3144753
Human Blastocyst Rep 7	GSM3144754
Human Blastocyst Rep 8	GSM3144755
Human Blastocyst Rep 9	GSM3144756
Bovine GV Rep 1	GSM1265758
Bovine GV Rep 2	GSM1265759
Bovine GV Rep 3	GSM1265760

Bovine GV Rep 4	GSM1511704
Bovine GV Rep 5	GSM1511705
Bovine GV Rep 6	GSM1511706
Bovine MII Rep 1	GSM1265761
Bovine MII Rep 2	GSM1265762
Bovine MII Rep 3	GSM1265763
Bovine MII Rep 4	GSM1429881
Bovine MII Rep 5	GSM1429882
Bovine MII Rep 6	GSM1511707
Bovine MII Rep 7	GSM1511708
Bovine MII Rep 8	GSM1511709
Bovine 2 Cell Rep 1	GSM1429883
Bovine 2 Cell Rep 2	GSM1429884
Bovine 8 Cell Rep 1	GSM1265767
Bovine 8 Cell Rep 2	GSM1265768
Bovine 8 Cell Rep 3	GSM1265769
Bovine 8 Cell Rep 4	GSM1429887

Bovine 8 Cell Rep 5	GSM1429888
Bovine 8 Cell Rep 6	GSM3520495
Bovine 8 Cell Rep 7	GSM3520496
Bovine 8 Cell Rep 8	GSM3520497
Bovine 8 Cell Rep 9	GSM2640582
Bovine 8 Cell Rep 10	GSM2640583
Bovine 8 Cell Rep 11	GSM2640584
Bovine 16 Cell Rep 2	GSM1265771
Bovine 16 Cell Rep 3	GSM1265772
Bovine 16 Cell Rep 4	GSM1429889
Bovine 16 Cell Rep 5	GSM1429890
Bovine Morula Rep 1	GSM1429893
Bovine Morula Rep 2	GSM1429894
Bovine Morula Rep 3	GSM1429891
Bovine Morula Rep 4	GSM1429892
Bovine Blastocyst Rep 1	GSM1265773
Bovine Blastocyst Rep 2	GSM1265774

Bovine Blastocyst Rep 3	GSM1265775
Bovine Blastocyst Rep 4	GSM1429895
Bovine Blastocyst Rep 5	GSM1429896
Bovine Blastocyst Rep 6	GSM4263616
Bovine Blastocyst Rep 7	GSM4263617
Bovine Blastocyst Rep 8	GSM4263618
Bovine Blastocyst Rep 9	GSM4263619
Bovine Blastocyst Rep 10	GSM4263620
Bovine Blastocyst Rep 11	GSM616070
Bovine Blastocyst Rep 12	GSM616070

3.10 Statistical Analysis

Genotypes

Observed ratios of heterozygous, wildtype and knockout mice (58:26:16) were compared to theoretical ratios (50:25:25) using a chi-squared goodness-of-fit test and found to not be significantly different (P=0.1023).

qRT-PCR

A one-way ANOVA was performed on each set of data from the different primers to check for differences in amount of RNA between stages of development. A Tukey's test was performed to identify specific differences between groups. The only primer set to show a significant difference was *Mthfr* Common (P=0.0004).

Bioinformatics

A one-way ANOVA was performed on each data set for each gene of interest in each species. This include MTHFR, BHMT, MTR, MAT1A, MAT2A, MAT2B, AHCY, SHMT1, SHMT2 in mouse, human and bovine. Each graph was analyzed using a Tukey's test to identify differences between groups. Many significant differences were found over the stages of development for each gene and each species.

Lambda Protein Phosphatase Experiments

The difference in molecular weight between treated (+LPP) and untreated (-LPP) samples was measured using peaks on the graphs in Prism. The molecular weight of the highest peak in the treated sample was subtracted from the molecular weight of the highest peak in the untreated

sample to give ΔMW. 3 replicates were used and compared using a two-tailed t-test between GVs and MIIs. A P value of less than 0.05 was determined as statistically significant.

4. **Results**

RT-PCR and qRT-PCR indicates that both *Mthfr* isoforms are present throughout development

RT-PCR

Expression of *Mthfr* A and *Mthfr* B were evaluated using isoform-specific primers in conventional PCR in GV oocytes, MII eggs, 2-cell embryos and blastocysts. Primers for a common region of *Mthfr* were used to detect total *Mthfr*. A control set of primers for *Ppia* was used to confirm the presence of cDNA. Figure 6 show the clear presence of both of the isoforms as well as the common region. *Ppia* was confirmed in all samples.

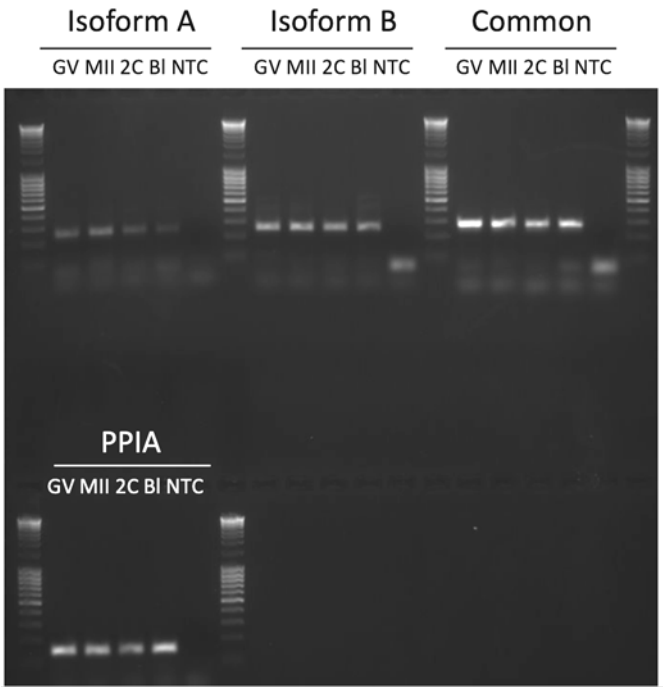

Figure 6. Presence of mRNA throughout oocyte and preimplantation embryo development.

RT-PCR performed with 6 oocytes or embryos per reaction, using the primers described in the Methods section for isoform specific regions of *Mthfr* A and B, a common region of *Mthfr* and *Ppia* as a reference gene. Isoform A band is at 251 bp, isoform B band is at 253 bp and the common band is at 283 bp. MassRuler (Thermo Scientific) was used to estimate amplicon size. Samples were run in a 1.5% agarose gel with ethidium bromide for 1 hour at 110V. GV: Germinal vesicle; MII: MII egg; 2C: 2-cell embryo; Bl: Blastocyst; NTC: No template control. One example of 3 similar independent repeats is shown.

qRT-PCR

As mentioned in the methods section, Allison Tscherner, a postdoctoral fellow in the lab, performed the qRT-PCR measurements as I was not permitted to be trained on the qPCR instrument due to Covid-19 restrictions. mRNA from *Mthfr* A and B, a common region of *Mthfr* and *Rnmt* were quantified. The same primers specified previously for conventional PCR were used for the qRT-PCR experiments for the *Mthfr* regions. Figure 7 shows the varying amounts of mRNA found in GVs, MIIs, 2-cells and blastocysts in femtograms for each set of primers. There is more mRNA found using the set of common primers compared to mRNA found in the primer sets for isoform A and B combined. This could be due to a lack of efficiency of the isoform specific primers as there was only a small area of base pairs that made each isoform different, which was not optimal for primer design. The common set of primers had a much larger range to be designed in and were more efficient, allowing for a greater yield of mRNA. Therefore, this does not allow for a conclusion based on amount of each isoform, rather that they are both present. *Rnmt* was chosen from RNA sequencing datasets as a reference gene since it appeared to have a similar amount of mRNA across the stages of development of interest. When used for qRT-PCR, there were not equal amounts at each stage so the *Mthfr* mRNA was not normalized to this and instead absolute quantification was used.

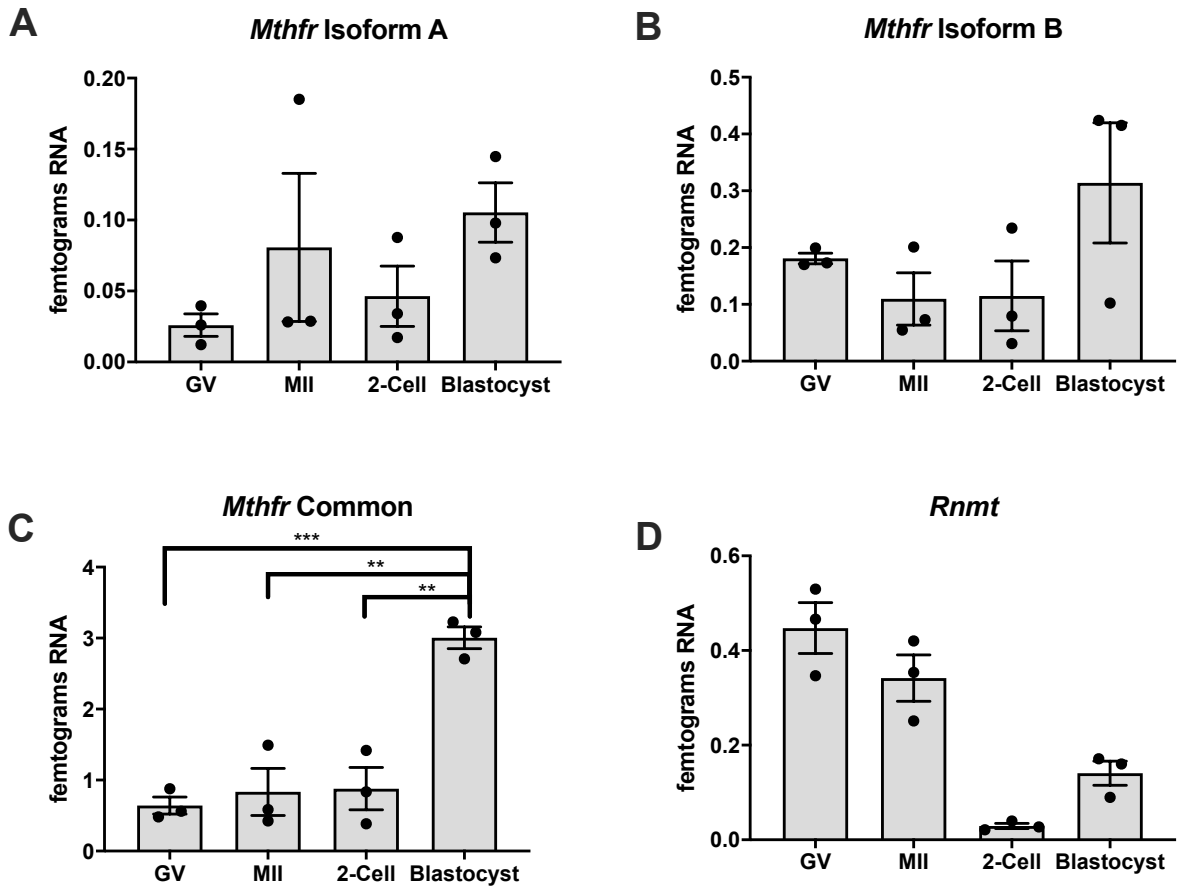

Figure 7. mRNA quantification.

qRT-PCR performed using 3 oocytes per reaction, using primers mentioned in the methods section. A) Amounts range from 0.025-0.1 fg for isoform A. B) Amounts range from 0.1-0.3 fg for isoform B. C) Amounts range from 0.6-3 fg for the common region. D) Amounts range from 0.02-0.4 fg for *Rnmt*. A one-way ANOVA was performed on each set with *Mthfr* Common being the only one to show statistical significance (P=0.0004). A post-hoc Tukey's test was performed and found GV and Blastocyst to be the most different (P=0.0006), MII and Blastocyst was also statistically different (P=0.0011) and 2-Cell and Blastocyst as well (P=0.0012).

Bioinformatics

Graphs are shown for each gene of interest including: *Mthfr*, *Bhmt*, *Mtr*, *Mat1a*, *Mat2a*, *Mat2b*, *Ahcy*, *Shmt1* and *Shmt2* in mouse, human and cow samples. These are all of the necessary components of OCM. The stages of development presented reflect the data that was available in the data sets. Averages are shown along with standard error (Figures 8). The amounts shown in the *Mthfr* mouse graph (Figure 8A) resemble what was found from the qRT-PCR data in that *Mthfr* RNA is low early on and increases as the embryo develops. These values are not directly comparable as the RNA sequencing data is counted as a proportion while the qRT-PCR values are absolute. All other datasets graphed are supplementary to the *Mthfr* data to show that the transcripts are present in the various stages investigated here and across species. The *Mthfr* human and bovine graphs (Figure 8B & 8C) both vary from what is identified in the mouse graph and do not seem to follow a pattern of embryonic genome activation.

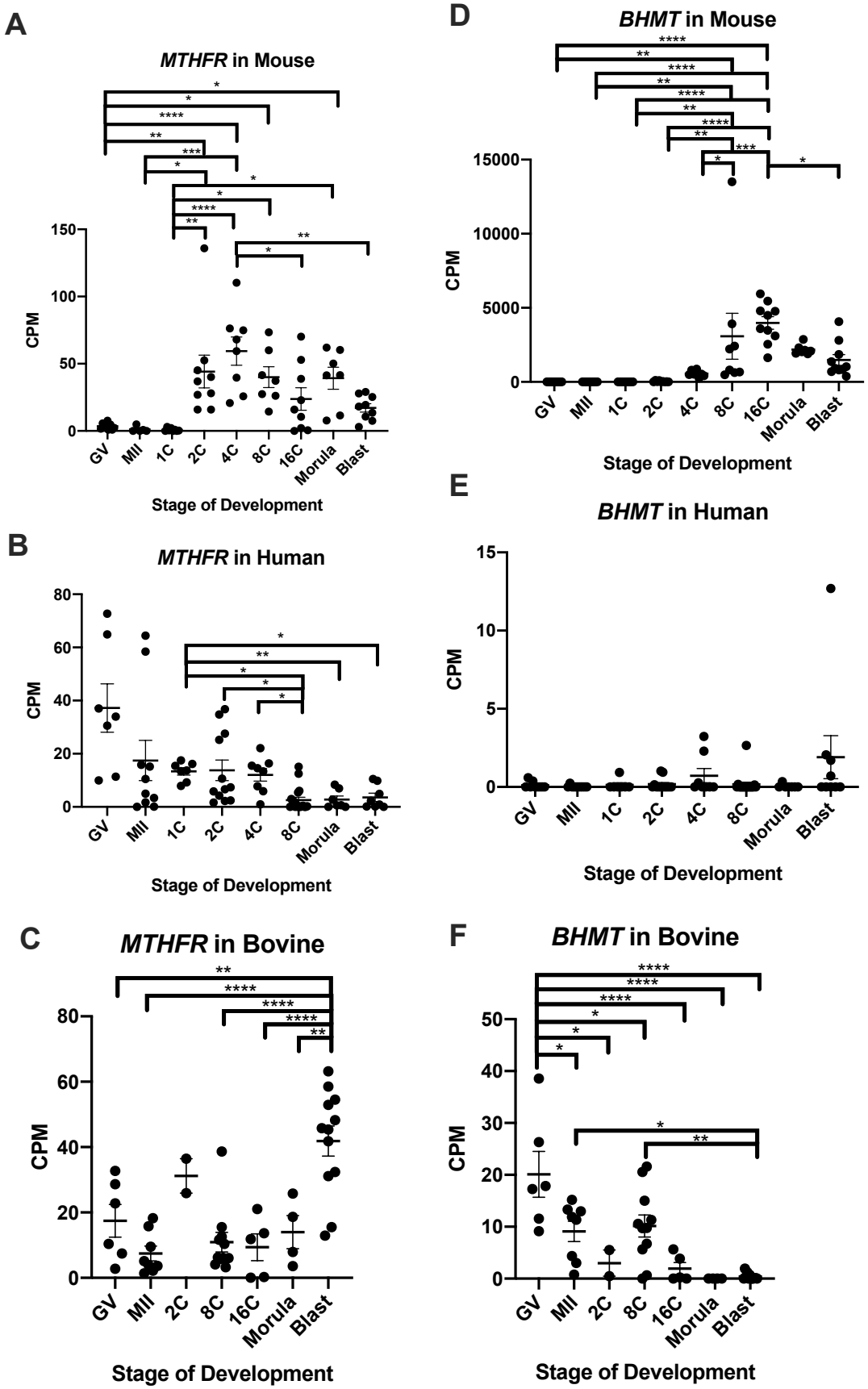
A
MTHFR in Mouse
CPM
Stage of Development
GV
MII
1C
2C
4C
8C
16C
Morula
Blast
B
MTHFR in Human
C
MTHFR in Bovine
D
BHMT in Mouse
E
BHMT in Human
F
BHMT in Bovine

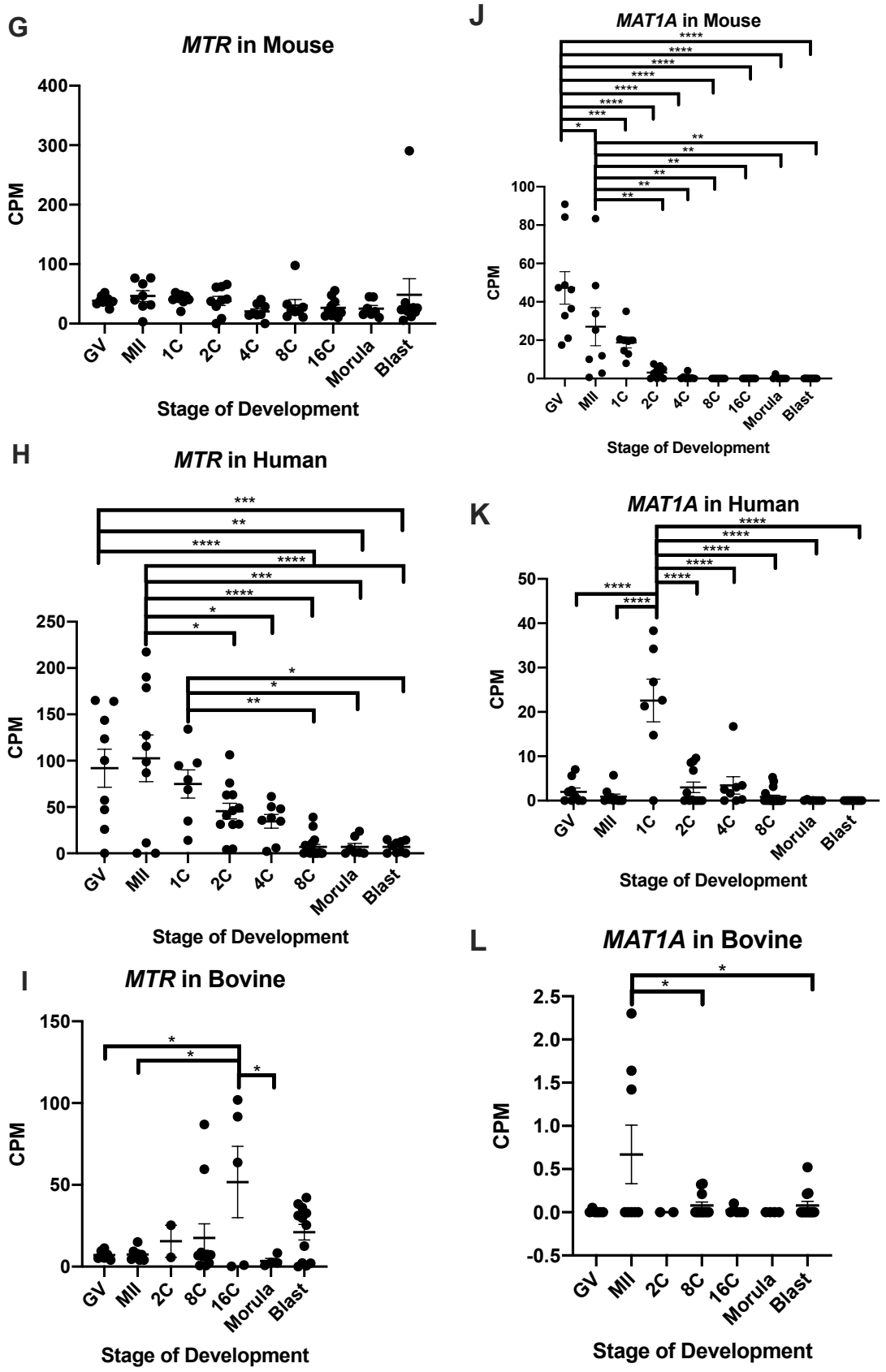
G
MTR in Mouse
CPM
Stage of Development
GV
MII
1C
2C
4C
8C
16C
Morula
Blast
J
MAT1A in Mouse
H
MTR in Human
K
MAT1A in Human
I
MTR in Bovine
L
MAT1A in Bovine

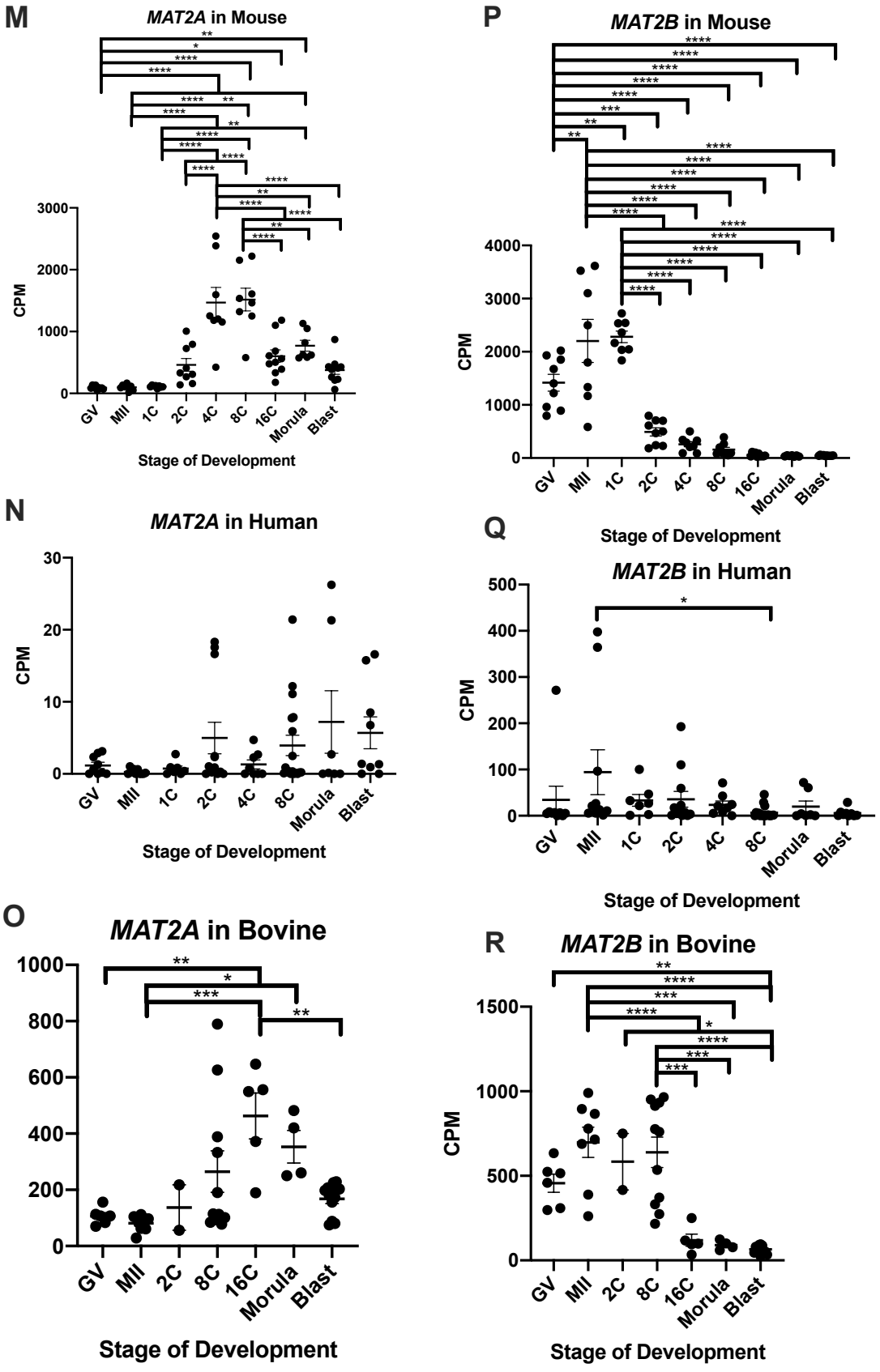
M
MAT2A in Mouse
CPM
Stage of Development
GV
MII
1C
2C
4C
8C
16C
Morula
Blast
P
MAT2B in Mouse
N
MAT2A in Human
Q
MAT2B in Human
O
MAT2A in Bovine
R
MAT2B in Bovine

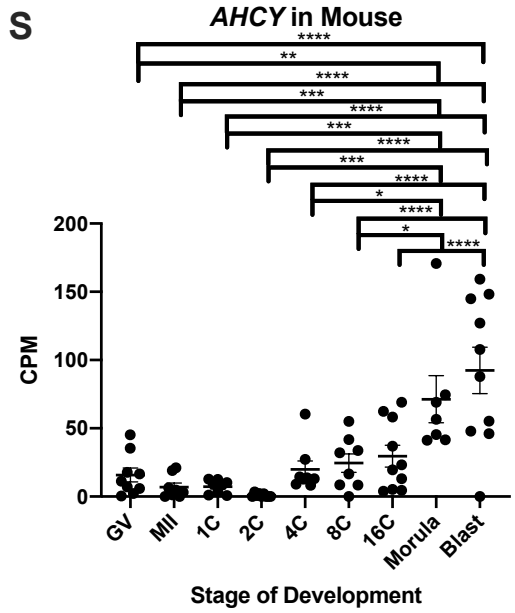
S
AHCY in Mouse
CPM
Stage of Development
GV
MII
1C
2C
4C
8C
16C
Morula
Blast

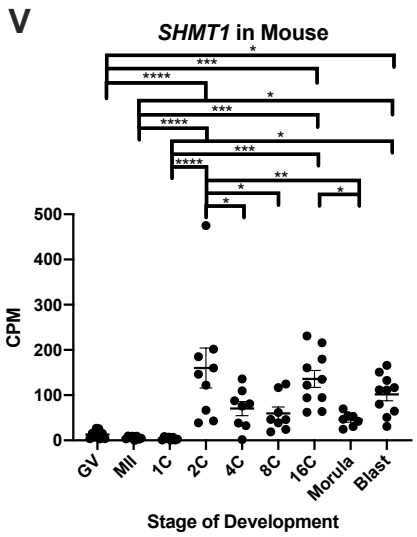
V
SHMT1 in Mouse
CPM
Stage of Development
GV
MII
1C
2C
4C
8C
16C
Morula
Blast

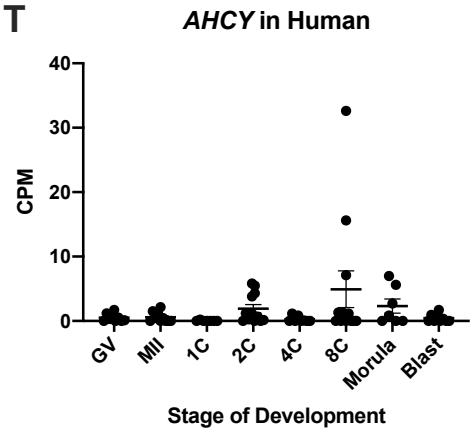
T
AHCY in Human
CPM
Stage of Development
GV
MII
1C
2C
4C
8C
Morula
Blast

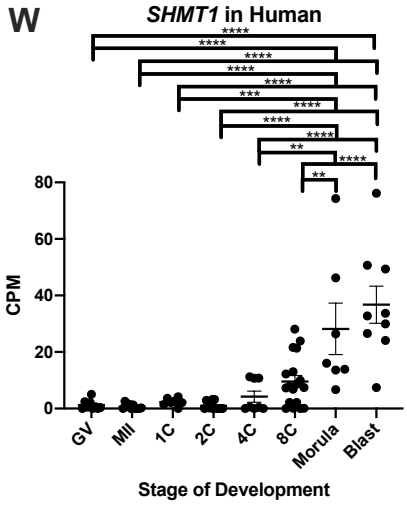
W
SHMT1 in Human
CPM
Stage of Development
GV
MII
1C
2C
4C
8C
Morula
Blast

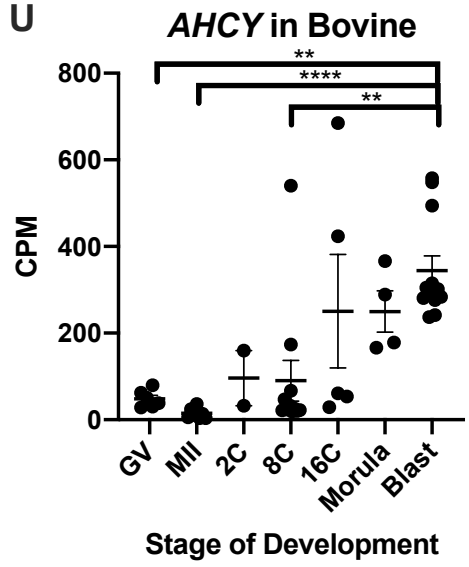
U
AHCY in Bovine
CPM
Stage of Development
GV
MII
2C
8C
16C
Morula
Blast

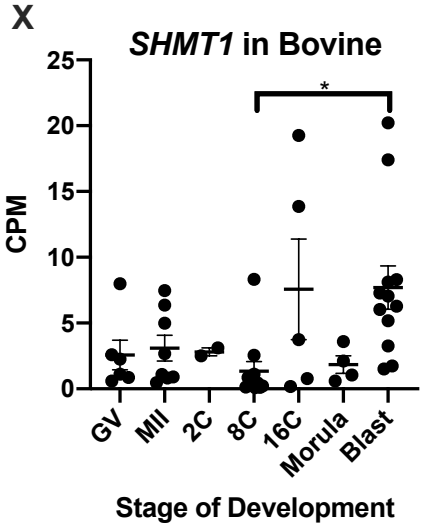
X
SHMT1 in Bovine
CPM
Stage of Development
GV
MII
2C
8C
16C
Morula
Blast

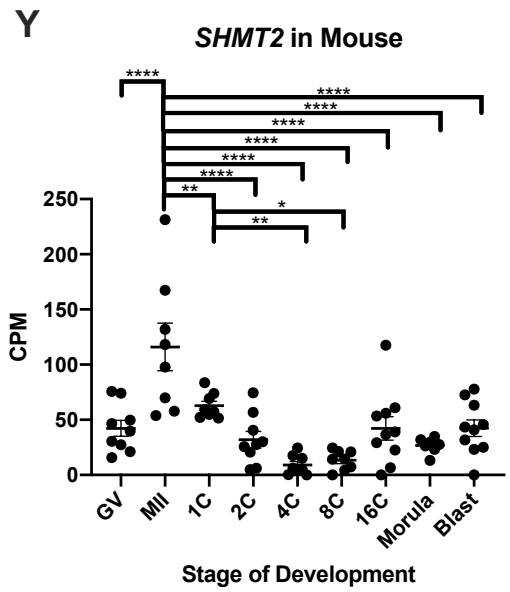
Y
SHMT2 in Mouse
CPM
Stage of Development
GV
MII
1C
2C
4C
8C
16C
Morula
Blast

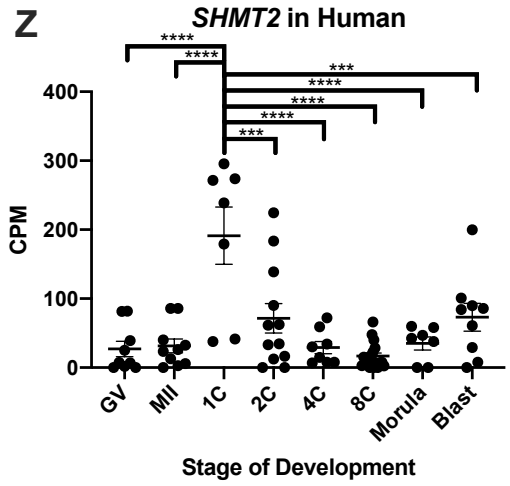
Z
SHMT2 in Human
CPM
Stage of Development
GV
MII
1C
2C
4C
8C
Morula
Blast

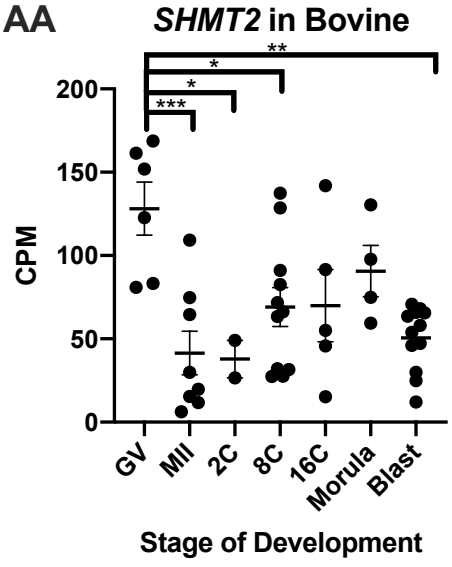
AA
SHMT2 in Bovine
CPM
Stage of Development
GV
MII
2C
8C
16C
Morula
Blast

Figure 8. Bioinformatics data from human, mouse and cow.

Genes relevant to the folate and methionine cycles shown. GV: GV oocytes; MII: MII eggs; 1C: 1 cell; 2C: 2 cell; 4C: 4 cell; 8C: 8 cell; 16C: 16 cell; Morula; Blast: Blastocyst. Amount of RNA shown in CPM: Counts per Million. This a proportion representing the amount of RNA out of the total. Asterisks denote level of significance.

Mthfr genotyping

PCR confirmed that the *Mthfr* knockout mice on the C57/Bl6 background had the expected genotypes. We have confirmed wildtypes, heterozygotes and knockout mice (Figure 9). The historical mouse data the lab has in the software SoftMouse shows 1183 offspring in the MTHFR -/+ x MTHFR +/- breeding scheme. Of these mice, 629 (53%) were male and 554 (47%) were female. From the 1183 mice we have had in our breeding scheme, 688 were heterozygous (357 male, 331 female) which is 58% of the total, 309 were wildtypes (175 male, 134 female) which is 26% of the total and 186 were knockouts (97 male, 89 female) which is 16% of the total. These genotypes deviated slightly from the expected Mendelian ratios of 50% heterozygous, 25% wildtype, and 25% knockout, but this did not reach significance using a Chi square test (P=0.1023). Genotyping was carried out by the technician in the laboratory, Taylor McClatchie.

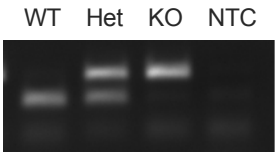

Figure 9. Genotyping of *Mthfr* mice.

Mthfr mouse ear notch samples were used for genotyping PCR. Wildtype, heterozygous and knockout mice were confirmed using specific primers for each. One example is shown. WT: wildtype; Het: heterozygous; KO: knockout; NTC: No template control.

Optimization of MTHFR antibody and western blot protocol

All preliminary western blot data collected for this project used an antibody produced by the Rozen Lab at McGill University (Chen et al., 2001). Frozen aliquots were kept in a -80°C freezer, which were used with the standard western blot protocol described in Materials and Methods. The Rozen antibody gave a similar result to the unpublished preliminary results obtained by previous lab members (Attempt 1 in Appendix A). The Rozen lab transferred this antibody to Sigma where it became commercially available. The purchased antibody from Sigma produced blots with very substantial background compared to the antibody supplied by the Rozen lab, using the same western blot protocol, as mentioned in Table 7, Attempt #2. The bands were much less visible. Thus, optimization for the antibody supplied by Sigma was attempted. Further details of this optimization can be found in Appendix A.

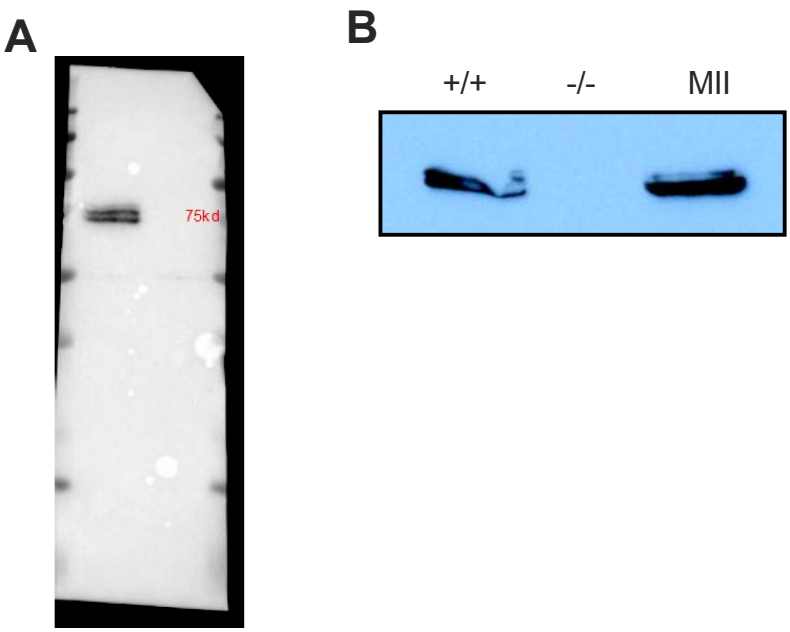

Figure 10. Attempts #68 and #69 from Table 7, Abcam antibody.

A) 5 µg of wildtype and knockout liver probed with 1:1000 Abcam anti-MTHFR. B) 5 µg of wildtype and knockout liver and 100 MII eggs probed with 1:1000 Abcam anti-MTHFR.

Abcam antibody is specific to MTHFR protein

The Abcam anti-MTHFR antibody is a rabbit monoclonal antibody that the manufacturer specifies shows reactivity with human and mouse MTHFR. The sample data on their website showed a band at approximately 75 kDa, which is what our lab previously found with the Rozen antibody and which is the approximate size in published western blots.

First, MII eggs were loaded on the same gel as wildtype and knockout liver to assess whether the antibody would show protein in MII egg lysates similar to the tissue samples (Figure 10).

Next, the optimal amount of liver protein to load as a control was assessed and while doing so, the difference between 2X and 4X loading dye was checked. The result showed no difference between loading dyes at either concentration and that 5 µg of liver protein was optimal (Figure 11).

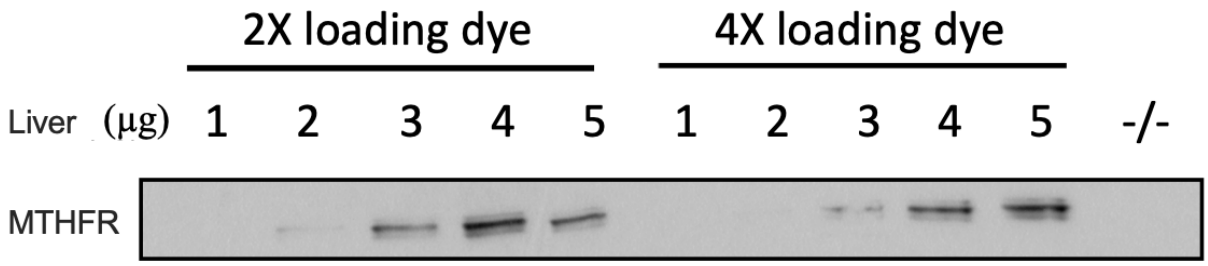

Figure 11. Optimization for Abcam antibody.

1 µg-5 µg of liver tissue, mixed with 2X loading dye or 4X loading dye, blocked with 5% milk, probed with 1:1000 anti-MTHFR Abcam antibody, 1:5000 secondary antibody. -/- indicates a lane with 5 µg knockout liver.

Once the protocol was optimized with liver samples, lysates of varying numbers of GV oocytes (10-100), were loaded on a gel in order to determine the limit of detection for the anti-MTHFR Abcam antibody in the samples of interest (Figure 12). 75 oocytes were determined to be the minimum amount to load per lane. Lysates of 75 oocytes or embryos were used for all future experiments as it was easily detectable using ECL Prime for a one-minute exposure.

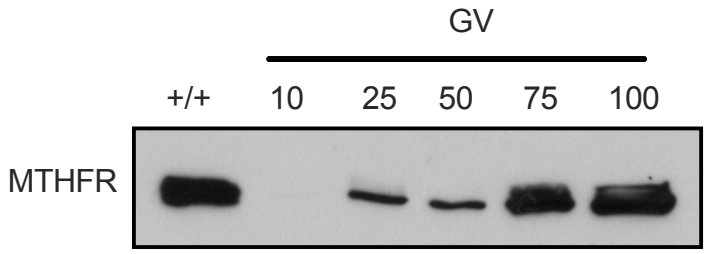

Figure 12. Abcam antibody test on GV oocytes.

5 µg of liver tissue, 10, 25, 50, 75 and 100 GV oocytes loaded onto a 10% acrylamide gel. Blocked with 5% milk, probed with 1:1000 anti-MTHFR Abcam antibody and 1:5000 HRP goat anti-rabbit secondary antibody.

Liver samples from age matched littermates of wild-type *Mthfr*$^{+/+}$, heterozygote *Mthfr*$^{+/-}$ and knockout *Mthfr*$^{-/-}$ animals from the *Mthfr* mutant mouse lines were used in a Western to confirm that the antibody was specific for MTHFR (Figure 13). The wildtype sample showed a dark set of bands near the expected MW of 75 kDa, while the heterozygote sample showed a faint set of bands and the knockout showed a complete lack of bands.

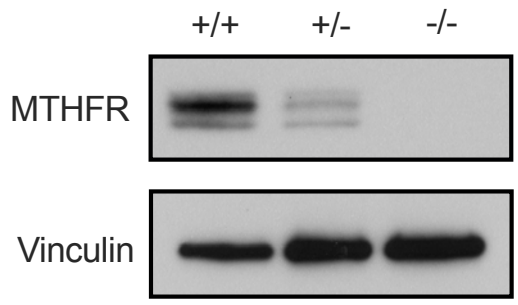

Figure 13. Wildtype, heterozygous and knockout mouse protein comparison.

5 µg of wildtype, heterozygous or knockout liver tissue blocked with 5% milk, probed with 1:1000 anti-MTHFR Abcam antibody and 1:1000 anti-vinculin as a loading control. The bands for MTHFR appear at the expected size of ~75 kDa.

MTHFR protein is present throughout mouse oocyte maturation and preimplantation embryo development

Western blots were used to determine if MTHFR protein was present in CD1 mouse oocytes and preimplantation embryos. To do this, 75 of each of GV oocytes, MII eggs, 1 cell embryos, 2 cell embryos, morulas and blastocysts were run in each lane of western blots (Figure 14). This confirmed that MTHFR protein was detectable throughout mouse oocyte maturation and preimplantation embryo development. The western blot results show three closely-spaced visible bands, varying in intensity depending on the stage. A clear difference visible in all replicates was that there was a higher band in MII egg samples with a lack of the lower band. The lower band seems to be at the same size across all other samples with a lack of the higher band. Quantification using ImageJ distance to peak analysis shows the differences between the samples are consistent (Figure 14).

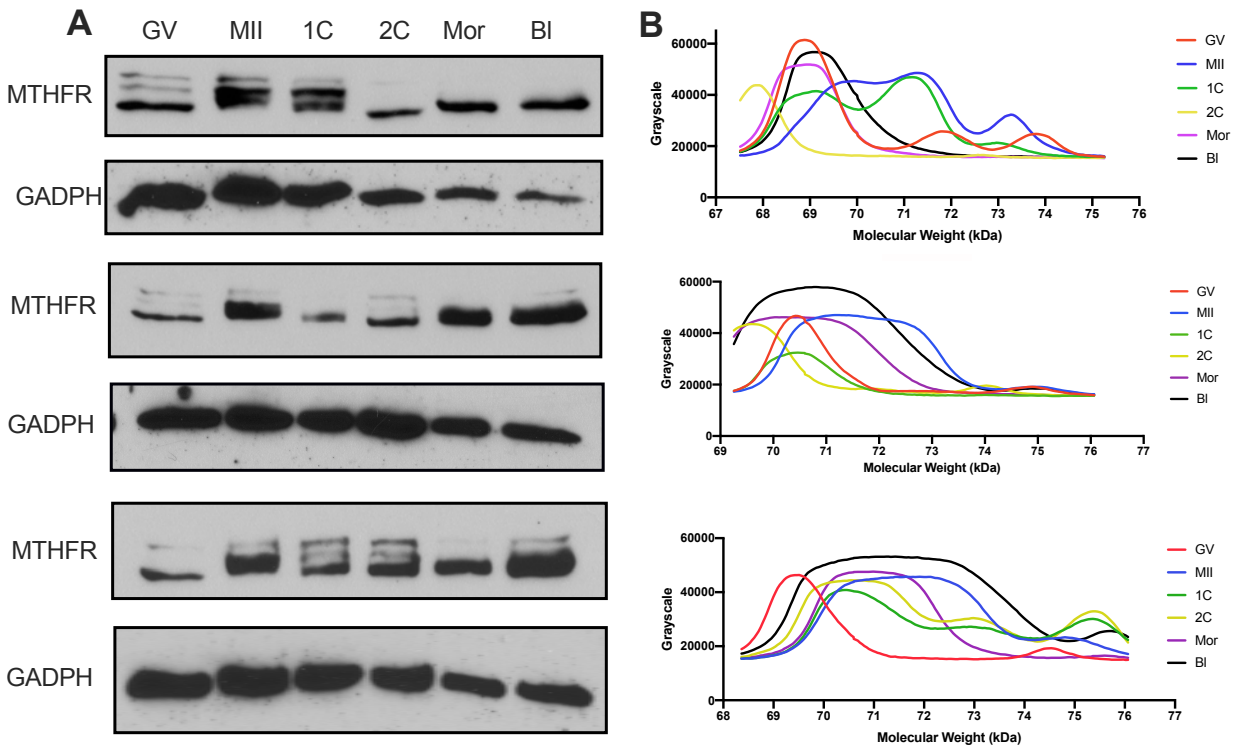

Figure 14. Developmental Series.

A) 3 independent replicates shown of 75 oocytes or embryos probed with anti-MTHFR Abcam antibody and 1:200 GADPH as a loading control. B) Molecular weight graphed against intensity of the bands on the blot for each stage loaded.

MII eggs have a higher MTHFR band on western blots that is suspected to be modified by phosphorylation and is less prominent in GVs, 2-cells and blastocysts

It was clear that the MII egg sample consistently had a band that ran at a higher MW as determined by western blot. It remained to be clarified whether this higher band was due to a different MTHFR isoform present in the MII egg or a modified version of the same isoform. The shift in MW was similar to what had previously been shown to result from phosphorylation of MTHFR in liver (Yamada et al, 2005; Megan Meredith, unpublished). To determine if it was a phosphorylation modification responsible for the band shift in MII eggs, Lambda Protein Phosphatase (LPP) treatment was used on the samples and compared to untreated samples.

GV oocytes and MII eggs were compared with or without LPP treatment (Figure 15). These blots revealed a clear shift from the dark upper band down to a lower band between the untreated and treated MII egg samples. However, no shift was visible in the GV oocytes samples. ImageJ was used to quantify these blots and the estimated molecular weight was plotted against the log10 of the grayscale values collected using the program. The same shift was visible clearly in the graphs when quantified (Figure 15). To test the significance of this finding, the difference between the molecular weights at their peak values between treated and untreated groups were compared between GV and MII and a two-tailed t-test was performed (N=3; P=0.026) (Figure 30).

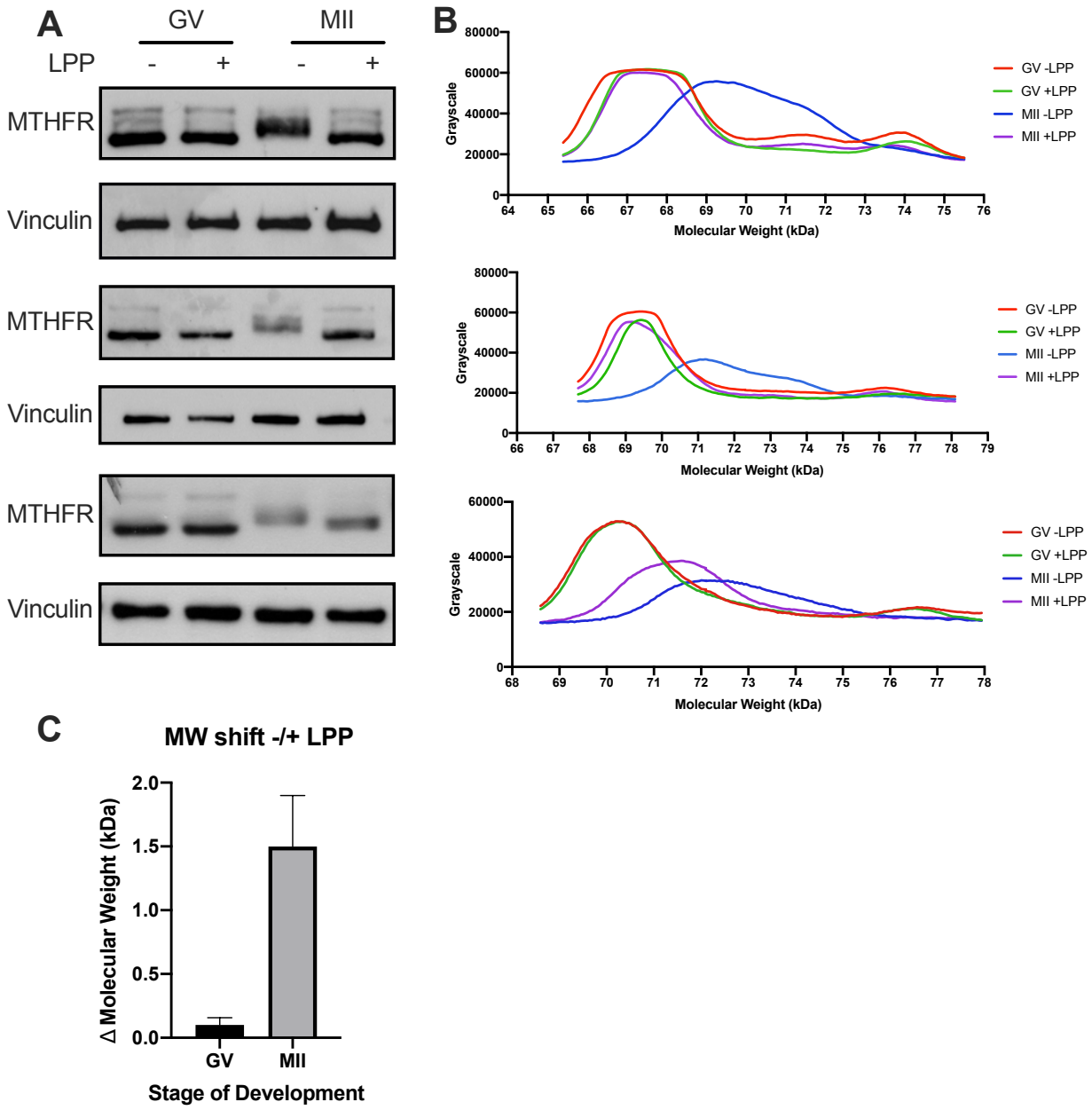

Figure 15. Lambda Protein Phosphatase (LPP) treatment on GV oocytes and MII eggs.

A) 3 independent replicates shown of 150 GV oocytes or MII eggs were pooled and separated into two groups of 75, one group as a control and one group to be treated with LPP for each of the GVs and MIIs. These groups were run on a western blot and probed with anti-MTHFR Abcam antibody and anti-vinculin as a loading control. B) The blot

was then analyzed using ImageJ and the data was graphed as molecular weight against the darkness of the bands. C) The difference between the molecular weights of the untreated and treated groups for GVs and MIIs were graphed and analyzed using a two-tailed unpaired t test and found to be significantly different (P=0.0257). This shows that the GVs are unaffected by the LPP treatment while the MIIs are affected significantly.

To determine if MTHFR in embryos was phosphorylated, the same treatment was used on 2-cell embryos and blastocysts (Figure 16). No shift was visible in either stage of development. ImageJ was used to quantify the molecular weights and the grayscale values and no changes were visible on the graph (P=0.3112). Thus, through meiotic maturation and preimplantation development, only mature MII eggs appear to have phosphorylated MTHFR.

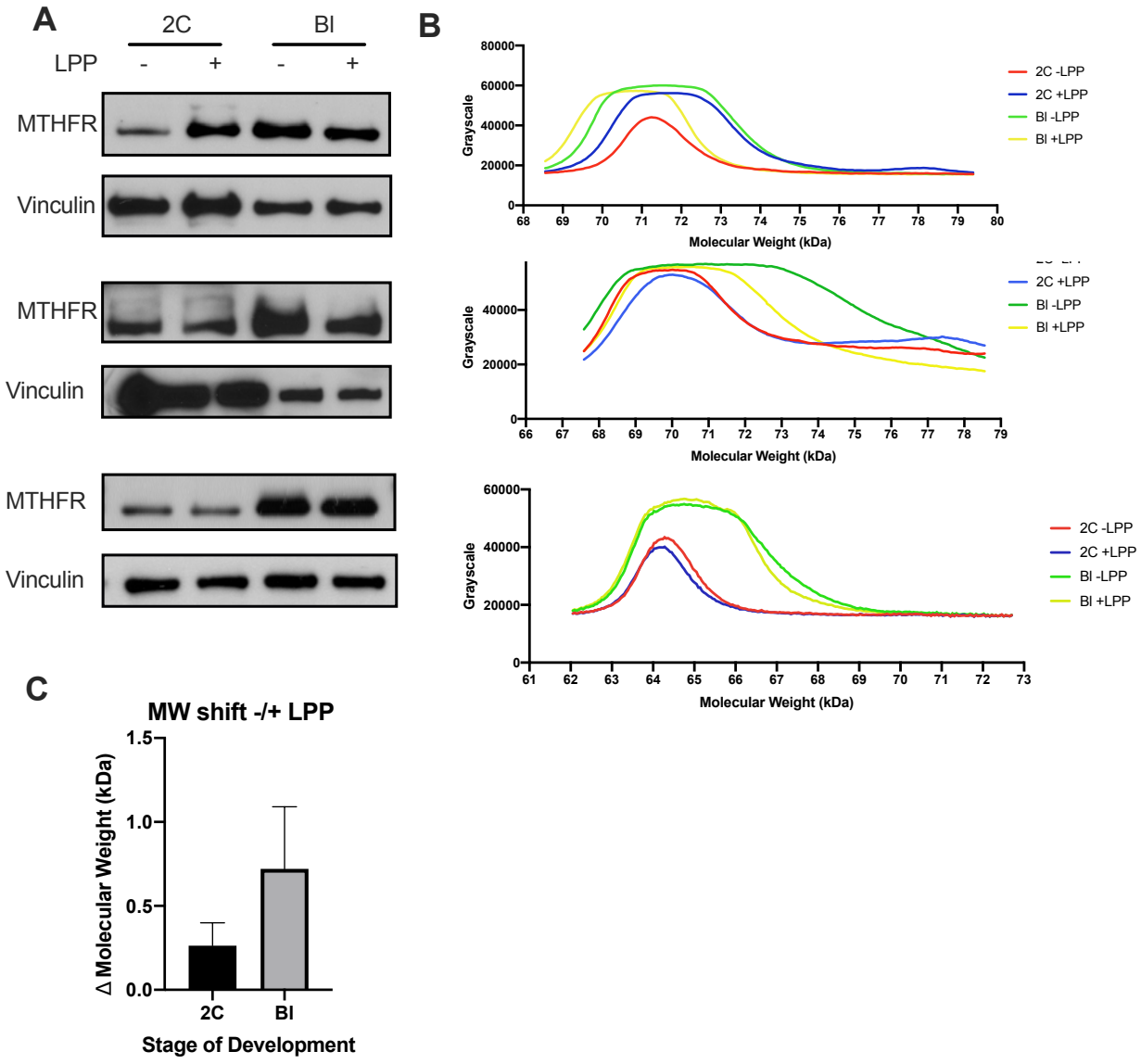

Figure 16. Lambda Protein Phosphatase (LPP) treatment on 2-cells and blastocysts.

A) 3 independent replicates shown of 150 2-cells or blastocysts were pooled and separated into two groups of 75 each, one group as a control and one group to be treated with LPP for each of the 2-cells and blastocysts. These groups were run on a western blot and probed with anti-MTHFR Abcam antibody. B) Lanes were analyzed using ImageJ and graphed by their molecular weight against the darkness of the band. No differences were

found between any groups. C) The difference between the molecular weights of the untreated and treated groups for 2 cells and blastocysts were graphed and analyzed using a two-tailed unpaired t test and found to not be different (P=0.3112). This shows that both the 2 cells and blastocysts are unaffected by the LPP treatment.

Determining the time course of MTHFR phosphorylation and dephosphorylation

Once the difference in phosphorylation between GV oocytes and MII eggs was confirmed, the *in vitro* culture of GV oocytes to MII eggs was investigated using a time course to evaluate if an upward shift occurred similar to what was found *in vivo*. To begin this set of experiments, GV oocytes were cultured in MEMα for 0 hours (i.e, not cultured), 6 hours or 20 hours and were run on a western blot (Figure 17). The 0 hour GV group looked as it did in all other experiments thus far, with a prominent lower band and faint upper bands. The 6 hour group is at a slightly larger molecular weight compared to the 0 hour group, which appears to be similar to *in vivo* MII eggs. The 20 hour group looked the same as *in vivo* collected MII eggs with only an upper band visible.

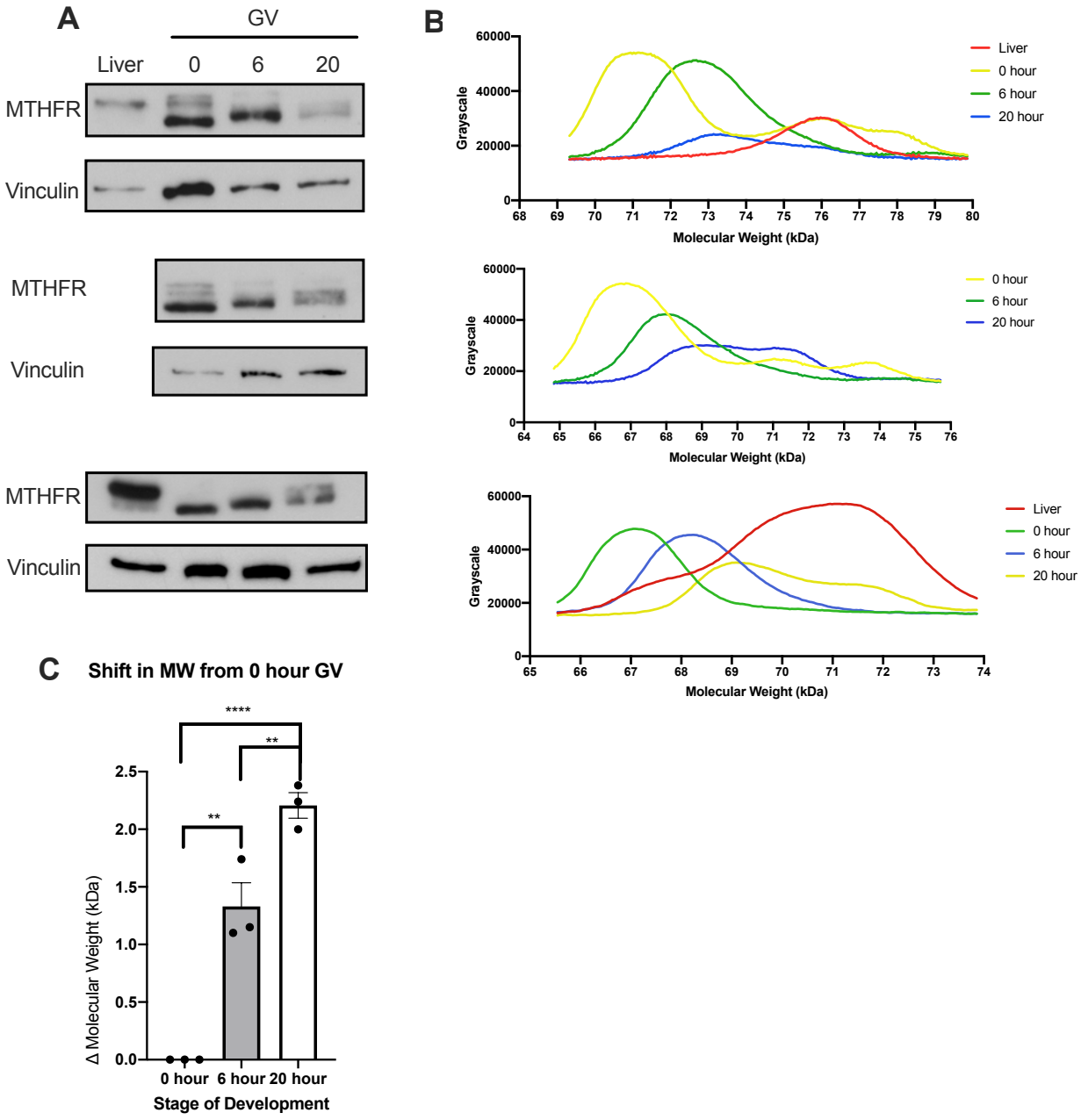

Figure 17. Time course of GV oocyte culture.

A) 3 independent replicates shown of GV oocytes cultured in MEMα for 0, 6 or 20 hours and then run in pools of 75 on a western blot and probed with anti-MTHFR Abcam antibody and anti-vinculin as a loading control. B) Lanes were analyzed using ImageJ

and graphed by molecular weight against darkness of the bands. C) The difference in molecular weight was measured from the 0 hour GV oocyte and a one way ANOVA was performed to check for statistical significance ($P<0.0001$). A post-hoc Tukey's test shows differences between all groups. The 0 hour to 6 hour group had a P-value of 0.0011. The 0 to 20 hour group had a P-value of <0.0001. The 6 hour to 20 hour group had a P-value of 0.0088.

I then sought to determine the time at which the phosphorylation occurs, focusing on the time between 0 to 6 hours. GV oocytes were cultured for 0 hours, 1 hour, 2 hours, 3 hours and 6 hours (Figure 18). The GV group at 1 hour was split into two groups: those which had undergone GVBD and those that had not. The results show a gradual change in molecular weight from the 0 hour GVs to the 6 hour GVs, the band appears to be at its highest by 3 hours and stays there until 6 hours. The GV status at 1 hour did not affect phosphorylation.

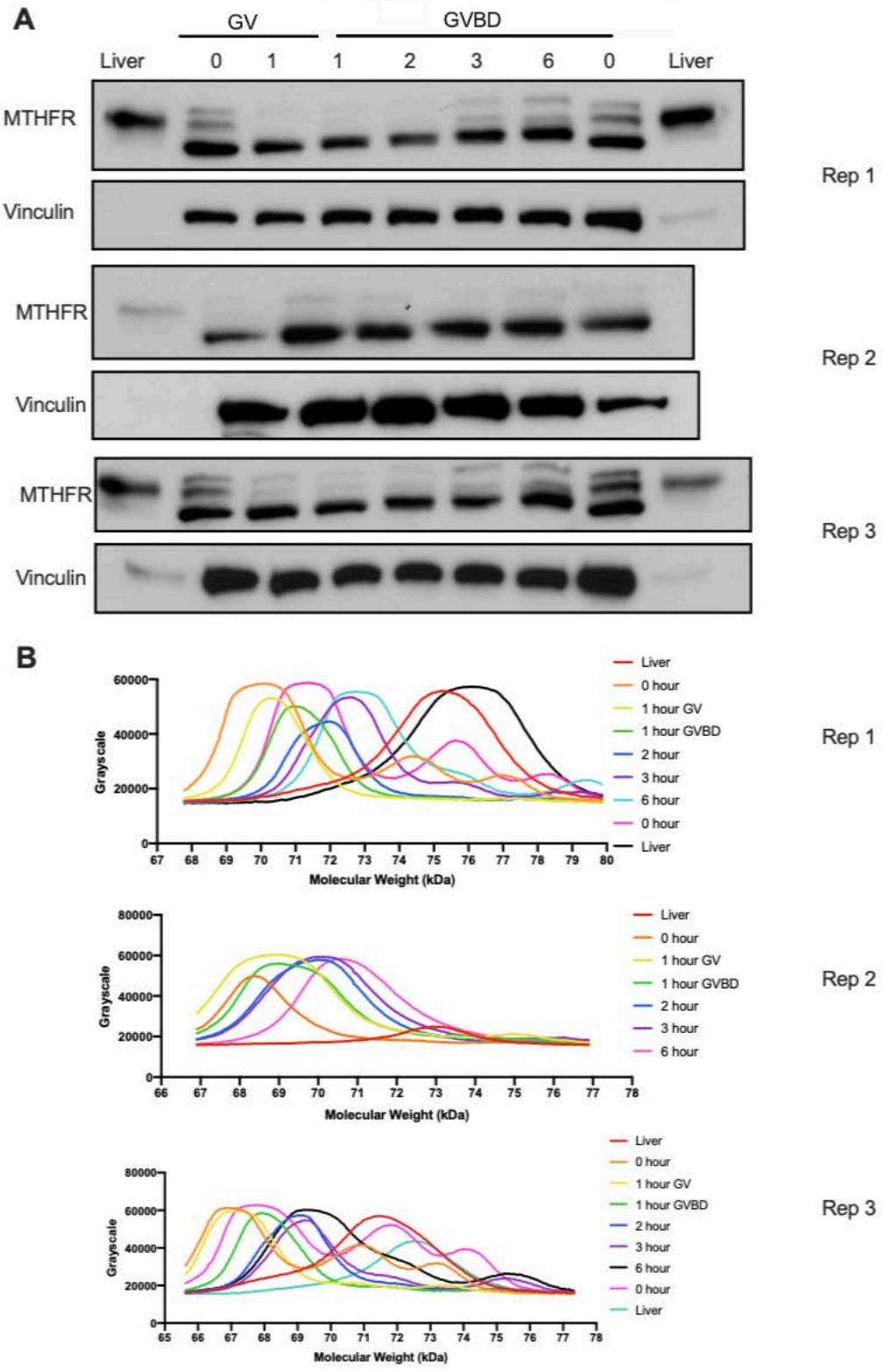
A
GV
GVBD
Liver
0
1
1
2
3
6
0
Liver
MTHFR
Vinculin
MTHFR
Vinculin
MTHFR
Vinculin
Rep 1
Rep 2
Rep 3
B
Grayscale
Molecular Weight (kDa)
Liver
0 hour
1 hour GV
1 hour GVBD
2 hour
3 hour
6 hour
0 hour
Liver
Rep 1
Rep 2
Rep 3

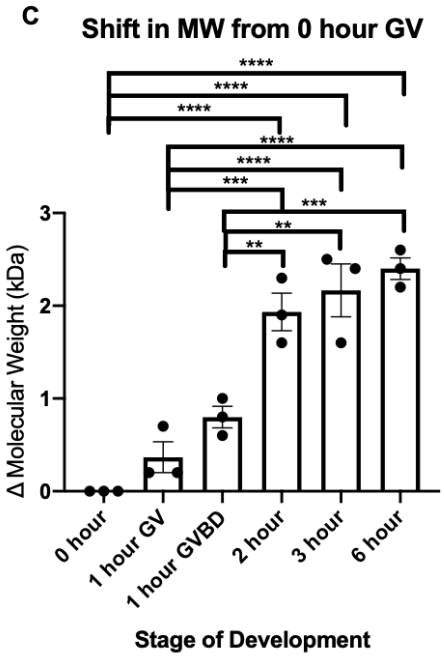

Figure 18. GV oocyte culture up to 6 hours.

A) GV oocytes cultured for 0, 1, 2, 3, or 6 hours in MEMα and then run in pools of 75 on a western blot. 1 hour culture was separated into those which had undergone GVBD and those which remained as intact GVs. Probed with anti-MTHFR Abcam antibody and anti-vinculin as a loading control. B) Lanes were analyzed using ImageJ and graphed by molecular weight against darkness of the bands. C) The difference in molecular weight was measured from the 0 hour GV oocyte and a one way ANOVA was performed to check for statistical significance ($P<0.0001$). A post-hoc Tukey's test shows differences between each the 2 hour, 3 hour and 6 hour group and the 0 hour, 1 hour GV and 1 hour GVBD groups.

It remained to be determined if the dephosphorylation from MII egg to 1-cell embryo happened just as quickly and matched the *in vivo* results. To examine this, strontium chloride was used to parthenogenetically activate MII eggs (Figure 19). The time points investigated initially were 0 hour, 2 hours, 3 hours, 6 hours and 24 hours (Figure 20). The shift appeared to happen within the first 2 hours, so another set of activations was performed and assessed the status of MTHFR by Western blot at 0 minutes, 30 minutes, 60 minutes, 90 minutes and 120 minutes post-activation (Figure 20). This showed the shift happened within the first 30 minutes. Therefore, another set of activations was performed and assessed by Western at 0 minutes, 15 minutes, 30 minutes and 60 minute post-activation. Because of the time needed to handle the eggs and change solutions, 15 minutes was the shortest interval post-activation that could be assessed. The blots revealed that the shift down towards the lower band happened within 15 minutes after the start of egg activation and thus that MTHFR is rapidly dephosphorylated upon egg activation (Figure 21).

Figure 19. MII egg activation with Strontium Chloride.

MII eggs flushed from mouse oviducts were cultured in strontium chloride-KSOM in order to parthenogenetically activate them. Photos taken at 0, 2, 3, 6 and 24 hours.

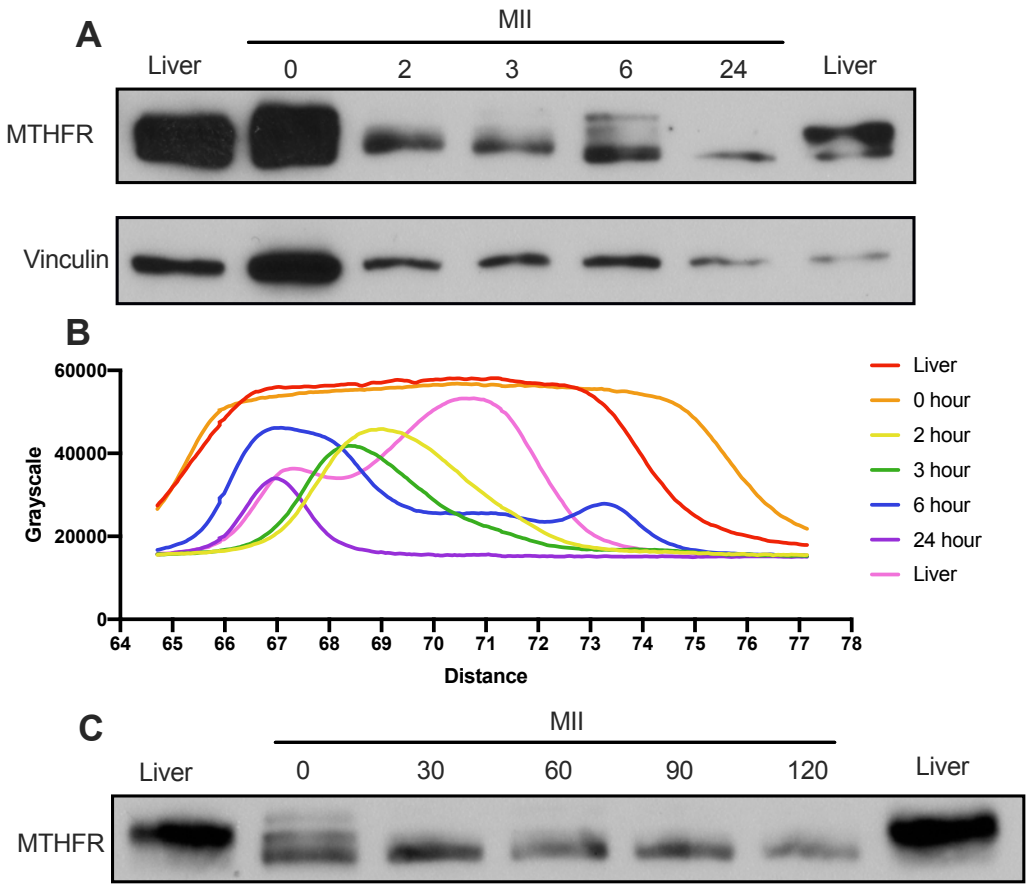

Figure 20. Time course of MII egg activation in Sr-KSOM.

A) 1 example of 2 independent replicates of MII eggs cultured in Sr-KSOM for 0, 2, 3, 6, or 24 hours pooled into groups of 75 and run on a western blot, probed with anti-MTHFR Abcam antibody and anti-vinculin as a loading control. B) Lanes were analyzed using ImageJ and plotted as molecular weight against darkness of the bands. C) MII eggs cultured in Sr-KSOM for 0, 30, 60, 90 or 120 minutes pooled into groups of 75 and run on a western blot, probed with anti-MTHFR Abcam antibody.

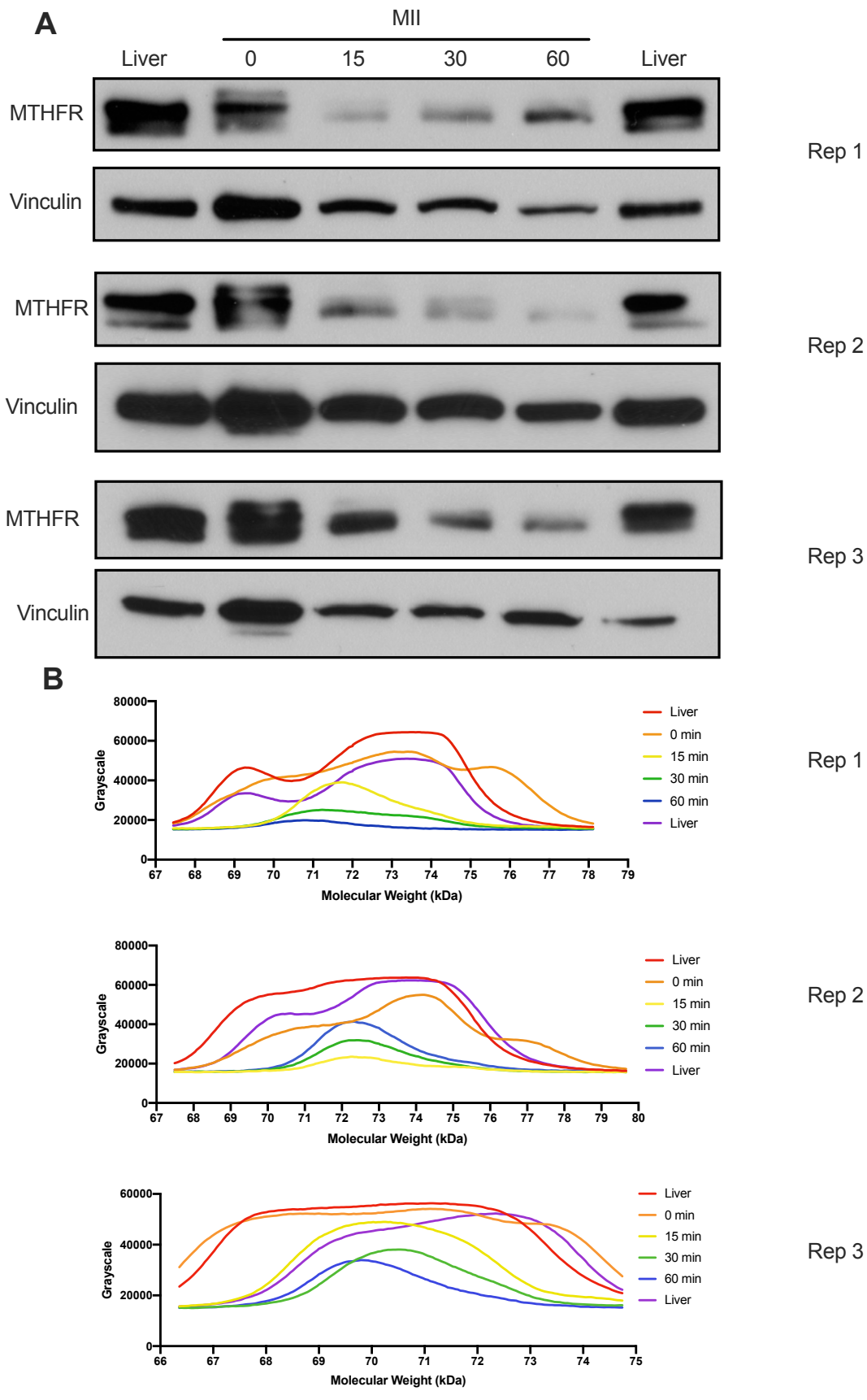
A
MII
Liver
0
15
30
60
Liver
MTHFR
Vinculin
MTHFR
Vinculin
MTHFR
Vinculin
Rep 1
Rep 2
Rep 3
B
Grayscale
Molecular Weight (kDa)
Liver
0 min
15 min
30 min
60 min
Liver
Rep 1
Rep 2
Rep 3

Figure 21. MII activation within the first hour of culture.

A) MII eggs cultured in Sr-KSOM for 0, 15, 30 or 60 minutes and pooled into groups of 75 to run on a western blot and probed with anti-MTHFR Abcam antibody. B) Lanes were analyzed using ImageJ and data was plotted as molecular weight against darkness of bands.

Inhibition of potential kinases responsible for phosphorylation show no effect at 1 μM or 10 μM concentration

Two kinases have been identified as mediating the phosphorylation of MTHFR in other cells: DYRK1A/2 and GSK3A/B (Zheng et al, 2019). Thus, these could be candidates for mediating the phosphorylation in oocytes during meiotic maturation. Inhibitors for each kinase have been characterized and are harmine for DYRK1A/2 and CHIR99021 for GSK3A/B. GV oocytes were cultured in MEMα with 1 μM of each inhibitor or DMSO as a vehicle control for ~20 hours and these samples were collected and run in a western blot to compare to GV oocytes that were not matured. If the inhibition worked, the treated samples would have a prominent, lower band similar to GV oocytes and the untreated, cultured samples with a darker, upper band as found in the control cultured oocytes that had progressed to the MII egg stage. This was not the case, since all cultured samples exhibited the normal shift upwards to the phosphorylated form of the protein, implying the kinases were not inhibited (Figure 22). A higher concentration, 10 μM, was attempted to ensure that there was enough inhibitor available. However, this too did not show any inhibition (Figure 22). To clarify if the inhibitor worked as it was supposed to, a cell line could be used to inhibit an *in vitro* phosphorylation reaction.

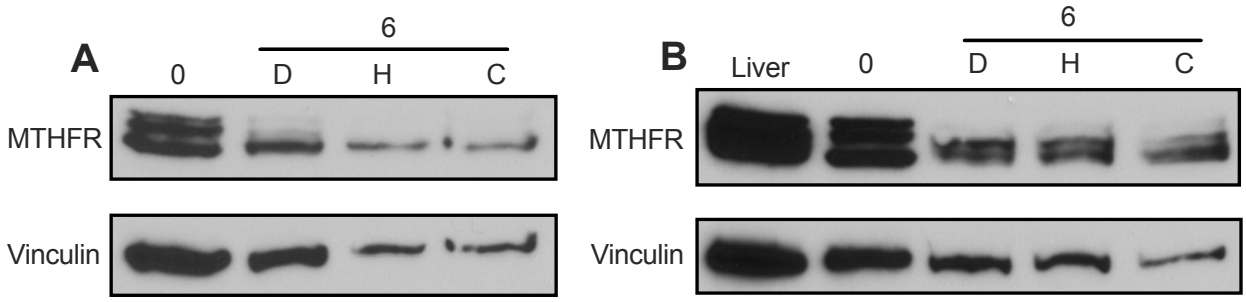

Figure 22. Kinase inhibition in GV oocytes.

A) GV oocytes were cultured in MEMα with the addition of inhibitor or DMSO as a vehicle control. Culture was in 1 μM of inhibitor and for 6 hours time. Inhibitors used were harmine for inhibition of DYRKs and CHIR99021 for inhibition of GSK3A/B. These were also compared to an untreated GV sample. B) GV oocytes were cultured in MEMα with the addition of inhibitor or DMSO as a vehicle control. Culture was in 10 μM of inhibitor for 6 hours time. 0: untreated GVs; D: cultured in DMSO; H: cultured in harmine; C: cultured in CHIR99021.

Phos-tag gel shows no differences from conventional gels between treated and untreated LPP groups of GV oocytes, MII eggs and liver samples

To further validate the idea of a phosphorylated protein at the MII stage, Phos-tag gels were acquired which contain manganese ions to selectively retain phosphate groups and isolate them from unphosphorylated proteins. The phosphorylated proteins run as they would in a regular PAGE gel, at the expected molecular weight, however since the unphosphorylated proteins do not bind to the manganese ions, they run much further than expected, at a smaller, unexpected, molecular weight. Since the most noticeable change is from the GV to MII stage, GV oocytes and MII eggs were collected and divided into untreated and treated with LPP groups and run in the Phos-tag gel, along with a liver control with and without LPP treatment. GVs treated with or without LPP were expected to show the same band pattern, but that they would be lower than expected as they are not phosphorylated. For the MII samples, two different band patterns were expected: the untreated MII group would show up at the expected molecular weight of approximately 75 kDA because it is phosphorylated and the treated MII group would look like the GV band pattern and only show a lower band which would run past the expected molecular weight as it is unphosphorylated. The liver would be expected to look similar to the MII band pattern as it has been shown to have the upper band, which implies phosphorylation. The results show no differences from conventional gels between treated and untreated samples across all of the groups, which implies that the LPP treatment does not completely dephosphorylate MTHFR, so it does not run through the gel much faster with treatment. (Figure 23).

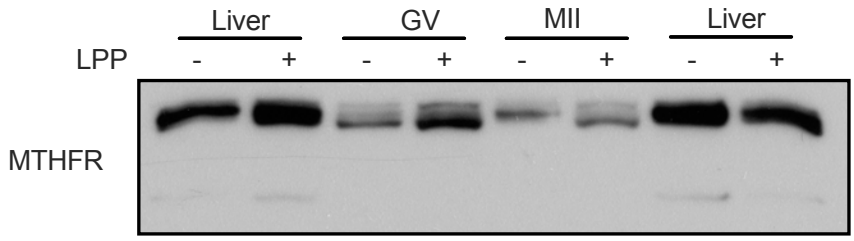

Figure 23. Phos-tag gel western blot.

150 GV oocytes or MII eggs were collected and separated into two pools of 75 each. One pool was treated with LPP and one pool was left as a control. These groups were run in a western blot and probed with anti-MTHFR Abcam antibody.

MTHFR Enzyme Assay Development

The synthesis of formaldemethone crystals began with the preparation of 0.4% dimedone solution in water and a formaldehyde solution. These two solutions were mixed together for approximately 24 hours and run through a Buchner funnel vacuum filtration. The crystals were then washed with distilled water and placed in a drying oven overnight. The dried crystals were dissolved in 99.9% methanol, an excess of water was added to re-precipitate the crystals and this was repeated twice. These were placed in a drying oven and weighed the next day for a yield calculation. The preparation had a 73% yield.

The mass spectrometry data indicated one clear, distinguishable peak to allow the experiment to proceed (Figure 24). The dilution series of formaldemethone crystals ranged from 0-100 ng dissolved in toluene. There were also quality control samples of 6.25, 18.75 and 62.5 ng. All of these samples were dried down for ~24 hours to allow for evaporation of the toluene as this could not be loaded in the LC-MS/MS system. Samples were resuspended in either 100 µL or 200 µL of 0.1% formic acid in acetonitrile:water (4:1). 10 µL of each sample was injected into the LC to allow for replicate measurements to be done. The limit of detection of the adduct was found to be ~5 ng in the 100 µL resuspension and ~10 ng in the 200 µL resuspension (Figure 24).

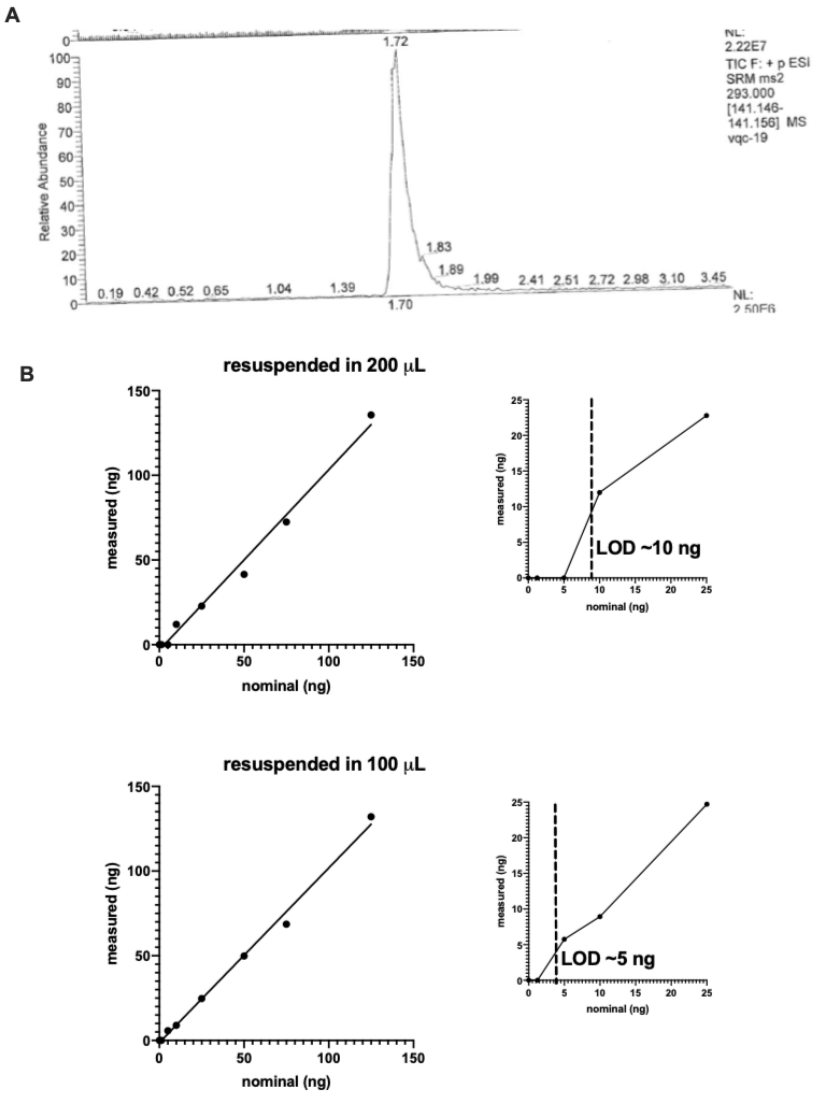

Figure 24. Limit of Detection of Formaldemethone crystals.

A) A single, distinguishable peak was found from the mass spectrometry. B) Formaldemethone crystals solubilized in toluene and then allowed to evaporate were resuspended in 100 µL or 200 µL of 0.1% formic acid in acetonitrile:water (4:1). 10 µL of each sample was loaded into the LC.

Once the limit of detection was found, wildtype and knockout liver samples were prepared for the LC system. Unfortunately, the results were unsuccessful as there is a large peak visible in all samples (blank, wildtype and knockout) where the adduct is expected to be, making it impossible to measure (Figure 25). The figures show the relative amount on the y-axis and the time it came off of the HPLC and entered the Mass Spec on the x-axis.

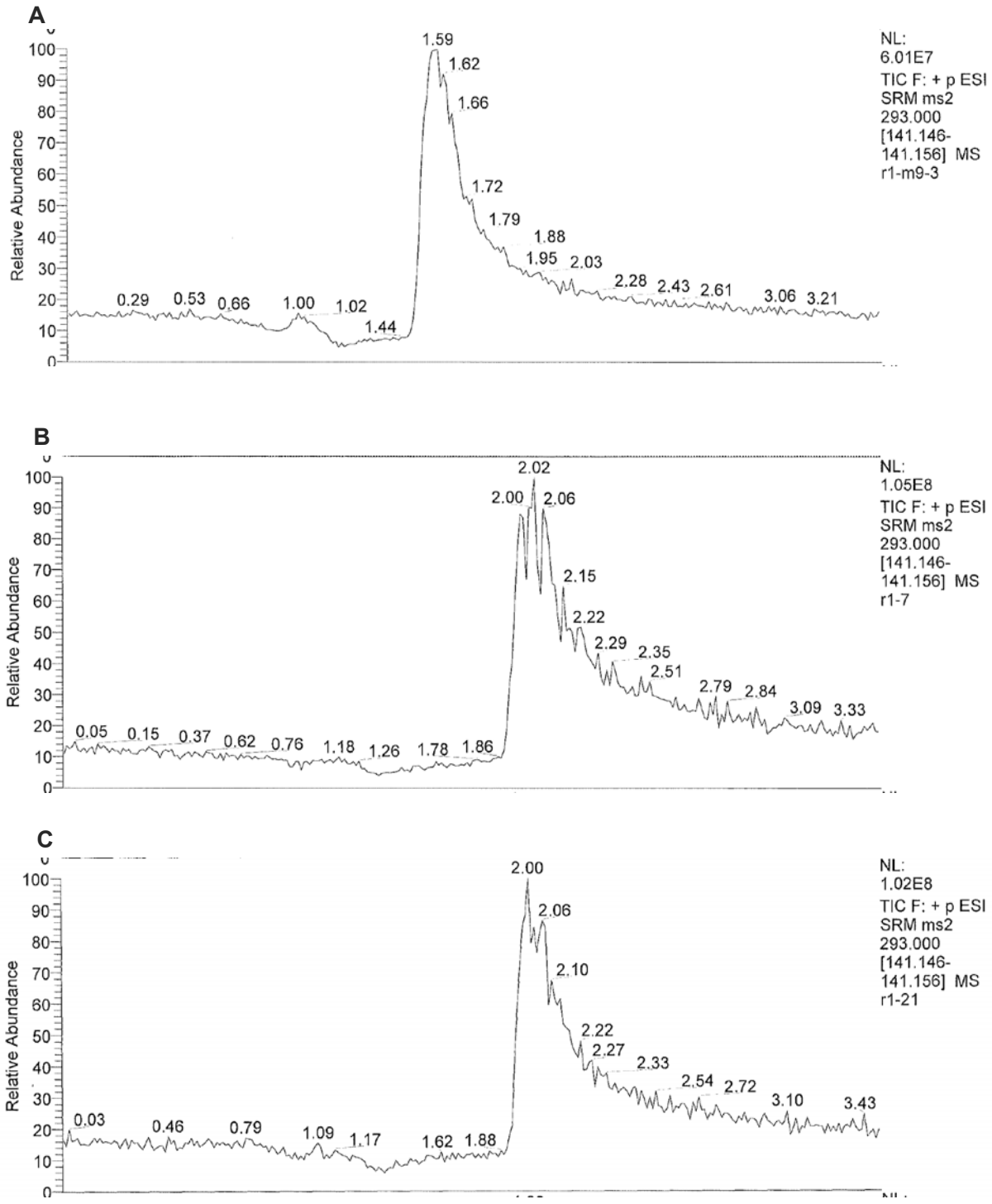

Figure 25. Traces of mouse liver sample from LC-MS/MS.

A Blank sample without liver, includes what was extracted from the reaction mix into the toluene phase. B. 200 µg of wildtype liver. C. 200 µg of knockout liver.

5. Discussion

MTHFR has previously been identified as an important contributor to the cellular methyl pool and is necessary for oocyte maturation and preimplantation embryo development in conjunction with BHMT to ensure adequate production of methionine (Appling 1991; Lee et al, 2012). The research we have done here has broadened the scope of knowledge of MTHFR and how it changes over the course of development, with regards to the isoforms that are present and phosphorylation modifications. The experiments completed in this thesis aimed to prove the presence or absence of *Mthfr* mRNA and MTHFR protein from the mature oocyte to the blastocyst stage and any changes in its phosphorylation occurring during this timeline.

Mthfr mRNA is present throughout oocyte maturation and preimplantation embryo development

qRT-PCR data shows a relatively low amount of *Mthfr* mRNA in GV oocytes, MII eggs, and 2-cell embryos and an increase in the blastocyst. The mouse bioinformatics data that we analyzed shows very little *Mthfr* mRNA in the GV and MII samples, a large increase in the 2-cells and then a slight decrease in blastocysts.

The relative expression patterns will not be identical for q-RT-PCR and RNAseq data due to the fact that the total amount of mRNA measured in the RNAseq data will not remain constant across all stages of development. Some maternal messages will be degraded during meiotic maturation while almost all messages will be degraded by the 2-cell stage. At the 2-cell stage, the embryonic RNA messages will begin to be expressed, changing the total amount of mRNA again. Therefore, in mice, total mRNA reaches a minimum at the 2-cell stage before increasing

during the remainder of preimplantation development. This affects the RNAseq data since the measurement yields a measure of a given transcript as a proportion of total transcripts. In contrast, q-RT-PCR yields an absolute measurement of transcripts that are present at each stage. This makes it difficult to make direct comparisons between the two. However, from our q-RT-PCR data, it is clear that *Mthfr* transcripts are present from the GV through blastocyst stages and increase in total amount by the blastocyst stage. From the bioinformatics analysis of the publicly-available RNAseq data, there is also a low level of *Mthfr* present from the GV stage through 1-cell embryos, and then a higher level from the 2-cell through blastocyst stages. The discrepancy between the q-RT-PCR and RNAseq data at the 2-cell stage is likely due to the level of *Mthfr* remaining essentially constant through the 2-cell stage (PCR data) and therefore being a higher proportion of the decreased total mRNA level at this stage (RNAseq data). This, however, remains to be directly shown.

Another contributing factor to the differences observed is biological variation. For the qRT-PCR data, we used CD1 mice, 4-6 weeks old, mated to BDF1 males for embryos. We super-ovulated the mice with PMSG and hCG. The timing of the injections could contribute to variations, as well as the exact timing of the collections, as there is a window of a couple of hours. Another biological variable is mouse strain. As shown in Figure 10, there is variability between CD1, CF1 and C57/Bl6 mice expressing MTHFR protein. We would expect to see similar differences at the transcript level between other strains of mice. Since the RNAseq data sets we compiled and normalized were done on various mouse strains and *in vitro* as well as *in vivo* oocyte maturation, these could be sources of biological variation as well.

Mthfr mRNA and protein is present throughout oocyte maturation and preimplantation embryo development

Mthfr mRNA was detected here using q-RT-PCR in samples of GV, MII, 2-cells and blastocysts. We used 6 oocytes per reaction for RT-PCR and 3 oocytes per reaction for q-RT-PCR with all primer sets which is more than our standard PCR protocol for most transcripts which calls for 1-2 oocytes per reaction. The protocol used here produced somewhat faint bands, but still allowed us to prove the presence of *Mthfr* mRNA across the stages. For reasons that are still unclear, *Mthfr* transcripts appear to be difficult to amplify by PCR. A previous postdoctoral fellow in the laboratory detected *Mthfr* transcripts using different sets of primers than used here and encountered the same difficulties with both mouse preimplantation embryos and liver (Baohua Zhang, unpublished data).

MTHFR protein was detected in samples of GV, MII, 1-cells, 2-cells, morulas and blastocysts with dark, solid bands at all stages using 75 oocytes or embryos. It has been previously shown that transcripts in the developing embryo are made several stages before they are translated (Israel et al, 2019). Our data are consistent with this idea, implying that the mRNA is transcribed during oocyte growth and stored so it is largely maternal in origin, allowing for high protein expression in stages that have low transcript levels. After the 2-cell stage, we hypothesize that new transcripts are being produced which explains the more prominent bands in the conventional PCR and the somewhat darker bands in the western blots, allowing for more protein translation as well. In the morula and blastocyst, there is an increased concordance between the transcript and protein expression (Israel et al, 2019), allowing for more robust translation.

In summary, MTHFR protein is present from GV stage oocytes through the blastocyst stage at levels that do not increase substantially. In contrast, *Mthfr* transcript levels are low until the 2-cell stage and then are higher during the remainder of preimplantation development. This is consistent with MTHFR being a maternal product at least until the embryonic genome is activated. Since GV oocytes already contain a high level of MTHFR protein, it was likely synthesized during oogenesis, although this remains to be shown. The MTHFR present in the later preimplantation stages may represent maternal protein that persists or may include newly-synthesized MTHFR translated from the *Mthfr* transcripts that appear after the 2-cell stage.

The pattern of MTHFR protein phosphorylation changes over the course of development

Two major isoforms of MTHFR are well established and give rise to two different size proteins (Tran et al, 2002). The predicted sizes of MTHFR A is 77 kDa and MTHFR B is 70 kDa, and each show temporal- and tissue-specific regulation (Pickell et al, 2011). Transcript variant 1 gives rise to the MTHFR A protein with 695 amino acids and transcript variant 2 translates to MTHFR B protein with 654 amino acids.

MTHFR is regulated by phosphorylation. The priming phosphorylation site is T34 in humans, T33 in mice (Yamada et al, 2005). T33 is only found in MTHFR B, as it is spliced out of MTHFR A. This means that only MTHFR B is likely able to be phosphorylated. The phosphorylated form of the protein is also the less active form (Yamada et al, 2005). After phosphorylation, MTHFR becomes more sensitive to inhibition by its ultimate product, SAM, so that the phosphorylated form has less enzyme activity for a given SAM concentration than the unphosphorylated form.

We compared the protein levels between GVs, MIIs, 1-cells, 2-cells, morulas and blastocysts to uncover any differences between the stages. We found a spread that MTHFR could usually be separated into 3 bands. We hypothesize that the lowest band is MTHFR B at approximately 70 kDA, the middle band is MTHFR B with phosphorylation modifications which migrates at approximately 72 kDA. The highest band may represent MTHFR A at 77 kDa. The molecular weight of one phosphoryl group is ~80 Da and there are 7 groups in fully-phosphorylated MTHFR, which would increase the calculated MW by ~0.56 kDa. However, phosphoproteins often migrate anomalously slowly in PAGE, exhibiting greater upward shifts than the increased MW would predict. This is true for MTHFR, where phosphorylated MTHFR migrates on gels with an apparent molecular weight between 70 kDa and 77 kDa (Yamada et al, 2005).

The pattern we see in our results shows three clear, separate bands in GVs, a loss of the lower band in the MIIs, a slight shift back down in the 1-cells and a consistent, dark lower band in the 2-cells and onwards. This implies that MTHFR may be less active in the MIIs than any other stage, as it loses the lower band, which corresponds to unphosphorylated MTHFR B. This deactivation of MTHFR could be due to a sufficient level of SAM in the oocyte. In mature oocytes, MTHFR could be less active as there is no need to produce methionine to make methyl groups. When re-methylation occurs, an increased number of methyl groups would need to be accessible so MTHFR would have to produce more 5-methylTHF and therefore be more active in its unphosphorylated form.

These results also support the qRT-PCR data we collected as there is more MTHFR B in all stages tested, compared to MTHFR A. In the MIIs, the amount of each transcript is most similar, which also lines up with the protein data. It should be emphasized, however, that further

studies would be needed to assign the bands observed on western blots to the MTHFR A and MTHFR B isoforms. Previous work in our lab attempted to knock down the MTHFR isoforms in embryos using antisense morpholinos, but this was unsuccessful (Baohua Zhang, unpublished), possibly because MTHFR protein does not turn over rapidly enough.

GVs are phosphorylated within 3 hours of culture to MII eggs

To isolate the time at which MTHFR in the GV is phosphorylated and therefore may decrease in enzyme activity, we cultured GVs in MEMα for up to 20 hours and compared the band shift between 0, 1, 2, 3, 6 and 20 hours. The shift appeared to be gradual between 1 and 3 hours, becoming fully phosphorylated by the 3-hour mark. We hypothesized that the shift occurred during GVBD, as that is when the oocyte exits meiotic arrest and begins maturation, so we separated the 1 hour group into intact GVs and GVs that had undergone GVBD. However, we saw no difference between the two. Instead, the gradual shift upwards suggests a slow addition of phosphate groups to the protein rather than an abrupt shift at GVBD. This phosphorylation would be predicted to make it gradually less active as it becomes phosphorylated, and fully deactivated by 3 hours after isolation from the follicle.

MII eggs are rapidly dephosphorylated after activation with Strontium Chloride

The western blots of oocyte and embryo stages indicated that MTHFR becomes dephosphorylated again after fertilization. To have a better understanding of the precise timeline of phosphorylation and dephosphorylation of MTHFR, we chose to parthenogenetically activate MII eggs with strontium chloride supplemented KSOM. The *in vivo* data shows three distinct bands in GV samples, the two upper bands in MII samples and a shift beginning to show the

lower band in 1-cell embryos after fertilization, but not always fully back down to the lower, dephosphorylated protein. Parthenogenetic activation allows precise control over timing unlike fertilization. The parthenogenetically activated MII eggs show a rapid dephosphorylation within the first 15 minutes after parthenogenetic activation, which was the earliest time point that could be assessed. It is not known why the dephosphorylation apparently is slower *in vivo*, where 1-cell embryos variably exhibit the higher phosphorylated bands, than in these parthenogenetically activated oocytes. It is possible that the method of parthenogenetic activation produces a stronger signal for dephosphorylation than for fertilization by sperm. Since the intracellular signaling controlling MTHFR phosphorylation in oocytes remains unknown (see below), resolving this question may have to wait until that is elucidated. Alternatively, it could simply be that one or two of the assumed 1-cell embryos in those samples were actually unfertilized, so that they still contained the phosphorylated MTHFR of MII eggs.

The kinase responsible for phosphorylating MTHFR in oocytes remains unknown

Studies on other cells and tissues have identified DYRK1A/2 and GSK3A/B as kinases that can be involved in the phosphorylation of MTHFR (Zheng et al, 2019). The use of harmine and CHIR99021, DYRK and GSK3 inhibitors respectively, with maturing oocytes did not affect their phosphorylation status implying that these are not the kinases at work in these samples or at least not the only kinases. A different experiment using a cell line could be done to prove that the inhibitors were working as they should have been and had not degraded on their delivery to the lab.

Another study has found that the surrounding amino acid sequence of MTHFR T34, the phosphorylation priming site in humans, matches with the substrate consensus motif for cyclin-

dependent kinases (CDKs) that control the cell cycle (Zhu et al, 2014). They proved that the CDK1/cyclin B complex efficiently phosphorylated HIS-tagged wild type MTHFR. However, it did not phosphorylate an MTHFR(T34A) mutant (Zhu et al, 2014), indicating that it targeted the initiating phosphorylation site at T34.

This is pertinent to the experiments here as CDK1 and cyclin B form a complex, producing MPF. MPF is not active in GV oocytes that are in prophase I arrest but is active in MI and MII eggs that are in meiotic metaphase, and then is not active again in interphase 1-cell embryos. This pattern matches the pattern we found of phosphorylation of MTHFR in oocytes and embryos. Inactive MPF allows GVs to remain arrested at prophase 1 and when activated will resume meiotic maturation. If CDK1 is the kinase responsible for phosphorylating MTHFR in oocytes, its activation at the MI and MII stages would correlate with the phosphorylation of MTHFR at these stages and its rapid dephosphorylation once it is inactivated after fertilization.

Testing this would prove difficult as any inhibition of CDK1 would not only inhibit the potential phosphorylation of MTHFR but would also block meiotic maturation, while any expression of constitutively-active MPF would induce meiotic maturation. It would be challenging to isolate the two events to prove that CDK1 is responsible for the phosphorylation in MII eggs independent of its role in control of meiotic maturation.

MTHFR Activity

Since MTHFR is less active when phosphorylated (Yamada et al, 2005) and we have proven that MTHFR is phosphorylated at MII, it would be expected that MTHFR activity would be lower in MII compared to any other stage of development investigated.

MTHFR activity has previously been measured by an activity assay where the physiological MTHFR reaction is run in reverse (Christensen et al, 1997). The reaction begins with radiolabelled methyltetrahydrofolate and, in the presence of MTHFR enzyme activity, this will be converted to methylenetetrahydrofolate, resulting in the methyl group being radiolabelled. Previous studies have done this with ^{14}C however in embryo samples, the specific activity is not high enough, so for this experiment to work ^{3}H would have to be used. The methylene group is what would need to be tritiated in the end, so the reaction would need to begin with ^{3}H-methyltetrahydrofolate. This product is no longer available commercially and we were not able to get it synthesized, therefore the activity of MTHFR could not be measured this way. This was confirmed by personal communication with Karen Christensen of the Rozen laboratory. Instead, we attempted to develop our own way of measuring MTHFR activity using LC-MS/MS.

We attempted to adapt the assay to use unlabeled 5-methylTHF and detect the product, dimedone formaldehyde adduct, by LC-MS/MS as described in the Materials and Methods section. We synthesized dimedone formaldehyde adduct and validated that it could be detected by LC-MS/MS in very low amounts. In this experiment, it was expected that the formaldehyde that would be produced by running the MTHFR reaction in reverse would then react with dimedone and would be traceable. In the radioactivity assay, this would be detected using a radiolabel and a scintillation counter. In the assay attempted here, this would be detected by extracting the dimedone formaldehyde adduct using toluene and detecting it using mass spectrometry.

When the assay was attempted using liver (comparing various amounts of MTHFR wild type and knockout liver from 1-200 ug plus controls with no liver), it became clear that one of the

components of the reaction mix produces a large peak that overlaps with the expected position of dimedone formaldehyde adduct (even in the controls) and made it impossible to detect. There was also no difference between KO and WT liver assays. Therefore, it was unfortunately not possible to confirm that MTHFR activity is lower in MII eggs than in GV oocytes as predicted by its phosphorylation pattern.

IVM/IVF clinical implications

Disruptions to one-carbon metabolism during the periconception period can impact IVF outcomes. Perturbations to the DNA methylation profile of IVF embryos can result in imprinting disorders and other negative outcomes (Odom & Segars, 2010). While it is well known that expecting mothers should have adequate levels of folate supplementation, the period at which a difference is observed in offspring is actually the periconception period, up to 8 weeks prior to conception. Without supplementation during this time, offspring can be born with hyperhomocysteinemia, elevated homocysteine levels, which can result in other comorbidities such as neural tube defects and increased aneuploidy (van der Put et al, 1998; Weisberg et al, 1998; Enciso et al, 2016). MTHFR is an important enzyme in ensuring that adequate levels of SAM be maintained, allowing methyl groups to be readily available for necessary processes. Since it is present and, except briefly in the unfertilized MII egg, in the apparently active, unphosphorylated form, this underscores the need for adequate folate to support its activity even before conception and during the preimplantation period, before pregnancies are even recognized.

Summary

When serine is consumed in the folate cycle, it donates its methyl group to THF and converts to glycine (Ikeda et al, 2012). Glycine reaches maximum levels by MII (Li et al, 2020; Tartia et al, 2009). This is largely due to the activation of glycine transport during meiotic maturation (Richard & Baltz, 2017; Tartia et al, 2009). However, this increase could also partly come from serine metabolism. Our lab has recently shown that serine is transiently transported into oocytes during MI (Zhang et al, 2020). Previous metabolomic data showed serine is low in GV oocytes, reaches its peak in MI and then decreases by MII (Li et al, 2020). This pattern is expected if serine is taken up until MTHFR becomes inactivated and SAM is no longer being produced at a high rate. High levels of glycine would also inhibit the use of serine, contributing to the suppression of SAM production and inactivation of MTHFR.

We propose that MTHFR is regulated by phosphorylation during the period of meiotic maturation in oocytes. SAM production reaches peak levels in MI oocytes and is then consumed for its methyl groups to be maintained at lower levels in the MII egg.

Since there is global DNA demethylation during the preimplantation period and remethylation begins at implantation, it would be expected that an increased amount of SAM would need to be accumulated to support this increase in methylation.

6. Conclusion

The research conducted in this thesis project shows that MTHFR changes over the course of oocyte maturation and preimplantation embryo development, with regards to mRNA and protein. *Mthfr* mRNA is present throughout and increases as the embryo develops. The protein pattern of MTHFR differs throughout the stages of development due to a phosphorylation modification. The GV oocyte is quickly phosphorylated as it matures to an MII egg and the MII egg is just as quickly dephosphorylated after activation with strontium chloride. The presence of phosphorylation was proven using LPP in assays with GV, MII, 2-cells and blastocysts.

The activity of MTHFR remains to be investigated as the present method for measuring has been unsuccessful on small samples equivalent to oocytes. The kinase responsible for this phosphorylation will also require further experiments to clarify which is responsible.

7. Literature Cited

An, Q., Sun, H., Zhang, J., Lu, Z., Peng, W., Xu, S., Zhang, Y., & Su, J. (2020). Methionine Adenosyltransferase 2β Participates in Mouse Oocyte Maturation by Regulating the MAPK Pathway. *Reprod Sci, 27*(1), 163-171. doi:10.1007/s43032-019-00015-6

Anderson, Robert, et al. "The Onset of Germ Cell Migration in the Mouse Embryo." *Mechanisms of Development*, vol. 91, no. 1, Elsevier Ireland Ltd, 2000, pp. 61–68, https://doi.org/10.1016/S0925-4773(99)00271-3.

Appling, D. R. (1991). Compartmentation of folate-mediated one-carbon metabolism in eukaryotes. *The FASEB journal*, *5*(12), 2645-2651.

Araújo, V. R., Gastal, M. O., Figueiredo, J. R., & Gastal, E. L. (2014). In vitro culture of bovine preantral follicles: a review. *Reproductive biology and endocrinology*, *12*(1), 1-14. < https://creativecommons.org/publicdomain/zero/1.0/>

Baiqiu, W., Songbin, F., Guiyin, Z., & Pu, L. (2000). Study of the relationship between psoriasis and the polymorphic site C677T of methylenetetrahydrofolate reductase. *Chinese medical sciences journal= Chung-kuo i hsueh k'o hsueh tsa chih*, *15*(2), 119-120.

Bartolomei, M. S., & Ferguson-Smith, A. C. (2011). Mammalian genomic imprinting. *Cold Spring Harbor perspectives in biology*, *3*(7), a002592.

Biggers, J. D., Bell, J. E., & Benos, D. J. (1988). Mammalian blastocyst: transport functions in a developing epithelium. *American Journal of Physiology-Cell Physiology*, *255*(4), C419-C432.

Biggers, J. D., Lawitts, J. A., & Lechene, C. P. (1993). The protective action of betaine on the deleterious effects of NaCl on preimplantation mouse embryos in vitro. *Molecular reproduction and development*, *34*(4), 380-390.

Bønaa, K. H., Njølstad, I., Ueland, P. M., Schirmer, H., Tverdal, A., Steigen, T., ... & Rasmussen, K. (2006). Homocysteine lowering and cardiovascular events after acute myocardial infarction. *New England Journal of Medicine*, *354*(15), 1578-1588.

Bonilla, L., Luchini, D., Devillard, E., & Hansen, P. J. (2010). Methionine requirements for the preimplantation bovine embryo. *Journal of Reproduction and Development*, 1006110280-1006110280.

Bottiglieri, T. (1996). Folate, vitamin B12, and neuropsychiatric disorders. *Nutrition reviews*, *54*(12), 382-390.

Boushey, C. J., Beresford, S. A., Omenn, G. S., & Motulsky, A. G. (1995). A quantitative assessment of plasma homocysteine as a risk factor for vascular disease: probable benefits of increasing folic acid intakes. *Jama*, *274*(13), 1049-1057.

Brachet, A. (1912). Development in vitro de blastodermes et de jeunes embryons de mammiferes. *C R Acad. Sci*. 55:119.

Burkart, A. D., Xiong, B., Baibakov, B., Jiménez-Movilla, M., & Dean, J. (2012). Ovastacin, a cortical granule protease, cleaves ZP2 in the zona pellucida to prevent polyspermyOvastacin cleaves ZP2 and prevents polyspermy. *The Journal of cell biology*, *197*(1), 37-44.

Cao, Y., Xu, J., Zhang, Z., Huang, X., Zhang, A., Wang, J., ... & Du, J. (2013). Association study between methylenetetrahydrofolate reductase polymorphisms and unexplained recurrent pregnancy loss: a meta-analysis. *Gene*, *514*(2), 105-111.

Cha, K. Y., Koo, J. J., Ko, J. J., Choi, D. H., Han, S. Y., & Yoon, T. K. (1991). Pregnancy after in vitro fertilization of human follicular oocytes collected from nonstimulated cycles, their culture in vitro and their transfer in a donor oocyte program. *Fertility and sterility*, *55*(1), 109-113.

Choi, S. W., & Mason, J. B. (2002). Folate status: effects on pathways of colorectal carcinogenesis. *The Journal of nutrition*, *132*(8), 2413S-2418S.

Christensen, B., Frosst, P., Lussier-Cacan, S., Selhub, J., Goyette, P., Rosenblatt, D. S., ... & Rozen, R. (1997). Correlation of a common mutation in the methylenetetrahydrofolate reductase gene with plasma homocysteine in patients with premature coronary artery disease. *Arteriosclerosis, thrombosis, and vascular biology*, *17*(3), 569-573.

Clare, C. E., Pestinger, V., Kwong, W. Y., Tutt, D. A. R., Xu, J., Byrne, H. M., Barrett, D. A., Emes, R. D., & Sinclair, K. D. (2021). Interspecific Variation in One-Carbon

Cockburn, K., & Rossant, J. (2010). Making the blastocyst: lessons from the mouse. *The Journal of clinical investigation*, *120*(4), 995-1003.

Cooper, G. M., & Hausman, R. (2000). A molecular approach. *The Cell. 2nd ed. Sunderland, MA: Sinauer Associates*.

Denomme, M. M., & Mann, M. R. (2012). Genomic imprints as a model for the analysis of epigenetic stability during assisted reproductive technologies. *Reproduction*, *144*(4), 393.

Enciso, M., Sarasa, J., Xanthopoulou, L., Bristow, S., Bowles, M., Fragouli, E., ... & Wells, D. (2016). Polymorphisms in the MTHFR gene influence embryo viability and the incidence of aneuploidy. *Human genetics*, *135*(5), 555-568.

Eppig, J. J. (2001). Oocyte control of ovarian follicular development and function in mammals. *Reproduction*, *122*(6), 829-838.

Fox, J. T., & Stover, P. J. (2008). Folate-mediated one-carbon metabolism. *Vitamins & hormones*, *79*, 1-44.

Gilula, N. B., Epstein, M. L., & Beers, W. H. (1978). Cell-to-cell communication and ovulation. A study of the cumulus-oocyte complex. *Journal of Cell Biology*, *78*(1), 58-75.

Ginsburg, M., et al. "Primordial Germ Cells in the Mouse Embryo During Gastrulation." *Development (Cambridge)*, vol. 110, no. 2, The Company of Biologists Limited, 1990, pp. 521–28.

Guerin, P., El Mouatassim, S., & Menezo, Y. (2001). Oxidative stress and protection against reactive oxygen species in the pre-implantation embryo and its surroundings. *Human reproduction update*, *7*(2), 175-189.

Harrouk, & Clarke, H. J. (1995). Mitogen-activated protein (MAP) kinase during the acquisition of meiotic competence by growing oocytes of the mouse. *Molecular Reproduction and Development*, *41*(1), 29–36. https://doi.org/10.1002/mrd.1080410106

Heape, W. (1891). III. Preliminary note on the transplantation and growth of mammalian ova within a uterine foster-mother. *Proceedings of the Royal Society of London*, *48*(292-295), 457-458.

Hudson, Q. J., Kulinski, T. M., Huetter, S. P., & Barlow, D. P. (2010). Genomic imprinting mechanisms in embryonic and extraembryonic mouse tissues. *Heredity*, *105*(1), 45-56.

Ikeda, S., Koyama, H., Sugimoto, M., & Kume, S. (2012). Roles of One-carbon Metabolism in Preimplantation Period—Effects on Short-term Development and Long-term Programming—. *Journal of Reproduction and Development*, *58*(1), 38-43.

Ikeda, S., Namekawa, T., Sugimoto, M., & Kume, S. I. (2010). Expression of methylation pathway enzymes in bovine oocytes and preimplantation embryos. *Journal of Experimental Zoology Part A: Ecological Genetics and Physiology*, *313*(3), 129-136.

Ishitani, H., Ikeda, S., Egashira, K., Sugimoto, M., Kume, S., Minami, N., & Ohta, T. (2020). Embryonic MTHFR contributes to blastocyst development. *Journal of Assisted Reproduction and Genetics*, *37*(8), 1807-1814.

Israel, S., Ernst, M., Psathaki, O. E., Drexler, H. C., Casser, E., Suzuki, Y., ... & Taher, L. (2019). An integrated genome-wide multi-omics analysis of gene expression dynamics in the preimplantation mouse embryo. *Scientific reports*, *9*(1), 1-15.

Iyer, R., & Tomar, S. K. (2009). Folate: a functional food constituent. *Journal of food science*, *74*(9), R114-R122.

Jacques, P. F., Bostom, A. G., Williams, R. R., Ellison, R. C., Eckfeldt, J. H., Rosenberg, I. H., ... & Rozen, R. (1996). Relation between folate status, a common mutation in methylenetetrahydrofolate reductase, and plasma homocysteine concentrations. *Circulation*, *93*(1), 7-9.

Jagarlamudi, K., & Rajkovic, A. (2012). Oogenesis: transcriptional regulators and mouse models. *Molecular and cellular endocrinology*, *356*(1-2), 31-39.

Kang, S. S., Passen, E. L., Ruggie, N., Wong, P. W., & Sora, H. (1993). Thermolabile defect of methylenetetrahydrofolate reductase in coronary artery disease. *Circulation*, *88*(4), 1463-1469.

Kidder, G. M., & Vanderhyden, B. C. (2010). Bidirectional communication between oocytes and follicle cells: ensuring oocyte developmental competence. *Canadian journal of physiology and pharmacology*, *88*(4), 399-413.

Kooistra, M., Trasler, J. M., & Baltz, J. M. (2013). Folate transport in mouse cumulus-oocyte complexes and preimplantation embryos. *Biology of reproduction*, *89*(3), 63-1.

Kwong, W. Y., Adamiak, S. J., Gwynn, A., Singh, R., & Sinclair, K. D. (2010). Endogenous folates and single-carbon metabolism in the ovarian follicle, oocyte and pre-implantation embryo. *Reproduction*, *139*(4), 705.

Lawitts, J. A., & Biggers, J. D. (1993). [9] Culture of preimplantation embryos. *Methods in enzymology*, *225*, 153-164.

Lee, M. B., Kooistra, M., Zhang, B., Slow, S., Fortier, A. L., Garrow, T. A., ... & Baltz, J. M. (2012). Betaine homocysteine methyltransferase is active in the mouse blastocyst and promotes inner cell mass development. *Journal of Biological Chemistry*, *287*(39), 33094-33103.

Li, L., Zhu, S., Shu, W., Guo, Y., Guan, Y., Zeng, J., ... & Wang, Q. (2020). Characterization of metabolic patterns in mouse oocytes during meiotic maturation. *Molecular cell*, *80*(3), 525-540.

Maller, J. L., Schwab, M. S., Gross, S. D., Taieb, F. E., Roberts, B. T., & Tunquist, B. J. (2002). The mechanism of CSF arrest in vertebrate oocytes. *Molecular and cellular endocrinology*, *187*(1-2), 173-178.

McKinnon, P. J., & Caldecott, K. W. (2007). DNA strand break repair and human genetic disease. *Annu. Rev. Genomics Hum. Genet.*, *8*, 37-55.

Mehlmann. (2005). Stops and starts in mammalian oocytes: recent advances in understanding the regulation of meiotic arrest and oocyte maturation. *Reproduction (Cambridge, England)*, *130*(6), 791–799. https://doi.org/10.1530/rep.1.00793

Menezo, Y., Khatchadourian, C., Gharib, A., Hamidi, J., Greenland, T., & Sarda, N. (1989). Regulation of S-adenosyl methionine synthesis in the mouse embryo. *Life sciences*, *44*(21), 1601-1609.

Meredith, M., MacNeil, A. H., Trasler, J. M., & Baltz, J. M. (2016). Growing mouse oocytes transiently activate folate transport via folate receptors as they approach full size. *Biology of reproduction*, *94*(6), 125-1.

Molyneaux, Kathleen A., et al. "Time-Lapse Analysis of Living Mouse Germ Cell Migration." *Developmental Biology*, vol. 240, no. 2, Elsevier Inc, 2001, pp. 488–98, https://doi.org/10.1006/dbio.2001.0436.

Monk, M., Boubelik, M., & Lehnert, S. (1987). Temporal and regional changes in DNA methylation in the embryonic, extraembryonic and germ cell lineages during mouse embryo development. *Development*, *99*(3), 371-382.

Odom, L. N., & Segars, J. (2010). Imprinting disorders and assisted reproductive technology. *Current opinion in endocrinology, diabetes, and obesity*, *17*(6), 517.

O'Neill, C. (1998). Endogenous folic acid is essential for normal development of preimplantation embryos. *Human Reproduction (Oxford, England)*, *13*(5), 1312-1316.

Park, J. Y., Su, Y. Q., Ariga, M., Law, E., Jin, S. L. C., & Conti, M. (2004). EGF-like growth factors as mediators of LH action in the ovulatory follicle. *Science*, *303*(5658), 682-684.

Pedersen, T., & Peters, H. (1968). Proposal for a classification of oocytes and follicles in the mouse ovary. *Reproduction*, *17*(3), 555-557.

Pepling, M. E., & Spradling, A. C. (2001). Mouse ovarian germ cell cysts undergo programmed breakdown to form primordial follicles. *Developmental biology*, *234*(2), 339-351.

Phillips, K. P., Petrunewich, M. A. F., Collins, J. L., Booth, R. A., Liu, X. J., & Baltz, J. M. (2002). Inhibition of MEK or cdc2 kinase parthenogenetically activates mouse eggs and yields the same phenotypes as Mos−/− parthenogenotes. *Developmental biology*, *247*(1), 210-223.

Pickell, L., Tran, P., Leclerc, D., Hiscott, J., & Rozen, R. (2005). Regulatory studies of murine methylenetetrahydrofolate reductase reveal two major promoters and NF-κB sensitivity. *Biochimica et Biophysica Acta (BBA)-Gene Structure and Expression*, *1731*(2), 104-114.

Pickell, L., Wu, Q., Wang, X. L., Leclerc, D., Friedman, H., Peterson, A. C., & Rozen, R. (2011). Targeted insertion of two Mthfr promoters in mice reveals temporal-and tissue-specific regulation. *Mammalian genome*, *22*(11), 635-647.

Ram, P. T., & Schultz, R. M. (1993). Reporter gene expression in G2 of the 1-cell mouse embryo. *Developmental biology*, *156*(2), 552-556.

Reik, W., & Walter, J. (2001). Genomic imprinting: parental influence on the genome. *Nature Reviews Genetics*, *2*(1), 21-32.

Richard, S., Tartia, A. P., Boison, D., & Baltz, J. M. (2017). Mouse oocytes acquire mechanisms that permit independent cell volume regulation at the end of oogenesis. *Journal of cellular physiology*, *232*(9), 2436-2446.

Rose, T. A., & Bavister, B. D. (1992). Effect of oocyte maturation medium on in vitro development of in vitro fertilized bovine embryos. *Molecular reproduction and development*, *31*(1), 72-77.

Rossant, J., & Tam, P. P. (2009). Blastocyst lineage formation, early embryonic asymmetries and axis patterning in the mouse.

SanMiguel, J. M., & Bartolomei, M. S. (2018). DNA methylation dynamics of genomic imprinting in mouse development. *Biology of reproduction*, *99*(1), 252-262

Schwahn, B., & Rozen, R. (2001). Polymorphisms in the methylenetetrahydrofolate reductase gene. *American journal of pharmacogenomics*, *1*(3), 189-201.

Smallwood, S. A., Tomizawa, S. I., Krueger, F., Ruf, N., Carli, N., Segonds-Pichon, A., ... & Kelsey, G. (2011). Dynamic CpG island methylation landscape in oocytes and preimplantation embryos. *Nature genetics*, *43*(8), 811-814

Sinclair, K. D., Allegrucci, C., Singh, R., Gardner, D. S., Sebastian, S., Bispham, J., ... & Young, L. E. (2007). DNA methylation, insulin resistance, and blood pressure in offspring determined by

maternal periconceptional B vitamin and methionine status. *Proceedings of the National Academy of Sciences*, *104*(49), 19351-19356.

Steptoe, P. C., & Edwards, R. G. (1978). Birth after the reimplantation of a human embryo. *The Lancet*, *312*(8085), 366.

Tartia, A. P., Rudraraju, N., Richards, T., Hammer, M. A., Talbot, P., & Baltz, J. M. (2009). Cell volume regulation is initiated in mouse oocytes after ovulation.

Tran, P., Leclerc, D., Chan, M., Pai, A., Hiou-Tim, F., Wu, Q., ... & Rozen, R. (2002). Multiple transcription start sites and alternative splicing in the methylenetetrahydrofolate reductase gene result in two enzyme isoforms. *Mammalian genome*, *13*(9), 483-492.

Tunquist, B. J., & Maller, J. L. (2003). Under arrest: cytostatic factor (CSF)-mediated metaphase arrest in vertebrate eggs. *Genes & development*, *17*(6), 683-710.

Vanderhyden, B. C., Caron, P. J., Buccione, R., & Eppig, J. J. (1990). Developmental pattern of the secretion of cumulus expansion-enabling factor by mouse oocytes and the role of oocytes in promoting granulosa cell differentiation. *Developmental biology*, *140*(2), 307-317.

van der Put, N. M., Gabreëls, F., Stevens, E. M., Smeitink, J. A., Trijbels, F. J., Eskes, T. K., ... & Blom, H. J. (1998). A second common mutation in the methylenetetrahydrofolate reductase

gene: an additional risk factor for neural-tube defects?. *The American Journal of Human Genetics*, *62*(5), 1044-1051.

Vasku, V., Bienertova-Vasku, J., Necas, M., & Vasku, A. (2009). MTHFR (methylenetetrahydrofolate reductase) C677T polymorphism and psoriasis. *Clinical and experimental medicine*, *9*(4), 327-331.

Walls, M. L., & Hart, R. J. (2018). In vitro maturation. *Best practice & research Clinical obstetrics & gynaecology*, *53*, 60-72.

Wassarman, P. M., Schultz, R. M., Letourneau, G. E., LaMarca, M. J., Josefowicz, W. J., & Bleil, J. D. (1979). Meiotic maturation of mouse oocytes in vitro. In *Ovarian follicular and corpus luteum function* (pp. 251-268). Springer, Boston, MA.

Wei, B., Xu, Z., Ruan, J., Zhu, M., Jin, K., Zhou, D., ... & Wang, Z. (2012). MTHFR 677C> T and 1298A> C polymorphisms and male infertility risk: a meta-analysis. *Molecular biology reports*, *39*(2), 1997-2002.

Weisberg, I., Tran, P., Christensen, B., Sibani, S., & Rozen, R. (1998). A second genetic polymorphism in methylenetetrahydrofolate reductase (MTHFR) associated with decreased enzyme activity. *Molecular genetics and metabolism*, *64*(3), 169-172.

Welch, G. N., Upchurch Jr, G., & Loscalzo, J. (1997). Hyperhomocyst (e) inemia and Atherothrombosis a. *Annals of the New York Academy of Sciences*, *811*(1), 48-59.

Welch, G. N., & Loscalzo, J. (1998). Homocysteine and atherothrombosis. *New England journal of medicine*, *338*(15), 1042-1050

Wu, W., Shen, O., Qin, Y., Lu, J., Niu, X., Zhou, Z., ... & Wang, X. (2012). Methylenetetrahydrofolate reductase C677T polymorphism and the risk of male infertility: a meta-analysis. *International journal of andrology*, *35*(1), 18-24.

Yamada, K., Strahler, J. R., Andrews, P. C., & Matthews, R. G. (2005). Regulation of human methylenetetrahydrofolate reductase by phosphorylation. *Proceedings of the National Academy of Sciences*, *102*(30), 10454-10459.

Yanagimachi, R. (1994). Fertility of mammalian spermatozoa: its development and relativity. *Zygote*, *2*(4), 371-372.

Zhang, B., Denomme, M. M., White, C. R., Leung, K. Y., Lee, M. B., Greene, N. D., ... & Baltz, J. M. (2015). Both the folate cycle and betaine-homocysteine methyltransferase contribute methyl groups for DNA methylation in mouse blastocysts. *The FASEB Journal*, *29*(3), 1069-1079.

Zhang, H., McClatchie, T., & Baltz, J. M. (2020). l-Serine transport in growing and maturing mouse oocytes. *Journal of cellular physiology*, *235*(11), 8585-8600.

Zhang, M., Su, Y. Q., Sugiura, K., Xia, G., & Eppig, J. J. (2010). Granulosa cell ligand NPPC and its receptor NPR2 maintain meiotic arrest in mouse oocytes. *Science*, *330*(6002), 366-369.

Zheng, W., Nagaraju, G., Liu, Z., & Liu, K. (2012). Functional roles of the phosphatidylinositol 3-kinases (PI3Ks) signaling in the mammalian ovary. *Molecular and cellular endocrinology*, *356*(1-2), 24-30.

Zheng, Y., Ramsamooj, S., Li, Q., Johnson, J. L., Yaron, T. M., Sharra, K., & Cantley, L. C. (2019). Regulation of folate and methionine metabolism by multisite phosphorylation of human methylenetetrahydrofolate reductase. *Scientific reports*, *9*(1), 1-11.

Zhu, B., Xiahou, Z., Zhao, H., Peng, B., Zhao, H., & Xu, X. (2014). MTHFR promotes heterochromatin maintenance. *Biochemical and biophysical research communications*, *447*(4), 702-706.

Appendix A

Attempts 3-6 in Table 7 used liver protein and a dilution series of the primary antibody including, 1:500, 1:1000, 1:1500 and 1:2000 all made in 5% milk, while keeping all other steps the same. This still produced an undesirable result due to the level of background (Figure 27).

Next, for attempts 7 and 8, extra washes in TBST were added after incubation in the secondary antibody to see if that would eliminate the very dark background. This was attempted with both a 10% acrylamide gel and a 12% acrylamide gel, giving similar results. It appeared to improve, but not entirely remove, the dark background.

To ensure that all the other reagents were working optimally apart from the primary antibody, lanes of the same liver sample were prepared using the standard protocol for attempts 9 and 10 from Table 7, and the membrane was cut into two pieces and each probed with a different primary antibody: the Sigma anti-MTHFR or anti-GAPDH that is commonly used as a loading control. The GAPDH antibody gave a clean band at the expected MW. This indicated the reagents were working at least for GAPDH detection and that the problem with the background was likely specific to the Sigma MTHFR antibody.

For attempts 11 and 12 from Table 7, the enzymatic reaction that produces the luminescence was manipulated. Two options available apart from the ECL Prime used in the standard protocol were ECL and Super Signal West Fento Maximum Sensitivity Substrate. The ECL appeared to help lighten the blot, however not enough for it to be clearly legible.

As the difference in ECL methods had looked promising, I changed conditions used after development with the Super Signal West Fento Maximum Sensitivity Substrate to see if it was possible to lighten the dark background. This included attempts 13 and 14 from Table 7. The membrane was washed in TBST for 15 minutes and developed again, this time with regular

ECL. This gave an interesting result where the background was dark but the bands of protein were light; this implies that the membrane was not being blocked adequately. The membrane was then washed for 15 minutes in TBST and then re-blocked, this time with 5% BSA overnight at 4°C. The membrane was not re-probed with antibody and developed immediately following the overnight block in BSA, which should have produced a blank film, however it was still dark and therefore still not blocked properly.

With this insight regarding the membrane not being blocked effectively for use with the Sigma anti-MTHFR antibody, a new gel was prepared using the standard western blot protocol (this is attempt 15 in Table 7). It was blocked with 5% milk using new Tween from another lab that had a working western blot protocol and developed following the blocking step. A blank film resulted as expected . Next, the same membrane was incubated with the primary Sigma anti-MTHFR antibody overnight and developed again, which resulted again in a blank film as expected (Attempt 16).

Thus, it appeared to be an issue with the secondary antibody, as all the steps leading up to the incubation with secondary antibody appeared as expected. I gave an aliquot of the Millipore anti-MTHFR antibody to another lab to use on their own membrane, with their own secondary antibody and this gave a clean result. At the same time, I tested the secondary antibody in our lab with a different primary antibody for attempt 17 in Table 7, anti-CHDH, and it appeared to work. The next logical step was to take the secondary antibody from the other lab and use it on my membrane. However, this still produced a very dark background when used in combination with the Sigma anti-MTHFR primary antibody. This led me to believe that the issue was a signal-to-noise problem for MTHFR, as the membrane from the other lab had more than 10 times the amount of protein loaded per lane and had developed without issue. New secondary antibody

was then obtained and tried with the same protocol for attempt #19 from Table 7. However, the new secondary developed dark background again . I then compared the three available secondary antibodies in attempts 19, 20 and 21 in Table 7, from two other labs and the new bottle our lab obtained, on three pieces cut from the same membrane, and all three turned out to have dark background again.

I then altered the blocking step of the protocol. For attempts 22 and 23, I ran another blot with 1 µg and 5 µg of liver protein loaded. The blot with 1 µg of liver was blocked with 5% milk and the blot with 5 µg of liver was blocked with 5% BSA. Upon developing these blots, both looked clean enough to move forward with either of the protocols. As the blots looked clean, for attempt #24, I used 5 µg of liver and 100 GVs to ensure the protocol would be satisfactory for the oocyte samples and developed a dark background again. To address the blocking issue for attempts 25-27, I obtained new milk and also tried to block with 2% ECL blocking solution or 1% BSA. All three attempts developed with dark background. I also tried fish skin gelatin which is sometimes used as a blocking agent. This is shown as attempts 28-43 in Table 7. I attempted to use this fish skin gelatin as a blocking agent and also diluted the primary antibody in this. I tried each combination on a nitrocellulose membrane and a PVDF membrane, some of which had dark background while some had no visible bands. I tried further optimizations with more concentrated fish skin gelatin block and less antibody, all of which did not produce a presentable blot. With the attempts on a PVDF membrane, I included a standard protocol with a 5% milk block and the primary antibody diluted in milk as our standard protocol used on nitrocellulose membranes.

I then attempted to systematically vary the dilutions of primary and secondary antibodies with the Sigma antibody, this accounts for attempts 44-66. This ranged from 1:2000 to 1:8000

for the primary antibody and 1:5000 to 1:100000 for the secondary antibody, none of which were successful in developing into a clean film with acceptable bands for MTHFR (Figure 28). Some of the dilutions showed potential as they were less dark, but the MTHFR bands were also very difficult to see on those, providing further evidence that the Sigma antibody had poor signal-to-noise. Next, I tried the variation of the dilutions that looked the best which was 1:4000 primary with 1:20000 secondary, but only incubated with secondary for 15 or 30 minutes. This was still unsuccessful (Figure 28).

The very extensive attempts to get the Sigma anti-MTHFR antibody to work similarly to the original Rozen antibody thus failed. I concluded that Sigma's Millipore-produced version of the Rozen antibody was not suitable for use with the small samples that can be obtained with mouse oocytes. This appeared due to a low signal-to-noise when using it with any secondary, which could not be remedied by changing reagents, different methods of blocking, different membranes, or different reagents for bioluminescence. The attempts would appear to have been justified, since previous work had been done in the laboratory using the Rozen anti-MTHFR, it had been extensively validated by the Rozen and Trasler groups at McGill (Chen et al., 2001), and it was previously shown to be specific using tissues and oocytes obtained from *Mthfr* knockout mice in our laboratory (Baohua Zhang, unpublished).

I then turned to testing other commercially available antibodies. I first tested anti-MTHFR antibody from GeneTex (Cat. No. GTX100535), in attempt #67. However, the GeneTex antibody showed several non-specific bands, so that was eliminated as a contender.

The next antibody tested was from Abcam (Cat. No. ab203786), which was attempt #68. I tested this antibody with wildtype and knockout liver lysate using our standard western blot protocol and it produced exactly what we were expecting: dark bands in the wildtype liver

sample but no bands visible in the knockout liver sample. Furthermore, the background was acceptable. I was then able to start optimizing the protocol using this Abcam antibody with oocytes (attempt #69) and to stop attempts at salvaging the Sigma anti-MTHFR antibody.

Table 7. Trouble-shooting the MTHFR antibody, listing all modifications attempted. Primary and secondary antibodies were made in 5% milk unless otherwise stated. Rozen Ab: the original anti-MTHFR antibody that the Rozen group produced and sent aliquots to our laboratory. Sigma Ab: the anti-MTHFR antibody from Sigma that is stated to be the same antibody as the Rozen antibody.

Attempt	Sample	Gel % acrylamide	Membrane	Blocking Agent	Primary Antibody	Secondary Antibody	Visualization Agent
1	Liver	10	Nitrocellulose	5% milk	1:2000 Rozen Ab	1:5000 Biorad	ECL Prime
2	Liver	10	Nitrocellulose	5% milk	1:2000 Sigma Ab	1:5000 Biorad	ECL Prime
3	Liver	10	Nitrocellulose	5% milk	1:500 Sigma Ab	1:5000 Biorad	ECL Prime
4	Liver	10	Nitrocellulose	5% milk	1:1000 Sigma Ab	1:5000 Biorad	ECL Prime
5	Liver	10	Nitrocellulose	5% milk	1:1500 Sigma Ab	1:5000 Biorad	ECL Prime
6	Liver	10	Nitrocellulose	5% milk	1:2000 Sigma Ab	1:5000 Biorad	ECL Prime
7	Liver	10	Nitrocellulose	5% milk	1:2000 Sigma Ab	1:5000 Biorad + extra washes	ECL Prime
8	Liver	12	Nitrocellulose	5% milk	1:2000 Sigma Ab	1:5000 Biorad + extra washes	ECL Prime
9	Liver	12	Nitrocellulose	5% milk	1:2000 Sigma Ab	1:5000 Biorad	ECL Prime

10	Liver	12	Nitrocellulose	5% milk	1:200 GADPH	1:5000 Biorad	ECL Prime
11	Liver	12	Nitrocellulose	5% milk	1:2000 Sigma Ab	1:5000 Biorad + extra washes	ECL
12	Liver	12	Nitrocellulose	5% milk	1:2000 Sigma Ab	1:5000 Biorad	Super Signal West Fento Maximum Sensitivity Substrate
13	Liver	12	Nitrocellulose	5% milk	1:2000 Sigma Ab	1:5000 Biorad	Washed + ECL
14	Liver	12	Nitrocellulose	5% milk Then 5% BSA	1:2000 Sigma Ab	1:5000 Biorad	None
15	Liver	12	Nitrocellulose	5% milk + NEW TBST	None	None	ECL Prime
16	Liver	12	Nitrocellulose	5% milk	1:2000 Sigma Ab	None	ECL Prime
17	Liver	12	Nitrocellulose	5% milk	1:1000 ProteinTech anti-CHDH	1:5000 Biorad	ECL Prime
18	Liver	12	Nitrocellulose	5% milk	1:2000 Sigma Ab	Secondary from lab on third floor	ECL Prime

19	Liver	12	Nitrocellulose	5% milk	1:2000 Sigma Ab	NEW 1:5000 Biorad	ECL Prime
20	Liver	12	Nitrocellulose	5% milk	1:2000 Sigma Ab	1:5000 Jackson Immunoresearch Cat. No. 111-035-003	ECL Prime
21	Liver	12	Nitrocellulose	5% milk	1:2000 Sigma Ab	1:5000 Jack Immunoresearch Cat. No. 111-035-144	ECL Prime
22	Liver	12	Nitrocellulose	5% BSA	1:2000 Sigma Ab	1:5000 Biorad	ECL Prime
23	Liver	12	Nitrocellulose	5% milk	1:2000 Sigma Ab	1:5000 Biorad	ECL Prime
24	Liver and 100xGV	12	Nitrocellulose	5% milk	1:2000 Sigma Ab	1:5000 Biorad	ECL Prime
25	Liver	12	Nitrocellulose	NEW 5% milk	1:2000 Sigma Ab	1:5000 Biorad	ECL Prime

26	Liver	12	Nitrocellulose	2% ECL	1:2000 Sigma Ab	1:5000 Biorad	ECL Prime
27	Liver	12	Nitrocellulose	1% BSA	1:2000 Sigma Ab	1:5000 Biorad	ECL Prime
28	Liver	12	PVDF	9% fish gelatin	1:4000 Sigma Ab in 0.9% fish gelatin	1:20000 Cell Signalling	ECL Prime
29	Liver	12	PVDF	9% fish gelatin	1:4000 Sigma Ab in TBST	1:20000 Cell Signalling	ECL Prime
30	Liver	12	PVDF	9% fish gelatin	1:4000 Sigma Ab	1:20000 Cell Signalling	ECL Prime
31	Liver	12	PVDF	5% milk	1:4000 Sigma Ab	1:20000 Cell Signalling	ECL Prime
32	Liver	12	Nitrocellulose	9% fish gelatin	1:4000 Sigma Ab in 0.9% fish gelatin	1:20000 Cell Signalling	ECL Prime

33	Liver	12	Nitrocellulose	9% fish gelatin	1:4000 Sigma Ab in TBST	1:20000 Cell Signalling	ECL Prime
34	Liver	12	Nitrocellulose	9% fish gelatin	1:4000 Sigma Ab	1:20000 Cell Signalling	ECL Prime
35	Liver	12	Nitrocellulose	5% milk	1:4000 Sigma Ab	1:20000 Cell Signalling	ECL Prime
36	Liver	12	PVDF	5% milk	1:2000 Sigma Ab	1:5000 Cell Signalling	Clarity Max
37	Liver	12	PVDF	5% milk	1:2000 Sigma Ab	1:10000 Cell Signalling	Clarity Max
38	Liver	12	PVDF	20% fish gelatin	1:2000 Sigma Ab in 2% fish gelatin	1:5000 Cell Signalling	Clarity Max
39	Liver	12	PVDF	20% fish gelatin	1:2000 Sigma Ab in TBST	1:5000 Cell Signalling	Clarity Max

40	Liver	12	Nitrocellulose	20% fish gelatin	1:4000 Sigma Ab in 2% fish gelatin	1:5000 Cell Signalling	Clarity Max
41	Liver	12	Nitrocellulose	20% fish gelatin	1:2000 Sigma Ab in 2% fish gelatin	1:5000 Cell Signalling	Clarity Max
42	Liver	12	Nitrocellulose	20% fish gelatin	1:2000 Sigma Ab in TBST	1:5000 Cell Signalling	Clarity Max
43	Liver	12	Nitrocellulose	20% fish gelatin	1:4000 Sigma Ab in TBST	1:5000 Cell Signalling	Clarity Max
44	Liver	12	Nitrocellulose	5% milk	1:2000 Sigma Ab	1:5000 Biorad	ECL Prime
45	Liver	12	Nitrocellulose	5% milk	1:2000 Sigma Ab	1:10000 Biorad	ECL Prime
46	Liver	12	Nitrocellulose	5% milk	1:2000 Sigma Ab	1:15000 Biorad	ECL Prime

47	Liver	12	Nitrocellulose	5% milk	1:2000 Sigma Ab	1:20000 Biorad	ECL Prime
48	Liver	12	Nitrocellulose	5% milk	1:4000 Sigma Ab	1:5000 Biorad	ECL Prime
49	Liver	12	Nitrocellulose	5% milk	1:4000 Sigma Ab	1:10000 Biorad	ECL Prime
50	Liver	12	Nitrocellulose	5% milk	1:4000 Sigma Ab	1:15000 Biorad	ECL Prime
51	Liver	12	Nitrocellulose	5% milk	1:4000 Sigma Ab	1:20000 Biorad	ECL Prime
52	Liver	12	Nitrocellulose	5% milk	1:4000 Sigma Ab	1:20000 Biorad + extra washes	ECL Prime
53	Liver	12	Nitrocellulose	5% milk	1:4000 Sigma Ab	1:20000 Biorad 45 min + extra washes	ECL Prime
54	Liver	12	Nitrocellulose	5% milk	1:4000 Sigma Ab	1:50000 Biorad	ECL Prime

55	Liver	12	Nitrocellulose	5% milk	1:4000 Sigma Ab	1:100000 Biorad	ECL Prime
56	Liver	12	Nitrocellulose	5% milk	1:4000 Sigma Ab	1:15000 Biorad	ECL Prime
57	Liver	12	Nitrocellulose	5% milk	1:8000 Sigma Ab	1:20000 Biorad	ECL Prime
58	Liver	12	Nitrocellulose	5% milk	1:8000 Sigma Ab	1:15000 Biorad	ECL Prime
59	Liver	12	Nitrocellulose	5% milk	1:4000 Sigma Ab	1:20000 Biorad	ECL Prime
60	Liver	12	Nitrocellulose	5% milk	1:4000 Sigma Ab	1:30000 Biorad	ECL Prime
61	Liver	12	Nitrocellulose	5% milk	1:4000 Sigma Ab	1:20000 Cell Signalling	ECL Prime
62	Liver	12	Nitrocellulose	5% milk	1:4000 Sigma Ab	1:30000 Cell Signalling	ECL Prime
63	Liver	12	Nitrocellulose	5% milk	1:6000 Sigma Ab	1:20000 Biorad	ECL Prime
64	Liver	12	Nitrocellulose	5% milk	1:6000 Sigma Ab	1:30000 Biorad	ECL Prime
65	Liver	12	Nitrocellulose	5% milk	1:6000 Sigma Ab	1:20000 Cell Signalling	ECL Prime
66	Liver	12	Nitrocellulose	5% milk	1:6000 Sigma Ab	1:30000 Cell Signalling	ECL Prime

67	Liver	12	Nitrocellulose	5% milk	1:2000 Genetex GTX100535 anti-MTHFR	1:5000 Biorad	ECL Prime
68	Liver	12	Nitrocellulose	5% milk	1:1000 Abcam anti-MTHFR	1:5000 Cell Signalling	ECL Prime
69	Liver and MII eggs	12	Nitrocellulose	5% milk	1:1000 Abcam anti-MTHFR	1:5000 Cell Signalling	ECL Prime

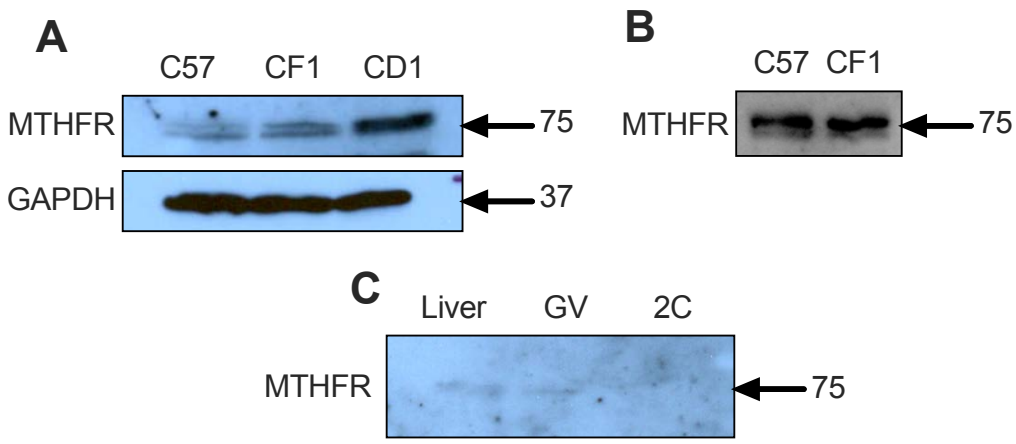

Figure 26. Attempt #1 and #2 from Table 7.

A) Example of western blot using the original Rozen antibody (done by author). 5 µg of liver tissue from each strain of mice, C57Bl6, CF1 and CD1 probed with 1:2000 anti-MTHFR Rozen antibody and 1:200 anti-GAPDH. B) Western done by Megan Meredith (lab technician) using the original Rozen antibody. 5 µg of liver tissue from C57Bl6 and CF1 mice probed with anti-MTHFR from the Rozen lab. C) Western blot with anti-MTHFR Sigma antibody that is supposed to be identical to the anti-MTHFR Rozen antibody (done by author). 5 µg liver, 100 GV oocytes and 100 2-cell embryos. Note the level of background obscuring the bands.

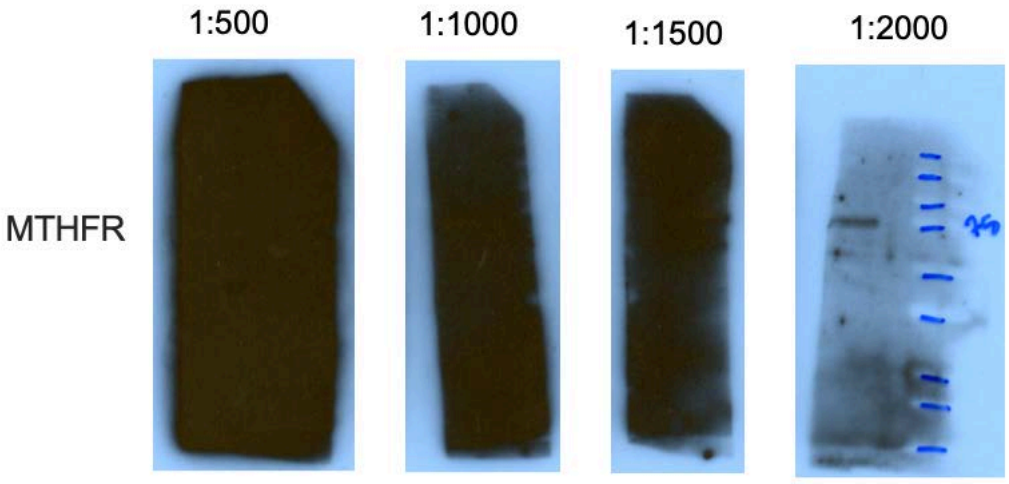

Figure 27. Attempts #3-#6 from Table 7: Dilution series of new Sigma anti-MTHFR antibody.

5 µg of C57Bl6 wildtype or knockout liver, probed with 1:500, 1:1000, 1:1500 and 1:2000 anti-MTHFR Sigma antibody using the standard western blot protocol for the anti-MTHFR Rozen antibody.

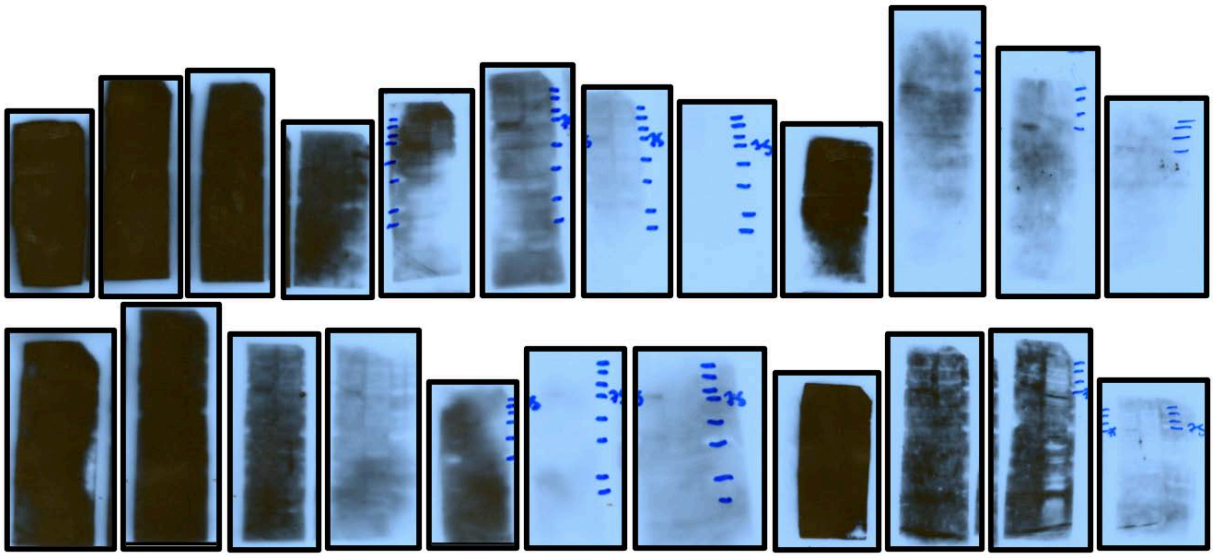

Figure 28. Attempts #44-#66 from Table 7. Dilutions of primary and secondary antibodies in 5% milk.

5 µg of liver tissue from wildtype or knockout mice probed with 1:2000-1:8000 anti-MTHFR Sigma antibody and 1:5000-1:100000 secondary antibody, attempted to be optimized.